Programa de Doctorado en Ingeniería Matemática, Estadística e Investigación Operativa

por la

Universidad Complutense de Madrid

y la

Universidad Politécnica de Madrid





Chaos and Dynamics in a Fractional Duffing Equation

Tesis Doctoral

Sara Hamaizia

Directores

Salvador Jiménez
M. Pilar Velasco

Año

2024





UNIVERSIDAD POLITÉCNICA DE MADRID
Escuela Técnica Superior de Ingenieros de Telecomunicación

Doctoral Degree in Mathematical Engineering, Statistics and Operational Research

Chaos and Dynamics in a Fractional Duffing Equation

D O C T O R A L T H E S I S

Submitted for the degree of Doctor by:

Sara Hamaizia
Master degree

Under the supervision of:
Dr. Salvador Jiménez
Dr. M. Pilar Velasco

Madrid, 2024

Title: Chaos and Dynamics in a Fractional Duffing Equation

Author: Sara Hamaizia

Doctoral Programme: Mathematical Engineering, Statistics and Operational Research

Thesis Supervision:

Dr. Salvador Jiménez, Associate professor of applied mathematics, Departamento de Matemática Aplicada a las T.I.C., E.T.S.I. Telecomunicación, Universidad Politécnica de Madrid, 28040-Madrid, Spain (Supervisor)

Dr. M. Pilar Velasco, Associate professor of applied mathematics, Departamento de Matemática Aplicada a las T.I.C., E.T.S.I. Sistemas de Telecomunicación, Universidad Politécnica de Madrid, 28038-Madrid, Spain

External Reviewers:

Thesis Defense Committee:

Thesis Defense Date:

This thesis has been partially supported by grant 048/PG/Espagne/2020-2021 of Ministère de l'Enseignement Supérieur et de la Recherche Scientifique, People's Democratic Republic of Algeria.

I thank ALLAH the Almighty for giving me the courage and the will to complete this work.

I dedicate this dissertation:

To my dear father: To my precious offering from God, who owes all my love and all my respect. To my lovely mother, to the woman who suffered without letting me suffer, and who spared no effort to make me happy. To my only sister Samia and her children Mouha, Amira, Oumaima and her husband, for his moral support and valuable advice throughout my studies. To my dear brothers: Said, Houcine, Ridha, Farid and his wife Amel and my big brother Walid and his wife Hana. To my younger brothers' children: Haboubti Amani, Salouma, Khaled, Anas. A special thank you to my friend and more than that to my second sister Hajoura, I wish her to succeed in her life. To all my friends Nour, Kenza, Chahi,... To everyone I love.

♡

Acknowledgement

First and foremost, I would like to praise God who gave me the will and the strength to carry out this work.

I would like to extend my deepest gratitude to my advisors: Prof. Salvador Jiménez and Prof. Maria Pilar Velasco.

Thank you, Prof. Jiménez, for your exceptional mentorship throughout my scientific research. Your insightful discussions, patience, and encouragement over the years have been invaluable. Your extensive knowledge and innovative ideas have played a crucial role in my journey, and I am truly honoured to have you as my mentor.

I extend my sincere thanks to Dr. M. Louaar for his valuable pieces of advice and for the guidance and information he regularly provided me.

I am deeply grateful to my family for teaching me that there are no barriers in life every opportunity can be accessed with determination and persistence.

A special thanks to my housemate, Nour, who has been a constant source of support and my go-to person for advice.

I am grateful to my friends Chahi, Kenza, and Hadjer for their constant emotional support.

Thank you to all those who contributed directly or indirectly, in my encouragement and moral support in the completion of my work. This work was made possible through the financial support of grant 048/PG/Spain/2020-2021 from the Ministry of Higher Education and Scientific Research of the People's Democratic Republic of Algeria.

Abstract

The Duffing equation is a nonlinear dynamical system known for exhibiting chaotic behaviour. It serves as a standard model for exploring chaos in a low-dimensional dynamical system.

In the work presented, we characterize the chaos in the Duffing equation with negative linear stiffness and a fractional damping term. The fractional form of the equation studied is a substitution of the first-order derivative in the Duffing equation with a Caputo fractional derivative of order α, ranging within the two intervals $(0, 1)$ and $(1, 2)$.

We determine that the phase space of the problem studied includes three dimensions, representing the parameters that define the system's state. However, with the phase remaining constant, we can effectively treat the phase space as two-dimensional, simplifying the analysis of the system's dynamics. We demonstrate that its regular solutions are not T-periodic.

We approximate the fractional Duffing equation using a new numerical method based on two approaches: by Strauss-Vázquez for conservative systems and by Odibat representation for the fractional derivative.

The purpose of the numerical simulations is to explore how the amplitude and the order of the fractional derivative α influence the system. The system displays a diverse range of behaviours depending on these two parameters. In our study, we have examined various values for amplitude and α to present the most significant solutions: regular solutions, chaotic solutions, long chaotic transient, solutions switching from regular or chaotic attractors and intermittent regime.

To clarify the various behaviours exhibited by the fractional system. We estimate the Lyapunov Characteristic Exponents (LCEs) and extend them to the whole range of values of α.

To analyze the threshold of chaos in this equation, we extend the Melnikov method to the fractional case and we conduct a comparative analysis between the analytical chaos threshold and its numerical counterpart.

The extension to values of $\alpha \in (1, 2)$ is also motivated by the fact that as $\alpha \to 2^-$, the fractional model becomes closer to a limit system where no damping and no saddle point exists. And that system can be seen as equivalent, at least for some range of the parameters, to the one obtained in the opposite limit, when $\alpha \to 0^+$. In this way, the fractional equations can be seen as an interpolation between the Duffing equation (limit $\alpha = 1$) and an undamped, forced system. In this work, we examine the behaviour of the fractional system in the vicinity of these limits.

For $\alpha \in (1, 2)$, the intermittent behaviour is notably common, with its manifestations influenced by the number of reinjection channels present, through the analysis of return map plots, which delineate these channels, along with approximations of the average laminar length corresponding to type I intermittency and the use of Floquet multipliers. We classify certain cases as type I intermittency.

Resumen

La ecuación de Duffing es un sistema dinámico no lineal conocido por presentar comportamiento caótico. Sirve como un modelo estándar para explorar el caos en sistemas dinámicos de baja dimensión.

En este trabajo, caracterizamos el caos en la ecuación de Duffing con rigidez lineal negativa y una disipación fraccional. La forma fraccional de la ecuación estudiada es una sustitución de la derivada de primer orden en la ecuación de Duffing con una derivada fraccional de Caputo de orden α, con valores dentro de los intervalos $(0, 1)$ y $(1, 2)$.

Establecemos que el espacio de fases del problema estudiado tiene tres dimensiones, representando los parámetros que definen el estado del sistema. Sin embargo, con la fase mantenida constante, podemos tratar de manera efectiva el espacio de fases como bidimensional, simplificando el análisis de la dinámica del sistema. Demostramos que los soluciónes regulares no son T-periódicas.

Aproximamos la ecuación de Duffing fraccional usando un nuevo método numérico basado en dos enfoques: el de Strauss-Vázquez para sistemas conservativos y la representación de Odibat para la derivada fraccional.

El propósito de las simulaciones numéricas es explorar cómo la amplitud y el orden de la derivada fraccional α influyen en el sistema. El sistema muestra una diversa gama de comportamientos dependiendo de estos dos parámetros. En nuestro estudio, hemos explorado varios valores para la amplitud y para α, para presentar las soluciones más significativas: soluciones regulares, soluciones caóticas, transitorios caóticos largos, soluciones que cambian de atractores regulares o caóticos y régimen intermitente.

Para aclarar los diversos comportamientos presentados por el sistema fraccionario, estimamos los Exponentes Característicos de Lyapunov (LCEs) y los extendemos a todo el rango de valores de α.

Para analizar el umbral del caos en esta ecuación, extendemos el método de Melnikov al caso fraccional y realizamos un análisis comparativo entre el umbral de caos analítico y su contraparte numérica.

La extensión a valores de $\alpha \in (1, 2)$ también está motivada por el hecho de que a medida que $\alpha \to 2^-$, el modelo fraccionario se aproxima a un sistema límite donde no existe amortiguamiento ni punto de silla. Y ese sistema puede considerarse equivalente, al menos para algunos rangos de los parámetros, al que se obtiene en el límite opuesto, cuando $\alpha \to 0^+$. De esta manera, las ecuaciones fraccionarios pueden verse como una interpolación entre la ecuación de Duffing (límite $\alpha = 1$) y un sistema forzado sin amortiguamiento. En este trabajo, examinamos el comportamiento del sistema fraccionario en la vecindad de estos límites.

Para $\alpha \in (1, 2)$, el comportamiento intermitente es notablemente común, con sus manifestaciones influenciadas por el número de canales de reinyección presentes. A través del análisis de gráficos de mapas de retorno, que delinean estos canales, junto con aproximaciones de la

longitud laminar promedio correspondiente a la intermitencia de tipo I y aprovechando los multiplicadores de Floquet, clasificamos ciertos casos como intermitencia de tipo I.

Résumé

L'équation de Duffing est un système dynamique non linéaire connu pour exhiber un comportement chaotique. Elle sert de modèle standard pour explorer le chaos dans un système dynamique de basse dimension.

Dans le travail présenté, nous caractérisons le chaos dans l'équation de Duffing avec une raideur linéaire négative et un terme dissipatif. La forme fractionnaire de l'équation étudiée est une substitution de la dérivée du premier ordre dans l'équation de Duffing par une dérivée fractionnaire de Caputo d'ordre α, variant dans les deux intervalles $(0, 1)$ et $(1, 2)$.

Nous établissons que l'espace des phases du problème étudié comprend trois dimensions, représentant les paramètres qui définissent l'état du système. Cependant, avec la phase restant constante, nous pouvons traiter effectivement l'espace des phases comme bidimensionnel, simplifiant ainsi l'analyse de la dynamique du système. Nous démontrons que ses solutions régulières ne sont pas T-périodiques.

Nous approchons l'équation de Duffing fractionnaire en utilisant une nouvelle méthode numérique basée sur deux approches : par Strauss-Vázquez pour systèmes conservatifs et par la représentation d'Odibat pour la dérivée fractionnaire.

Le but des simulations numériques est d'explorer comment l'amplitude et l'ordre de la dérivée fractionnaire α influencent le système. Le système montre une gamme diversifiée de comportements en fonction de ces deux paramètres. Dans notre étude, nous avons examiné différentes valeurs pour l'amplitude et α afin de présenter les solutions les plus significatives : solutions régulières, solutions chaotiques, transitoires chaotiques longs, solutions changeant d'attracteurs réguliers ou chaotiques et régime intermittent.

Pour discerner les différents comportements exhibés par le système fractionnaire, nous éstimons les Exposants Caractéristiques de Lyapunov (LCEs) et étendons à toute la plage de valeurs de α.

Pour analyser le seuil du chaos dans cette équation, nous étendons la méthode de Melnikov au cas fractionnaire et réalisons une analyse comparative entre le seuil de chaos analytique et son équivalent numérique.

L'extension aux valeurs de $\alpha \in (1, 2)$ est également motivée par le fait qu'à mesure que $\alpha \to 2^-$, le modèle fractionnaire se rapproche d'un système limite où il n'existe ni amortissement ni point de selle. Et ce système peut être considéré comme équivalent, du moins pour certaines plages de paramètres, à celui obtenu dans la limite opposée, lorsque $\alpha \to 0^+$. De cette manière, l' équation fractionnaire peut être vue comme une interpolation entre l'équation de Duffing (limite $\alpha = 1$) et un système forcé sans amortissement. Dans ce travail, nous examinons le comportement du système fractionnaire à proximité de ces limites.

Pour $\alpha \in (1, 2)$, le comportement intermittent est notablement commun, avec ses manifestations influencées par le nombre de canaux de réinjection présents. À travers l'analyse des graphiques des cartes de retour, qui délimitent ces canaux, ainsi que des approximations de

la longueur laminaire moyenne correspondant à l'intermittence de type I et en utilisant les multiplicateurs de Floquet, nous avons classé certains cas comme intermittence de type I.

Table of Contents

Acknowledgement v
Abstract vi
Resumen vii
Résumé ix
Conclusions xii
List of Figures xii
List of Tables xvi
Notation xviii

1 Introduction **1**
1.1 A brief history of factional calculus 2
1.1.1 Fractional integral and derivatives 5
1.1.2 Solving fractional nonlinear problems 14
1.2 A brief history of Duffing equation 14
1.3 Main objectives 17
1.4 Thesis organisation 18
1.5 Published Manuscript 18

2 Classical Duffing equation **19**
2.1 Undamped unforced Duffing equation 23
2.2 Damped unforced Duffing equation 24
2.3 Damped forced Duffing equation 26
2.4 Numerical solution of classical Duffing equation 27

3 Fractional Duffing equation and its numerical simulation **33**
3.1 Introduction 33
3.1.1 State of the art 33
3.2 The Considered problem 34
3.2.1 Phase space of fractional Duffing equation 35
3.2.2 Periodicity of solution 37
3.3 Numerical methods for the fractional Duffing equation 38
3.3.1 SV + Diethelm method for $\lceil\alpha\rceil = 1$ and $\lceil\alpha\rceil = 2$ 39
3.3.2 SV + Odibat method for $\lceil\alpha\rceil = 1$ and $\lceil\alpha\rceil = 2$ 41
3.4 Numerical results 45
3.4.1 Phenomenology of solutions 45

4 Characterizing chaos in the fractional Duffing equation **57**
4.1 Lyapunov characteristic exponents (LCEs) . . . 57
4.1.1 Computations of the LCEs . . . 59
4.2 LCEs for $\lceil\alpha\rceil = 1$ . . . 60
4.2.1 Analytical Approximation . . . 61
4.2.2 Numerical Results . . . 62
4.3 LCEs for $\lceil\alpha\rceil = 2$ . . . 65
4.3.1 Analytical Approximation . . . 65
4.3.2 Numerical Results . . . 68
4.4 Extension of Melnikov method . . . 71
4.4.1 Melnikov method for the classical Duffing equation . . . 71
4.4.2 Melnikov method for fractional Duffing equation . . . 73
4.4.3 Numerical integration of the fractional integral K_α . . . 76
4.4.4 Numerical and analytic onset of chaos . . . 80
4.5 Limiting cases . . . 82
4.5.1 Non-fractional equation: undamped forced Duffing equation . . . 83
4.5.2 Fractional Duffing equation near the limits . . . 86

5 Intermittency **91**
5.1 Theory of the main types of chaotic intermittency . . . 91
5.1.1 Type I intermittency . . . 93
5.1.2 Type III intermittency . . . 96
5.1.3 Type II intermittency . . . 97
5.1.4 Cases of intermittency in the classical Duffing equation . . . 99
5.2 Different cases of intermittency in the fractional Duffing equation . . . 111
5.2.1 Intermittency with two reinjection channels . . . 113
5.2.2 Intermittency with one reinjection channel . . . 119
5.2.3 Future research . . . 121

6 Conclusions **123**

A Stability of periodic solutions: Floquet theory **127**

References **133**

List of Figures

1.1 Hook Law. 15

2.1 Potential of Duffing oscillator: $U(x) = -\frac{a}{2}x^2 + \frac{b}{4}b^4$, $a < 0$ and $b > 0$ with hardening stiffness $k = a - bx^2$ under random excitation. 21
2.2 Potential well: $U(x) = -\frac{ax^2}{2} + \frac{bx^4}{4}$, $a < 0$ and $b < 0$. 21
2.3 Modelling of double twin wells potential Duffing equation: $U(x) = -\frac{ax^2}{2} + \frac{bx^4}{4}$, $a > 0$ and $b > 0$ 22
2.4 Cantilever beam in the nonuniform field of two permanent magnets. 22
2.5 Potential function $U(x)$ given by (2.16). 23
2.6 Orbits of the unforced Duffing oscillator. 24
2.7 Vector field of undamped, unforced, Duffing equation. 26
2.8 Trajectories attracted to the the fixed point $(1, 0)$ for small values of f_0: $f_0 = 0.001, \gamma = 0.25, x_0 = v_0 = 0$. 27
2.9 Strange attractor of classical Duffing equation for $f_0 = 0.3$. 27
2.10 Orbits in phase space and stroboscopic map (red points) for different periodic attractors for $x_0 = 0.5.$, $v_0 = 0.2$ 30
2.11 Strange attractors for different values of f_0. 31

3.1 Phase space and stroboscopic map for a regular solution that tends towards a T-periodic curve with $\alpha = 0.5$, $f_0 = 0.1$, $x_0 = v_0 = 0$. 46
3.2 Phase space and stroboscopic map of a regular solution tends towards a $3T$-periodic curve with $\alpha = 0.8$, $f_0 = 2$, $x_0 = v_0 = 0$. 46
3.3 Multiplicity of limit cycles in the regular regime: for different initial conditions with the same set of parameters: $\alpha = 0.6$, $f_0 = 0.2409$. 47
3.4 Regular attractors of the fractional Duffing equation for several values of α. 48
3.5 Comparison of fractional Duffing equation solutions: with phase $\phi = 0$ and phase-shifted solution ($\phi = \pi$) 49
3.6 Strange attractors of the fractional Duffing equation for several values of α. 50
3.7 Time series for chaotic and regular solutions for $\alpha = 0.1$, $f_0 = 0.16$ for two different initial conditions. In (b) the solution tends to a regular attractor after a chaotic transient. 51
3.8 The solution regularised after a long chaotic transient and tends towards a closed curve of period $8T$ (and a limit set of 8 points in the stroboscopic map), $\alpha = 0.3$, $f_0 = 3$, $x_0 = 1.23$, $v_0 = 1.21$. 51

3.9 Stroboscopic map of different chaotic transients for $\alpha = 0.25$, $f_0 = 0.229$ shows that two solutions with nearby initial conditions, display transients of different lengths. 52
3.10 Stroboscopic map with intermittent chaotic transient for $\alpha = 1.1$, $f_0 = 0.25$. 52
3.11 Phase space and Stroboscopic map of the transition from a T-periodic attractor to a $2T$ attractor, $\alpha = 1.1$, $f_0 = 0.2$, $x_0 = 0$, $v_0 = 0.5$. 53
3.12 Phase space and Stroboscopic map of the transition from a $2T$-periodic attractor to a $4T$ attractor, $\alpha = 1.2$, $f_0 = 0.19$, $x_0 = 0.5$, $v_0 = 0.5$. 53
3.13 Phase space and Stroboscopic map of the transition from a T-periodic attractor to a 3T attractor via a chaotic-like transition for $\alpha = 1.1$, $f_0 = 0.2$, $x_0 = 0.5$, $v_0 = 0.5$. 54
3.14 Switching from a regular attractor to a chaotic one, for $\alpha = 1.1$, $f_0 = 0.4$, $x_0 = 1.05$, $v_0 = 1.06$. 54
3.15 Switching from a regular $(T)-$chaotic$-$regular $(5T)-$regular $(7T)-$chaotic attractor, for $\alpha = 1.1$, $f_0 = 0.387$, $x_0 = 1.05$, $v_0 = 1.06$. 55
3.16 Intermittency with oscillations around one center $(-1, 0)$, for $\alpha = 1.25$, $f_0 = 0.2271$, $x_0 = 0.00101$, $v_0 = 0.002$. 55
3.17 Intermittency with oscillations around any of the two centers $(\pm 1, 0)$, for $\alpha = 1.35$, $f_0 = 0.2119$, $x_0 = v_0 = 0$. 56
3.18 Intermittency with oscillations around the two centres, $\alpha = 0.1$, $f_0 = 0.778, x_0 = 1$, $v_2 = 0$. 56

4.1 Estimates of the LCEs for the fractional Duffing's equation, chaotic solution with $\alpha = 0.8$, $f_0 = 0.3$, $x_0 = 0.8, v_0 = 0$ (SV + Diethelm method). 63
4.2 Estimation of LCEs shows the agreement between the positive Lyapunov exponent λ_1 and $\lambda_{\max}$: chaotic solution for $\alpha = 0.5$, $f_0 = 0.3$, $x_0 = 0.8$, $v_0 = 0$ (SV + Odibat method). 64
4.3 Estimation of LCEs shows the agreement between the positive Lyapunov exponent λ_1 and $\lambda_{\max}$: regular solution for $\alpha = 0.5$,$f_0 = 0.15$, $x_0 = 0.8$, $v_0 = 0$ (SV + Odibat method). 64
4.4 Accuracy of the conservation law (4.26) for $\alpha = 0.5$. 65
4.5 Estimation of Lyapunov Characteristic Exponents (LCEs) for a chaotic solution, for $\alpha = 1.1$, $x_0 = v_0 = 0$,$f_0 = 0.29$. 68
4.6 Estimation of Lyapunov Characteristic Exponents (LCEs) for a regular solution, $f_0 = 0.12$. 69
4.7 Accuracy of the conservation law (4.26) for $\alpha = 1.1$. 69
4.8 Estimation of the LCEs for a solution with a long regular phase, $\alpha = 1.1$, $f_0 = 0.4$, $x_0 = 1.05$, $v_0 = 1.06$. 70
4.9 Estimates of the Lyapunov dimension D_L versus α. 70
4.10 Graphics representations of the two functions V_0 (4.72) and V_0' (4.73). 75
4.11 Functions x' and x'' in semi-logarithmic scale compared to the exponential. . 76
4.12 Chaos threshold Obtained by the Melnikov extension for $0 < \alpha < 2$ 80
4.13 Numerical threshold for chaos. 81
4.14 Comparison of theoretical and numerical chaos thresholds Derived from the Melnikov extension method 82

4.15 Stroboscopic maps for Equation (4.100). Different colors correspond to different initial conditions. 85
4.16 Stroboscopic maps for equation (4.100) for value of $f_0 = 1$, shows a different chaotic attractors. 85
4.17 Stroboscopic maps for Equation (4.100) for $f_0 = 0.03$, shows a different chaotic attractors. 86
4.18 Stroboscopic maps for both limits with $f_0 = 0.13$, $\gamma = 0.01$, $\omega = 1$ shows the similarity to the classical case (Figure 4.15(a)). 87
4.19 Stroboscopic maps for α near to 1 and 2 for $f_0 = 0.03$, $\gamma = 0.25$, $\omega = 1$. . . . 87
4.20 Stroboscopic maps for α near to 1 and 2 for $f_0 = 1$, $\gamma = 0.9$, $\omega = 1$, $x_0 = v_0 = 0$. 88
4.21 Stroboscopic maps for α near to 1 and 2 for $f_0 = 0.03$, $\gamma = 0.9$, $\omega = 1$. . . . 88
4.22 Stroboscopic maps showing the chaotic region of both limit cases: $f_0 = 0.1$. 89

5.1 Floquet multipliers μ: type I. 93
5.2 Type I intermittency, Tangent bifurcation. (a) Existence of two fixed points: one stable x_s and the other one unstable x_u. (b) Coalescence of both fixed points into a single fixed point. (c) Intermittency: occurrence of the channel [23]. 94
5.3 Lorenz system: transitioning to chaos through type I intermittency. 96
5.4 Floquet multipliers: type III. 97
5.5 Floquet multipliers: type II. 98
5.6 Intermittent behaviour in (5.16). 100
5.7 Third return maps constructed from experimental data of the Poincaré map for$f = 0.542152$, $x_0 = v_0 = 0$. 101
5.8 x_{n+3} versus x_n near $x = -0.633$ showing the slow passage of x thereby forming a laminar phase. 101
5.9 Intermittency patterns for $f_0 = 0.3603208$. 102
5.10 The bifurcation diagram for equation $\ddot{x} + 0.25\dot{x} - x + x^3 = f\cos(\omega t)$. 103
5.11 Regular solution for $f_0 = 0.26496$. 103
5.12 Intermittency for $f_0 = 0.2649622$. 104
5.13 Intermittent behaviour for $f_0 = 0.287644871$. 104
5.14 Intermittent behaviour for $f_0 = 0.320452$: the blue curve represents the solution $x(t)$ and the red dots are the stroboscopic map corresponding to this solution. 105
5.15 Intermittent behaviour for $f_0 = 0.34856$. 105
5.16 Intermittent behaviour for $f_0 = 0.40214$. 106
5.17 Third return map corresponds to $f_0 = 0.2649622$. 107
5.18 Third return map x_{n+3} versus x_n in the neighbourhood of the fixed point $x = 1.28563$. 107
5.19 Double logarithmic scale of the maximum length l of the laminar sections in dependence of ϵ with slope equals to -0.5147. 108
5.20 Floquet multipliers corresponding to Figure 5.12: The first crossing with the unit circle was throughout μ_2. 109
5.21 Intermittency type III in (5.19). 110
5.22 Type III intermittency $x_0 = v_0 = 0.1$. 111
5.23 Intermittency with one channel of reinjection around both centres, $\alpha = 0.1$, $f_0 = 0.778, x_0 = 1, v_2 = 0$. 111

5.24 Intermittency for $\alpha = 0.99999, \quad f_0 = 0.26497, \quad x_0 = 1.2, v_0 = 0.3.$ 112
5.25 Intermittency for $\alpha = 1.000001, f_0 = 0.4057, x_0 = 0, v_0 = 0.$ 112
5.26 Intermittency for $\alpha = 1.000001, f_0 = 0.4057, x_0 = 0, v_0 = 0.$ 113
5.27 Intermittency with one channel, $\alpha = 1.25$, $f_0 = 0.2271$, $x_0 = 0.00101$, $v_0 = 0.002$. 113
5.28 Intermittency with two channels, $\alpha = 1.35, f_0 = 0.2119, x_0 = v_0 = 0.$ 114
5.29 Phase space and stroboscopic map for regular solution $f_0 = 0.25000699$. . . . 114
5.30 Chaotic intermittent behaviour with two re-injection channels $f_0 = 0.250007$. 115
5.31 Stroboscopic map of two re-injection channels, $f_0 = 0.250007$. 115
5.32 Stroboscopic map and solution $x(t)$ showing the intermittent behaviour as f_0 increases with two re-injection channels. 116
5.33 Stroboscopic map for $f = 0.250027$, where there exist two laminar phases. . 117
5.34 First return map for $f = 0.250027$, with two distinct re-injection channels. . 117
5.35 Two channels shown by the first return maps for $f = 0.250027$. 118
5.36 Power law for the mean value of the laminar phases with slope $\beta = -0.59$. . 118
5.37 Stroboscopic map and solution $x(t)$ showing the intermittent behaviour as f_0 increases with one re-injection channel. 119
5.38 Estimation of the LCEs for an intermittent behaviour, $\alpha = 1.3$, $f_0 = 0.221$, $x_0 = 0.85$, $v_0 = 0.12$. 120
5.39 The Floquet multipliers associated with the data in Figure 5.37(a) intersect the +1 level line. The solid black lines represent the levels +1 and -1. . . . 120
5.40 Return map of intermittent behaviour. 121

A.1 A schematic illustrating the Floquet multipliers and the corresponding possible bifurcations. 130
A.2 Comparison between exact and numerical Floquet multipliers (real and imaginary part). 132

List of Tables

4.1 Dependency scheme illustrating the calculation of K_α using coefficients ω_i, roots t_i, and functions v_k, λ_k based on the chosen value of β 80

5.1 Numerical data of the Floquet multipliers near the first crossing with the unit cycle. 109

Notation

This thesis adopts a systematic notation to facilitate readability. Below, we present the key notations employed throughout this work:

x	Displacement
x_0	Initial displacement
$\dot{x} = v$	Velocity
v_0	Initial velocity
t	time
$f^{(m)}$	Derivative of order m of f with respect to the variable
$\triangle t$	time step
γ	Damping term
ω	Angular frequency
f_0	Amplitude of external force
$U(x)$	Potential
H	Hamiltonian function
Γ	Euler's gamma function
$[.]$	integer part
$\lceil . \rceil$	ceiling function
$\lfloor . \rfloor$	Floor function
${}_aI_t^\alpha$	RL fractional integral
${}_aD_t^\alpha$	RL fractional derivative
${}_a^CD_t^\alpha$	Caputo fractional derivative
λ_i	Lyapunov Characteristic Exponent
λ_{max}	Maximum Lyapunov Characteristic Exponent
J	Jacobi matrix
M	Fundamental solution matrix
μ	Floquet mutipliers
RL	Riemann–Liouville
GL	Grünwald Letnikov derivative
SV	Straus-Vázquez conservative method
FDE	Fractional differential equation
ODE	Ordinary differential equation
LCE	Lyapunov Characteristic Exponent

Chapter 1

Introduction

In the realm of mathematical modelling, the classical theory of dynamical systems has long been a basis, guiding our understanding of how various phenomena evolve. Differential equations, which represent the essence of change in a system, are at the core of classical dynamical systems. To explain how variables change over time, these equations use integer-order derivatives, which reflect instantaneous rates of change. This approach has been extremely helpful in understanding how physical, chemical, biological, and social systems behave. However, it is not always enough to capture the entire range of complex interactions and changing patterns displayed by the real world.

Fractional dynamical systems, an extension of classical dynamical systems theory, integrate the concept of fractional calculus. By generalizing differentiation and integration to non-integer orders through fractional derivatives and integrals, this framework offers a more flexible representation.

Models incorporating fractional calculus employ these fractional-order derivatives to represent and analyse various systems that exhibit non-local behaviour. Within this mathematical framework, nonlinear differential equations with fractional-order derivatives, known as fractional differential equations (FDEs), play an important role. These equations expand upon ordinary differential equations (ODEs) by including fractional derivatives. The FDEs have the property of capturing memory effects and long-range dependencies. This makes them useful in modelling complex systems with non-local behaviours.

This property can be illustrated using the Fundamental Theorem of Calculus. We introduce a special function F as the primitive of a function f.

$$\frac{dF(t)}{dt} = f(t), \quad F(0) = F_0, \tag{1.1}$$

this can be represented in integral form as:

$$F(t) = F_0 + \int_0^t 1 \cdot f(\tau) d\tau. \tag{1.2}$$

Its general representation (the generalized primitive) can be achieved by replacing the

constant 1 with a convolution kernel that introduces the memory element:

$$F(t) = F_0 + \int_0^t K(t-\tau)f(\tau)d\tau, \tag{1.3}$$

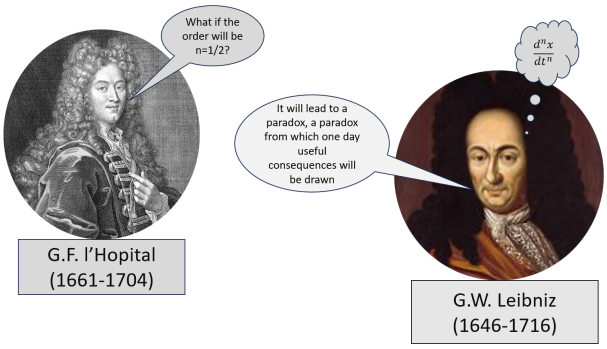
the convolution kernel K is a memory term which captures this influence of past values on the current behaviour of the function and it is an essential aspect of fractional calculus equations. It signifies the non-local nature of fractional derivatives and integrals, as they involve a weighted average of past values rather than just the value at a single point [127]. Multiple definitions of fractional derivatives have been progressively formulated to extend the fundamental notion of the ordinary derivative D, in such a manner that the conventional operator is retrievable when its order is an integer.

1.1 A brief history of factional calculus

The history of fractional calculus traces back to ancient times, but formalisation and development occurred over centuries. We provide an overview of significant milestones and contributors in the evolution of fractional calculus below [102, 21, 101, 65].

The first question that prompted the term fractional calculus was: can we give meaning to the derivative $d^n x/dt^n$ when n is a fraction? Later, the question became: can n take on any value: fractional, irrational, or even complex? This shift occurred after the affirmative resolution of the latter question.

This notation of the derivative of integer order was invented by Leibniz when he was naive playing with symbols. This promotes L'Hopital in 1695 to ask Leibniz: "What if n is $\frac{1}{2}$?" Leibniz's replay was prophetic: "You can see by that, sir, that one can express by an infinite series a quantity such as $d^{1/2}\overline{xy}$ or $d^{1:2}\overline{xy}$. Although infinite series and geometry are distant relations, infinite series admits only the use of exponents that are positive and negative integers and does not, as yet, know the use of fractional exponents. Thus it follows that $d^{1/2}x$ will be equal to $x\sqrt{dx : x}$. This is an apparent paradox from which, one day, useful consequences will be drawn."



Leibniz mentioned derivatives of "general order" during his discussion with Johann Bernoulli [67]. In his conversation with John Wallis, he suggested that differential calculus could potentially be utilized to obtain Wallis's infinite product for $\frac{1}{2}\pi$ [66], introducing the notation $d^{1/2}y$ to represent a derivative of order 1/2.

Since that time, many scientists and mathematicians, proposed several fractional integral formulations, such as Euler, Lagrange, Laplace, Fourier, Abel, Liouville, Riemann, Cayley, Weyl, Laurent, Hadamard, Lévy, Hardy, Littlewood, Zygmund, Marcel Riesz, Lions, Guelfand, Shilov $\cdots$ [21]

In [25], Euler discussed the concept of fractional calculus, particularly the differentiation of functions when the exponent n is a fraction rather than a positive integer. Euler acknowledges that when n is a positive integer, differentiation is straightforward and can be expressed algebraically. He said "When n is a positive integer, and if p should be a function of x, the ratio $d^n p$ to dx^n can always be expressed algebraically, so that if $n = 2$ and $p = x^3$, then d^2x^3 to dx^2 is $6x$ to 1".

However, Euler is interested in the question of what happens when n is a fraction. He notes the difficulty in finding the derivative when n is not an integer, as the process of continued differentiation doesn't readily apply. Euler suggests that interpolation already explained as a mathematical technique for estimating values between known data points, might offer a solution to this challenge.

In [61], Lagrange formulated the law of exponents for the differential operator as follows:

$$\frac{d^m}{dx^m} \cdot \frac{d^n}{dx^n} y = \frac{d^{m+n}}{dx^{m+n}} y, \tag{1.4}$$

then, the point is omitted, to avoid misunderstanding it as multiplication.

By the theory of fractional calculus, and the idea to replace m and n with non-integer order, Lacroix [60] generalized the expression of the nth derivative, starting with the function $y = x^m$ and using the factorial notion !, then the symbol Γ to generalize it. He expressed it as:

$$\frac{d^n}{dx^n} y = \frac{m!}{(m-n)!} x^{m-n} = \frac{\Gamma(m+1)}{\Gamma(m-n+1)} x^{m-n}, \quad m, n \in \mathbb{N}, m \geq n. \tag{1.5}$$

Replacing n with $1/2$ and m with arbitrary real number, he obtains:

$$\frac{d^{\frac{1}{2}}}{dx^{\frac{1}{2}}} y = \frac{\Gamma(m+1)}{\Gamma(m+\frac{1}{2})} x^{m-\frac{1}{2}}. \tag{1.6}$$

In 1822, Joseph P. J. Fourier [28] also used the derivative of arbitrary order. He generalized his integral representation of a function $f(t)$ by replacing the integer order n with an arbitrary number u positive or negative, to obtain:

$$\frac{d^u}{dt^u} f(t) = \frac{1}{2\pi} \int_{-\infty}^{+\infty} f(s) ds \int_{-\infty}^{+\infty} p^u \cos\Big(p(t-s) + \frac{u\pi}{2}\Big) dp. \tag{1.7}$$

Lacroix's method and Fourier's generalization for derivatives of arbitrary order did not indicate a potential practical application.

Niels Henrik Abel was the first one who use fractional calculus, employing it in 1823 to solve an integral equation linked to the tautochrone problem. This problem seeks to determine the

configuration of a frictionless wire positioned vertically, ensuring that regardless of the initial placement of a bead on the wire, the time taken for the bead to slide to the wire's lowest point remains constant [1].

Abel started by solving the integral equation:

$$k = \int_0^t \frac{f(\tau)}{(t-\tau)^{\frac{1}{2}}}\, d\tau, \tag{1.8}$$

where k is a constant. It is a particular case of a defined fractional integration of order $1/2$. Abel wrote the right-hand side of (1.8) by means of a fractional derivative of order $1/2$,

$$k = \sqrt{\pi}\Big(\frac{d^{-1/2}}{dt^{-1/2}}\Big(f(t)\Big)\Big). \tag{1.9}$$

Abel's formulation (1.8) was not completed to generalize differentiation but it was exceptionally elegant, likely capturing the attention of Liouville, who undertook the pioneering effort to establish a formal definition of a fractional derivative. Liouville's foundation begins with established results concerning derivatives of integer order m:

$$D_t^m e^{at} = a^m e^{at}, \tag{1.10}$$

and extended it to arbitrary order α :

$$D_t^\alpha e^{at} = a^\alpha e^{at}. \tag{1.11}$$

Through Fourier expansion, a broad range of functions can be represented as a combination or superposition of complex exponentials.

$$f(t) = \sum_{n=0}^{+\infty} c_n e^{a_n t}, \quad Re(a_n) > 0. \tag{1.12}$$

The arbitrary derivative of such function (1.12) of order α is:

$$D_t^\alpha f(t) = \sum_{n=0}^{+\infty} c_n a_n^\alpha e^{a_n t}, \tag{1.13}$$

this is the Liouville's first formula [72].

After several attempts to find a suitable general definition of a fractional derivative. G. F. Bernhard Riemann [99] formulated a somewhat distinct theory concerning fractional operations where he used a generalization of a Taylor series to derive a formula for the integration of arbitrary order:

$$D^{-\alpha} f(t) = \frac{1}{\Gamma(\alpha)} \int_c^t f(\tau)(t-\tau)^{\alpha-1} d\tau + \psi(t). \tag{1.14}$$

In fact, the derived expression stands as the prevailing contemporary definition of fractional integral. To address the ambiguity associated with the lower limit of integration c, Riemann

introduced a complementary function $\psi(t)$ to his definition. However, the current definition of fractional integration eliminates this complementary function. Neither Riemann nor Liouville resolved the issue of the complementary function, making it historically intriguing to understand how the present-day Riemann-Liouville definition eventually emerged.

However, the formal development of fractional calculus gained momentum in the 20th century. Notably, mathematicians like Riemann, Grünwald, and Letnikov made significant contributions. In the mid-20th century, the subject gained broader recognition with the works of renowned mathematicians such as Kolwankar, Bagley, and Oldham.

1.1.1 Fractional integral and derivatives

Fractional integral

A fundamental role of fractional calculus is illustrated through the gamma function $\Gamma(z)$, which serves to generalize the concept of factorial $z!$, enabling the inclusion of not only non-integer but also complex values for z. Its definition is:

$$\Gamma(z) = \int_0^\infty s^{z-1}e^{-s}ds,\ z \in \mathbb{C},\ Re(z) \in \mathbb{R}^+. \tag{1.15}$$

The gamma function (1.15) exhibits complex mathematical properties. After integration by parts in equation (1.15), we obtain the following property:

$$\Gamma(z) = (z-1)\Gamma(z-1),\ Re(z) > 0, \tag{1.16}$$

which allows giving the gamma function of a positive integer number as:

$$\Gamma(n) = (n-1)!. \tag{1.17}$$

The following property allows for the extension of the function to negative values and provides a way to compute the gamma function for complex numbers:

$$\Gamma(z)\Gamma(z-1) = \frac{\pi}{\sin(\pi z)}\cdot \tag{1.18}$$

Fractional operators are used as a way to include memory effects in differential models.

fractional calculus extends the concepts of integration and differentiation to include non-integer order fundamental operations. In 1869, N. Ya. Sonin [117] expressed what is now called the Riemann-Liouville integral using the Cauchy integral formula that represents the iteration of integrals an integer number n of times with a the lower bound of each integral:

$${}_aI_t^n f(t) = \int_a^t dt_1 \int_a^{t_1} dt_2\ \ldots \int_a^{t_{n-1}} f(\tau)\,d\tau = \frac{1}{(n-1)!}\int_a^t (t-\tau)^{n-1} f(\tau)\,d\tau, \tag{1.19}$$

However, the equation (1.19) remains valid for any strictly positive real value of n. This can be achieved using the gamma function (1.17). We thus obtain a definition of the primitive of positive real order $n = \alpha$ and lower bound a of the function f:

$${}_aI_t^\alpha f(t) = \frac{1}{\Gamma(\alpha)}\int_a^t (t-\tau)^{\alpha-1} f(\tau)\,d\tau. \tag{1.20}$$

This is the Riemann-Liouville (RL) integral formula. It can be stated in two cases depending on its bounds as follows:

- **Definition 1** *Left-side Riemann–Liouville Fractional Integral of order, $\alpha > 0$:*

$$ {}_aI_t^{\alpha} f(t) = \frac{1}{\Gamma(\alpha)} \int_a^t f(\tau)(t-\tau)^{\alpha-1} d\tau,\ a \in \mathbb{R}. \tag{1.21} $$

- **Definition 2** *Right-side Riemann–Liouville Fractional Integral of order, $\alpha > 0$:*

$$ {}_bI_t^{\alpha} f(t) = \frac{1}{\Gamma(\alpha)} \int_t^b f(\tau)(\tau-t)^{\alpha-1} d\tau,\ t < b,\ b \in \mathbb{R}. \tag{1.22} $$

- **Properties**:
  The operator (1.21), which is non-local, follows the following fundamental properties:
  - The integral is well defined if $f \in L^1[a,b]$.
  - The operator has a semi-group property:
    Let be $f \in L^p(a,b)$ $(1 \leq p \leq \infty)$ and $\alpha, \beta > 0$, then, for every $t \in [a,b]$,

$$ {}_aI_t^{\alpha}\, {}_aI_t^{\beta} f(t) = {}_a\, I_t^{\alpha+\beta} f(t). \tag{1.23} $$

  - The integral of a power is a power:
    Let be $\beta > 0$ and $\alpha > 0$, then

$$ {}_aI_t^{\alpha} (t-a)^{\beta-1} = \frac{\Gamma(\beta)}{\Gamma(\beta+\alpha)}\ (t-a)^{\beta+\alpha-1}. \tag{1.24} $$

Fractional derivatives

The fundamental concept behind non-integer order derivation involves extending or generalizing the traditional notion of derivative of different orders:

- Beginning with a function f, we can initiate its differentiation once, we obtain f':

$$ f'(t) = \lim_{\triangle t \longrightarrow 0} \frac{f(t+\triangle t) - f(t)}{\triangle t}. \tag{1.25} $$

- Subsequently, upon further differentiation of f', we obtained the second derivative, denoted as f''. This process clarifies the significance of the n^{th} derivative (or derivative of order n) of the function f, where n is a positive integer:

$$ \frac{d^n f(t)}{dt^n} = \lim_{\triangle t \longrightarrow 0} \frac{1}{\triangle t^n} \sum_{m=0}^{n} (-1)^m \begin{pmatrix} n \\ m \end{pmatrix} f\Big(t + (n-m)\triangle t\Big), \tag{1.26} $$

  where :

$$ \begin{pmatrix} n \\ m \end{pmatrix} = \frac{n!}{m(n-m)!},\ 0 \leq m \leq n. \tag{1.27} $$

If we consider the generalization of the concept of factorial through the function gamma (1.15), we obtain the definition of the fractional derivative of Grünwald-Letnikov (GL):

- **Definition 3** ***Grünwald Letnikov (GL) derivative***

$$ {}_aD_t^q f(t) = \lim_{\triangle t \to 0} \triangle t^{-q} \sum_{m=0}^{\infty} (-1)^m \left(\begin{array}{c} q \\ m \end{array} \right) f\Big(t + (q-m)\triangle t\Big), \quad t,\, \triangle t \in \mathbb{R},\, q \in \mathbb{N}. \tag{1.28} $$

For a function $f(t)$ defined on the interval $t \in [a, b]$ with $\triangle t > 0$ and $\alpha \in \mathbb{R}^+$:

$$ {}_aD_t^\alpha f(t) = \lim_{\triangle t \to 0} \triangle t^{-\alpha} \sum_{m=0}^{\infty} (-1)^m \left(\begin{array}{c} \alpha \\ n \end{array} \right) f^*(t - m\triangle t), \tag{1.29} $$

where:

$$ f^*(t) = \begin{cases} f(t), & t \in [a, b], \\ 0 & t \notin [a, b]. \end{cases} \tag{1.30} $$

The series in (1.29) converges absolutely and uniformly for each $\alpha > 0$ and for every bounded function $f(t)$. It is acceptable to rewrite (1.29) in terms of the function $f(t)$ itself, avoiding its continuation as a vanishing function, in the forms:

$$ {}_aD_t^\alpha f(t) = \lim_{\triangle t \to 0} \triangle t^{-\alpha} \sum_{m=0}^{[x]} (-1)^m \left(\begin{array}{c} \alpha \\ m \end{array} \right) f(t - m\triangle t), \tag{1.31} $$

where $[x]$ is a the integer part of x, with $x = \frac{t-a}{\triangle t}$, and the binomial coefficient $\left(\begin{array}{c} \alpha \\ m \end{array} \right)$ is generalized using the gamma function:

$$ \left(\begin{array}{c} \alpha \\ m \end{array} \right) = \begin{cases} \dfrac{\Gamma(\alpha+1)}{m!\Gamma(\alpha-m+1)}, & \alpha \in \mathbb{C},\, \alpha \notin \mathbb{Z}^-,\, m \in \mathbb{N}, \\ 1 \quad m = 0, & \\ \dfrac{(-1)^n(-\alpha)^m}{m!}, & \alpha \in \mathbb{C},\, m \in \mathbb{N}. \end{cases} \tag{1.32} $$

- **Definition 4** ***Riemann-Liouville fractional derivative***

The Riemann-Liouville fractional derivative is defined as follows:

$$ {}_aD_t^\alpha f(t) = D_t^n\, {}_aI_t^{n-\alpha} f(t) = \frac{1}{\Gamma(n-\alpha)} \frac{d^n}{dt^n} \int_a^t f(\tau)(t-\tau)^{-\alpha+n-1} d\tau, \quad n-1 < \alpha \leq n. \tag{1.33} $$

Properties [56]

– The left and rigth derivative is defined for functions $f \in AC^n[a,b]$: $C^{n-1}[a,b]$, $f^{(n-1)} \in AC[a,b]$.
Lipschitz $\subset$ Continuous $\subset$ Absolutly Continuous $\subset$ Differentiable .

Each inclusion can be expressed mathematically as:

$$Lip[a,b] \subset C[a,b] \subset AC[a,b] \subset C^1[a,b]. \tag{1.34}$$

The space $AC([a,b])$ is a space of an absolutely continuous function.

Definition 5 *A function f: $f : [a,b] \to \mathbb{R}$ is absolutely continuous on $[a,b]$, if $\forall \quad \epsilon > 0$, there exists $\delta > 0$, such that for any collection of pairwise disjoint intervals $\{[a_j, b_j]\}_j$ in $[a,b]$, we have:*

$$\sum_j (b_j - a_j) < \delta \Longrightarrow \sum_j \Big(f(b_j) - f(a_j) \Big) < \epsilon. \tag{1.35}$$

Definition 6 *A function f: $f : [a,b] \to \mathbb{R}$ is Lipschitz function on $[a,b]$ if and only if:*

$$|f(x) - f(y)| \leq c|x - y|, \quad \forall x, y \in [a,b]. \tag{1.36}$$

We denote the space of Lipschitz functions as $Lip[a,b]$.

∗ Let us prove that Lipschitz function on $[a,b]$ is absolutely continuous on $[a,b]$, i.e., $Lip[a,b] \subset AC[a,b]$.

Proof 1 *We have $f \in Lip[a,b]$ and $[a_j, b_j] \subset [a,b]$, then we have:*

$$|f(a_j) - f(b_j)| \leq c|a_j - b_j|, \tag{1.37}$$

hence:

$$\sum_j |f(a_j) - f(b_j)| \leq c \sum_j |a_j - b_j|, \tag{1.38}$$

given: $\sum_j |a_j - b_j| < \delta$ and multiply both sides by c:

$$c \sum_j |a_j - b_j| < c\delta. \tag{1.39}$$

Let choose $\delta = \frac{\epsilon}{c}$, then $c\delta = \epsilon$, and we have:

$$c \sum_j |a_j - b_j| < c\delta = \epsilon \tag{1.40}$$

– Limit at integer order:

$$\lim_{\alpha \to n} {}_aD_t^\alpha f(t) = D_t^n f(t) = f^{(n)}(t). \tag{1.41}$$

– Derivative of a power: let be $\beta > 0$ and $\alpha > 0$, then:

$$ {}_aD_t^{\alpha}(t-a)^{\beta-1} = \frac{\Gamma(\beta)}{\Gamma(\beta-\alpha)}\ (t-a)^{\beta-\alpha-1}. \tag{1.42} $$

– Derivative of a constant: let be $0 < \alpha < 1$, then:

$$ {}_aD_t^{\alpha}1 = \frac{(t-a)^{-\alpha}}{\Gamma(1-\alpha)}. \tag{1.43} $$

On the other hand, for $\alpha > 0$ with $n = \lceil \alpha \rceil$,

$$ {}_aD_t^{\alpha} f(t) = 0 \iff f(t) = \sum_{j=1}^{n} c_j (t-a)^{\alpha-j}, \tag{1.44} $$

with c_j arbitrary constants.

– Index laws:

⋆ Let be $f \in L^1(a,b)$, $\alpha, \beta > 0$, such that $n = \lceil \alpha \rceil$, $m = \lceil \beta \rceil$, $(n, m \in \mathbb{N})$ and $\alpha + \beta < n$. Then:

$$ {}_aD_t^{\alpha} f(t)\, {}_aD_t^{\beta} f(t) =_a D_t^{\alpha+\beta} f(t) - \sum_{j=1}^{m} {}_aD_t^{\beta-j} f(a) \frac{(t-a)^{-j-\alpha}}{\Gamma(1-j-\alpha)}. \tag{1.45} $$

⋆ Let be $f \in L^1(a,b)$, we have:

$$ {}_aD_t^{\alpha}\, {}_aI_t^{\alpha} f(t) = f(t) \tag{1.46} $$

$$ {}_aD_t^{\beta}\, {}_aI_t^{\alpha} f(t) = {}_aI_t^{\alpha-\beta} f(t), \qquad \alpha \geq \beta \tag{1.47} $$

$$ {}_aD_t^{\beta}\, {}_aI_t^{\alpha} f(t) = {}_aI_t^{\beta-\alpha} f(t), \qquad \alpha \leq \beta \tag{1.48} $$

a.e. in $[a,b]$.

⋆ Let be $f \in L^1(a,b)$, $\alpha > 0$, $n = \lceil \alpha \rceil$. Then:

$$ {}_aI_t^{\alpha}\, {}_aD_t^{\alpha} f(t) = f(t) - \sum_{j=1}^{n} \frac{f^{(n-j)}(a)}{\Gamma(\alpha-j+1)} (t-a)^{\alpha-j}. \tag{1.49} $$

– **Cauchy problem with the Riemann-Liouville derivative**

Consider the fractional equation:

$$ {}_aD_t^{\alpha} x(t) = f\Big(t, x(t)\Big), \quad \alpha > 0,\ t > a, \tag{1.50} $$

with $n = \lceil \alpha \rceil$. The model's initial conditions are:

$$ {}_aD_t^{\alpha-k} x(a) = b_k,\ b_k \in \mathbb{R},\ k = 1, 2, \ldots, n, \tag{1.51} $$

with: ${}_aD_t^{\alpha-k} x(a) = \lim_{t \to a} {}_aD_t^{\alpha-k} x(t)$.

They ensure the existence and unicity of a continuous solution provided f is continuous in t and Lipshitz in x [56].

- **Definition 7** ***Caputo fractional derivative***

  The Caputo fractional derivative is closely related to the Riemann-Liouville derivative. It is defined by:

$$ {}_a^C D_t^\alpha f(t) = \frac{1}{\Gamma(n-\alpha)} \int_a^t \frac{f^{(n)}(\tau)}{(t-\tau)^{\alpha-n+1}} d\tau, \quad n-1 < \alpha < n, \tag{1.52} $$

  where $f^{(n)}$ is the derivative of f of order $n \in \mathbb{N}$.

  Properties [56]

  – Relationship between Caputo and Riemann-Liouville fractional derivative

  When subjected to homogeneous initial conditions, the Riemann-Liouville and Caputo derivatives are equivalent. The relation between them is:

$$ {}_a D_t^\alpha f(t) = {}_a^C D_t^\alpha f(t) + \sum_{k=0}^{n-1} \frac{(t-a)^{k-a}}{\Gamma(k-\alpha+1)} f^{(k)}(a), \tag{1.53} $$

  with $f^{(k)}(a) = 0, (k = 0, 1, ..., n-1)$.

  – Relationship between Caputo and Riemann-Liouville fractional integral

  If $\alpha \in \mathbb{N}$, $\alpha \leq 0$, $f \in AC^n[a, b]$:

$$ {}_a^C D_t^\alpha f(t) = {}_a I_t^{n-\alpha} D^n f(t) = \frac{1}{\Gamma(n-\alpha)} \int_a^t \frac{f^{(n)}(\tau)}{(t-\tau)^{\alpha-n+1}} d\tau. \tag{1.54} $$

  – Limits of derivatives of integer order:

  * If $\alpha = n \in \mathbb{N}$

$$ \lim_{\alpha \to n} {}_a^C D_t^\alpha f(t) = f^{(n)}(t). \tag{1.55} $$

  * If $\alpha = n = 0$

$$ \lim_{\alpha \to 0^+} {}_a^C D_t^\alpha f(t) = f(t). \tag{1.56} $$

  – If $\alpha = 1 + \beta$, $\alpha \in \mathbb{R}$

$$ {}_a^C D_t^\alpha f(t) = {}_a^C D_t^{\beta+1} f(t) = {}_a^C D_t^\beta f'(t). \tag{1.57} $$

  – Cauchy problem with the Caputo derivative:

  Let be the fractional equation:

$$ {}_a^C D_t^\alpha x(t) = f\Big(t, x(t)\Big), \quad \alpha > 0, \ a \leq t \leq b, \tag{1.58} $$

  with $n = \lceil \alpha \rceil$. The model's initial conditions are:

$$ D_t^k x(a) = b_k, \ b_k \in \mathbb{R}, \ k = 0, 2, \ldots, n-1. \tag{1.59} $$

For this initial problem also, they ensure the existence and unicity of a continuous solution provided f is continuous in t and Lipshitz in x. In this case, the initial conditions are integer order derivatives at the initial time.

The solution $x(t)$ satisfies the relation (1.58) with (1.59) if and only if $x(t)$ satisfies the Volterra integral equation [56]:

$$x(t) = \sum_{j=0}^{n-1} \frac{b_j}{j!}(t-a)^j + \frac{1}{\Gamma(\alpha)} \int_a^y \frac{f(t,x(t))}{(y-t)^{1-\alpha}} dt, \quad a \leq y \leq b. \tag{1.60}$$

– Derivative of a constant. If $\alpha \notin \mathbb{N}$:

$${}_a^C D_t^\alpha a = 0. \tag{1.61}$$

On the other hand, for $\alpha > 0$ with $n = \lceil \alpha \rceil$,

$${}_a^C D_t^\alpha x(t) = 0 \iff x(t) = \sum_{j=1}^{n-1} c_j (t-a)^j, \tag{1.62}$$

with $c_j = \frac{b_j}{j!}$ and b_j arbitrary constants.

Fractional differential equations find applications in various fields, including physics, engineering, finance, biology, and more. In electrochemical systems, diffusion plays a crucial role in the transport of ions or molecules to and from electrodes.

Some nonlinear differential equations with fractional-order terms are commonly used to model various phenomena in biology, the Lotka-Volterra equations are a classic model used to describe the dynamics of predator-prey interactions in ecological systems which is studied as a fractional model. Fractional-Order Models for Cell Proliferation [116] and Fractional-Order Reaction-Diffusion equations [110] are two examples that illustrate how fractional-order differential equations can be applied to model various biological processes. There are also fractional-order differential equations that can be used to model the complex viscoelastic behaviour of materials as the Fractional Zener Model for viscoelasticity [69] and the Fractional Burgers Model for viscoelasticity [55].

In physics, The Schrödinger equation is a fundamental equation in quantum mechanics that describes the behaviour of wavefunctions representing particles. Introducing fractional derivatives into this equation can model systems with memory effects or subdiffusion behaviour [63]. Also, the classical Duffing equation stands as an example of such equations that have been adapted to analyse the dynamics of fractional-order systems. This adaptation hinges on the specific fractional derivative under consideration and the corresponding integer-order derivative it replaces. It is the application that we are interested in within this work.

Numerical Integration of Caputo fractional derivative

Numerous works within the literature have delved into the examination of analytical solutions employing techniques such as Laplace transforms, Fourier transforms, Mellin transforms, and

the method of separation of variables [93]. Some of the authors transform the initial problem:

$$ {}_{t_0}^{C}D_t^{\alpha}x(t)x(t) = f(t, x(t)), \quad n-1 < \alpha < n \tag{1.63} $$

with initial conditions

$$ x^{(k)}(t_0) = x_0^{(k)}, k = 0, 1, ..., n-1, \tag{1.64} $$

in terms of the Volterra integral equation of the second kind and solve it. Lubich [75] solved this kind of equation using the general Runge-Kutta method. The finite difference method and finite element method are used to build numerical algorithms of fractional differential equations as is done in [138].

Despite the existence of numerous numerical techniques, our study collaborates on two numerical algorithms for the Caputo fractional derivative. Diethelm et al. [18] sought a new approach to numerically solve the nonlinear fractional differential equation described in (1.63), alongside its initial conditions as specified in (1.64). Initially, they revisited the concept underlying the classical one-step Adams–Bashforth–Moulton algorithm. Following this, they devised a formula that extends this concept, incorporating the product trapezoidal quadrature, and subsequently established theorems concerning the accuracy of this Adams scheme.

Remark 1 *We will use the notation* ${}_{t_0}D_t^{\alpha}x$ *instead of* ${}_{t_0}^{C}D_t^{\alpha}x$ *to denote the Caputo fractional derivative.*

In 2005, Diethelm et al. [17] introduced a new numerical method for computing the Caputo fractional derivative, for $0 < \alpha < 2, \alpha \neq 1$:

Diethelm approximation
For the interval $[0, a]$ with the grid $\{x_k = k\triangle t : k = 0, 1, 2, ..., n\}$ and $\triangle t = a/n$, compute:

$$ D_t^{\alpha}x_n(\triangle t) = \frac{\triangle t^{-\alpha}}{\Gamma(2-\alpha)} \sum_{k=0}^{n} c_{k,n} \left(x_{n-k} - \sum_{j=0}^{\lfloor \alpha \rfloor} \frac{(n-k)^j \triangle t^j}{j!} x_{0^+}^{(j)} \right), \tag{1.65} $$

where

$$ D_t^{\alpha}x(a) = D_t^{\alpha}x_n(\triangle t) + \mathcal{O}(\triangle t^{2-\alpha}). \tag{1.66} $$

The coefficients $c_{k,n}$ [17] are obtained by the quadrature weights (derived from the Trapezoidal rule):

$$ \begin{cases} c_{0,n} = 1, \\ c_{k,n} = (k+1)^{1-\alpha} - 2k^{1-\alpha} + (k-1)^{1-\alpha}, \quad 0 < k < n, \\ c_{n,n} = (1-\alpha)n^{-\alpha} - n^{1-\alpha} + (n-1)^{1-\alpha}. \end{cases} \tag{1.67} $$

The second method we are interested in is the Odibat approach, initially proposed by Odibat et al. [87]. Odibat introduced a specific algorithm for approximating the Caputo fractional derivative when $\alpha > 0$, which relies on two distinct definitions: the trapezoidal rule and the Modified trapezoidal rule [87].

Odibat approximation

The approximation of the Caputo fractional derivative for a function f is defined on the interval $[0, a]$ with a step size denoted by $t_j = j\triangle t$ with $j = 1 : k$. The approximation is given as follows:

$$C(f, \triangle t, \alpha) = \frac{\triangle t^{m-\alpha}}{\Gamma(m+2-\alpha)} \left(\Big((k-1)^{m-\alpha+1} - (k-m+\alpha-1)k^{m-\alpha} \Big) f^{(m)}(0) \right)$$
$$+ \frac{\triangle t^{m-\alpha}}{\Gamma(m+2-\alpha)} \left(\sum_{j=1}^{k-1} \Big((k-j+1)^{m-\alpha+1} - 2(k-j)^{m-\alpha+1} + (k-j-1)^{m-\alpha+1} \Big) f^{(m)}(t_j) \right)$$
$$+ \frac{\triangle t^{m-\alpha}}{\Gamma(m+2-\alpha)} f^{(m)}(a) \quad a > 0, \quad m-1 < \alpha < m, \quad (1.68)$$

where:

$$\Big(D_t^{\alpha} f(t) \Big)(a) = C(f, \triangle t, \alpha) - E_C(f, \triangle t, \alpha), \quad a > 0. \quad (1.69)$$

Error analysis

The error analysis of this method, if $f(t) \in C^{m+2}\Big([0, a]\Big)$ is:

$$|E_C(f, \triangle t, \alpha)| \leq C'_{m-\alpha} \left\| f^{(m+2)} \right\|_{\infty} a^{m-\alpha} \triangle t^2 = \mathcal{O}(\triangle t^2), \quad m-1 < \alpha < m. \quad (1.70)$$

- **The estimation of the Caputo fractional derivative for** $0 < \alpha < 1$:

$$\begin{aligned} C(f, \triangle t, \alpha) &= \frac{\triangle t^{1-\alpha}}{\Gamma(3-\alpha)} \Big[\Big((k-1)^{3-\alpha} - (k+\alpha-2)k^{1-\alpha} \Big) f'(0) \\ &+ \sum_{j=1}^{k-1} \Big((k-j+1)^{2-\alpha} - 2(k-j)^{2-\alpha} + (k-j-1)^{2-\alpha} \Big) f'(t_j) \\ &+ f'(a) \Big], \quad 0 < \alpha < 1. \end{aligned} \quad (1.71)$$

- **The estimation of the Caputo fractional derivative for** $1 < \alpha < 2$:

$$\begin{aligned} C(f, \triangle t, \alpha) &= \frac{\triangle t^{2-\alpha}}{\Gamma(4-\alpha)} \Big[\Big((k-1)^{2-\alpha} - (k+\alpha-2)k^{2-\alpha} \Big) f''(0) \\ &+ \sum_{j=1}^{k-1} \Big((k-j+1)^{3-\alpha} - 2(k-j)^{3-\alpha} + (k-j-1)^{3-\alpha} \Big) f''(t_j) \\ &+ f''(a) \Big], \quad 1 < \alpha < 2. \end{aligned} \quad (1.72)$$

In 2009, Z. M. Odibat [88] introduced a supplementary method, building upon his previous work [87], where he clarified numerical algorithms. This method employs a set of finite difference formulas as the initial step in formulating the algorithm for numerical computations of fractional derivatives.

1.1.2 Solving fractional nonlinear problems

Solving fractional nonlinear problems is a topic of interest to many authors for partial fractional differential equations or ordinary fractional differential equations that must be solved according to appropriate initial and boundary conditions [16].

Kilbas et al. consider the concept of the uniqueness and existence of the solution for some generalized differential models related to the dynamics of a sphere immersed in an incompressible viscous fluid with oscillatory processes that have fractional damping terms [56].

Mainardi [76] studied the oscillatory processes with fractional damping based on the fractional Caputo derivative through the following initial values problem:

$$\begin{cases} \ddot{x}(t) + \gamma_0^C D_t^\alpha x(t) + bx(t) = g(t), \\ x(0) = C_0, \quad \dot{x}(0) = C_1, \end{cases} \tag{1.73}$$

where $\gamma > 0$ and $0 < \alpha < 2$. He successfully tackled this challenge using the Laplace transform. This equation has a unique solution similar to the fractional Duffing equation we are studying, except it does not include the nonlinear cubic term x^3. In the case of Caputo fractional differential equations, the initial conditions, as detailed in (1.58) with (1.59), resemble those observed in classical ordinary differential equations (ODEs), and are therefore familiar to us. Consequently, the necessity to resolve FDEs justifies the preference for adopting Caputo's derivative(1.52) for fractional differentiation over the more prevalent Riemann Liouville definitions.

1.2 A brief history of Duffing equation

The realm of nonlinear dynamics has an expansive history with diverse threads, spanning from the deeply mathematical to the practical and applied domains. The idea of nonlinear vibrations [1] had been recognized well before Duffing penned his treatise on oscillations, where he introduced his renowned equation. Yet, it was Duffing who methodically untangled the complexities of a nonlinear oscillator in an organized fashion by applying concepts from the linear oscillator framework. Furthermore, he systematically studied the impacts of quadratic and cubic stiffness nonlinearities [2]on the system's behaviour [108, 58, 11].

He stressed the differences between the linear and the nonlinear oscillators for both free and forced vibrations [3], also considering the effects of damping.

Before Duffing's contributions, there where some research focused on the mathematical examination of nonlinear oscillators. Within the context of nonlinear dynamics history, the pendulum assumes a prominent position, thus making it fitting to commence the narrative

[1]Nonlinear vibrations: involve recurring motion patterns in systems where the restoring force is not strictly proportional to the displacement from equilibrium.

[2]Stiffness is the extent to which an object resists deformation in response to an applied force.

[3]Forced vibration is an external factor acting on an oscillatory system that has the influence to command and modify its oscillations.

with Galileo. Galileo Galilei contemplated various concepts concerning the typical frequency and amplitude of oscillation [74]. To improve these ideas and explain them clearly, he devised a device known as an escapement to experimentally validate his hypotheses. After that Huygens proved that the Pendulum is nonlinear [137].

The interaction between the stiffness and the mass leads to several behaviours in different vibration systems. Hooks was the first who discover the law of elasticity in 1660 which states that when an object undergoes small deformations, the extent of displacement or deformation size directly corresponds to the applied deforming force or load and the object returns to its first shape once this force is removed. The amount of force F required to stretch or compress a spring by a certain distance (displacement) x increases proportionally as the distance increases [41].

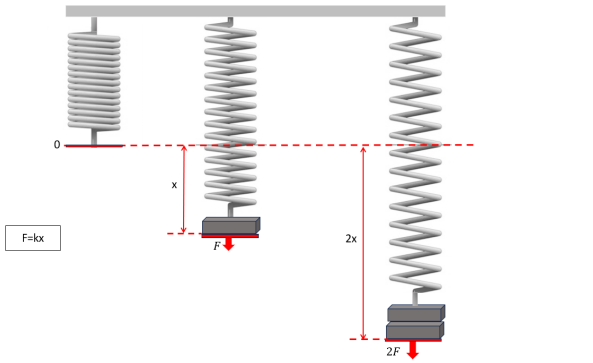


Figure 1.1: Hook Law.

The quantity $F = kx$ is the applied force, x is the displacement and k is a constant. Then, Leibniz [124] extended Hooke's law to a system involving moments, specifically in the context of bending a beam. Leibniz's insight was that this bending moment is proportional to the second moment of the area of the beam. Then, from the analysis side, Euler is credited as the first individual to formulate the equation of motion of a harmonically forced, undamped, linear oscillator [26]:

$$m\ddot{x} + kx = F\sin(\omega t). \tag{1.74}$$

A non-linear stiffness component was introduced into the equation of motion, which Euler initially developed. Helmholtz was the first to incorporate this addition, as follows:

$$m\ddot{x} + k_1 x + k_2 x^2 = F\sin(\omega t). \tag{1.75}$$

where $f = k_1 x + k_2 x^2$ is the restoring force [38].

Rayleigh studied the same model but with a cubic restoring force $f = k_1 x + k_2 x^3$ which is close to the Duffing equation with a null external force $F = 0$, [59]. Rayleigh's contribution included a limited analysis, demonstrating that nonlinear systems will experience vibrations at a primary frequency along with their harmonics. These harmonic occurrences depend on the vibration amplitude and the particular characteristics of the nonlinear stiffness force.

Despite the challenges in accurately describing physical systems, the Duffing equation serves as an approximate model that facilitates qualitative analysis of their behaviour.

There are various forms of the Duffing equation linear or non-linear are used to describe several systems.

In the subsequent chapter, we commence by introducing the classical Duffing equation, both with and without external force and viscous damping force. We explore its solutions and the array of behaviours demonstrated by the system, including periodic motion, chaotic motion, doubling bifurcation, and intermittency.

Due to the diverse behaviours exhibited in dynamical systems, which often challenge explanation and prediction, chaos theory has emerged as a method for both qualitative and quantitative analysis to investigate these behaviours. Chaotic systems, are characterised by their sensitive dependence on initial conditions: a small change in one state of a deterministic nonlinear system may lead to a completely different result in a later state. We use the following operative definition of chaos:

Definition 8 *We call chaos in a dynamical system an aperiodic behaviour for long times of the bounded solutions that are sensitive to the initial conditions.*

The aperiodicity for long times supposes that there are trajectories in the phase space that do not converge to a critical point, to a limit cycle or to periodic or almost-periodic orbits as times go to $+\infty$. The set of these trajectories is of significance and the part of phase space affected is important. The sensitivity to the initial conditions suppose that there are solutions that start in neighbouring values and separate exponentially.

This divergence described by exponential separation is fundamental to understanding chaotic behaviour in dynamical systems. It can be quantified by approximating the Characteristic Lyapunov Exponents (LCEs).

The LCEs are an essential tool used to characterise chaos. They measure the rate at which nearby trajectories separate or converge in phase space, providing crucial insights into the system's predictability and stability. Therefore, examining the LCEs helps to understand the system's dynamic behaviours.

These dynamic behaviours can be characterised also by unpredictable behaviours such as strange attractor or intermittency [133, 112, 62, 118, 132]. The presence of a strange attractor is often shown in stroboscopic phase space maps by the emergence of a region covered by a "cloud" of points, indicating the aperiodic behaviour.

Intermittency is a phenomenon characterised by irregular alternation between chaotic and regular behaviour where chaotic bursts intermittently disrupt the regular phases.

Duffing equation is a paradigmatic model among systems of nonlinear dynamics that exhibit chaos [12, 133, 36, 91, 45, 32].

It can be used to present a diversity of physical systems. It can be considered as a benchmark for studying chaos in a low-dimensional dynamical system [4]. It has been extended to the fractional case. Depending on which fractional derivative is used (Riemann-Liouville, Caputo, Grünwald-Letnikov, etc.) and what integer order it replaces, different systems are obtained

[4] A low-dimensional dynamical system is a mathematical model that describes the evolution of a system over time, where the state of the system is characterized by a small number of variables or dimensions.

which are not in principle equivalent [136, 71, 123, 4, 43, 70, 104].

1.3 Main objectives

In our study outlined in this thesis, we have studied a fractional Duffing equation, with specific regularity conditions, that ensure the existence and unicity of solutions [49], replacing the first-order derivative in the Duffing equation by a Caputo fractional derivative of order α ranging within the two intervals $(0, 1)$ and $(1, 2)$. This system has the particularity of corresponding to feasible physical systems.

In [51], Jiménez et al. studied the effects of chaos in this very same fractional equation and presented a way to estimate all the LCEs, to establish the chaoticity or regularity of the solutions and the onset of chaos as a function of the parameters. They also analysed the controlling effect of anharmonic external perturbations and the existence of geometric resonances that suppress the chaotic behaviour.

In our study, we expand on the results presented in [51], which showed that solution behaviours in a particular fractional order range $0 < \alpha < 1$ are complex and deserve more research. To enhance understanding, we undertake a more detailed analysis in this work.

Once the fractional model is set, a numerical method has to be used to approximate it and, in practice, one ends up studying a discrete system, close to the continuous one. This supposes that not only the choices related to the fractional derivatives but, also, the choice of a numerical technique may be relevant. Different methods may be considered (see, for instance, [115, 9]).

In our case, we use a numerical scheme based on the conservative Strauss-Vázquez method (SV method) [48], to approximate the non-fractional terms, and the Odibat representation [87, 88] for the fractional derivative. This new method improves the one used a previous studies [51].

Besides, these studies were limited to the case with a fractional derivative of order $\alpha \in (0, 1)$ and in this present work we extend to include also the range $\alpha \in (1, 2)$.

Equations with fractional derivatives present a computational challenge due to the non-locality. It is thus worth to use different numerical methods and contrast the agreement of their results. In our case, we use this new method (SV + Odibat method) and the one used in [51]. Since that method was only valid for $0 < \alpha < 1$, we extended it to include $1 < \alpha < 2$.

Understanding chaotic behaviour is a complex task, and different methods and approaches have been employed to detect it. See for instance [140, 114, 47, 120] and, more recently, [13, 14]. In our work, we estimate the LCEs using two different techniques: the fiduciary orbit and linearization. This second method cannot be applied in the range $(1, 2)$ as is done for $(0, 1)$ and the extension requires some adaptations, using several tools that differ from the previous technique.

With all these tools, we have sampled the different behaviours exhibited by the solutions of the fractional system, which appear to have a rich phenomenology: transition between regular

and chaotic regimes inside the solution, bifurcation in time, and intermittency.

We also study the appearance of chaos by estimating its threshold and examining how the system parameters influence this threshold by extending the Melnikov method to the fractional case.

The chaotic behaviour in the limit systems $\alpha \to 0^+$ and $\alpha \to 2^-$ is due to the perturbation caused by the external forcing on a Hamiltonian. In these limit cases, chaos is present in the central region of the phase space independently of the parameter's values with a chaotic region tending to fill a two-dimensional area of the phase space. This is quite different to the phenomenology of Duffing equation where the chaos is directly related to the perturbation of the stable and unstable manifolds around the saddle point. In this work, we study the behaviour of the fractional system near these limits.

1.4 Thesis organisation

After this introductory Chapter 1, our thesis aims to study the different dynamics of the fractional Duffing equation, which contains five chapters.

- Chapter 2 covers various aspects of the classical Duffing equation to allow the comparison with the results for the fractional model. It begins by introducing the general form of the equation itself and then presents different models described by this equation. Additionally, the chapter discusses numerical methods for solving the Duffing equation when analytical solutions are not possible. Overall, the chapter provides a comprehensive overview of the behaviours exhibited by the classical Duffing equation.
- Chapter 3 explores the fractional Duffing equation, its solution's periodicity and numerical simulation. It covers concepts of fractional calculus, especially the two approaches used to approximate the Caputo fractional derivative.
- Chapter 4 explores two tools to characterise chaos in the fractional Duffing equation. It presents the approximation of the Lyapunov Characteristic Exponents (LCEs), an extension of the Melnikov method to the fractional case, and an examination of limiting cases.
- Chapter 5 focuses on the theory of the main types of chaos intermittency. It explores intermittency in both the classical Duffing equation and the fractional Duffing equation. It provides a numerical analysis of intermittent behaviour in the fractional case for specific cases.

1.5 Published Manuscript

- Hamaizia, S., Jiménez, S. and Velasco, M.P. Rich phenomenology of the solutions in a fractional Duffing equation. Fract Calc Appl Anal (2024). https://doi.org/10.1007/s13540-024-00269-1

Chapter 2

Classical Duffing equation

The Duffing oscillator exemplifies a periodically driven system with nonlinear elasticity. It is a nonlinear differential equation that is used to illustrate diverse physical and engineering phenomena. In the field of nonlinear dynamics, the Duffing oscillator is represented by [133, 62, 58]:

$$My''(s) + Dy'(s) + \frac{dU(y(s))}{dy(s)} = F\cos(\Omega s + \Phi), \tag{2.1}$$

where the primes in (2.1) denote the derivative with respect to time s, y'' is, thus, the acceleration of the system, y' the velocity and y the displacement. The parameters M, D, F, Φ, Ω are real constants.

- According to Newton's second law, the term My'' represents the system's resistance to changes in motion caused by its mass M.
- The term Dy' represents the viscous damping force with D the viscous damping parameter (damping is an impact inside or upon an oscillatory framework that diminishes or forestals its oscillation).
- The term U represents the potential energy function with quadratic and quartic terms in a symmetric disposition:

$$U(y) = -\frac{A}{2}y^2 + \frac{B}{4}y^4. \tag{2.2}$$

- F represents the amplitude of the periodic driving force.
- Ω represents the angular frequency of the periodic driving force.
- Φ represents the phase angle.

Rescalling the equation (2.1)

To make the equation more concise and easier to work with we rescale the equation (2.1). First, we need to perform a few transformations. Let:

$$t = \alpha s,\ x(t) = \beta y(s),\ \alpha, \beta > 0, \tag{2.3}$$

be the new variables. Thus:

$$y = \frac{1}{\beta}x, \quad y' = \frac{\alpha}{\beta}\dot{x}, \quad y'' = \frac{\alpha^2}{\beta}\ddot{x}. \tag{2.4}$$

Substitute the new variables in (2.1), we find:

$$\frac{\alpha^2 M}{\beta}\ddot{x} + \frac{D\alpha}{\beta}\dot{x} - \frac{A}{\beta}x + \frac{B}{\beta^3}x^3 = F\cos\Big(\frac{\Omega}{\alpha}t + \Phi\Big), \tag{2.5}$$

to make the coefficient of $\ddot{x}$ equal to one, we multiply the entire equation by the coefficient $\frac{\beta}{\alpha^2 M}$, and we obtain:

$$\ddot{x} + \frac{D}{M\alpha}\dot{x} - \frac{A}{\alpha^2 M}x + \frac{B}{\beta^2\alpha^2 M}x^3 = \frac{F\beta}{\alpha^2 M}\cos\Big(\frac{\Omega}{\alpha}t + \Phi\Big), \tag{2.6}$$

Now, we rescale the coefficients and define:

$$\gamma = \frac{D}{M\alpha}, \tag{2.7}$$

$$a = \frac{A}{\alpha^2 M}, \tag{2.8}$$

$$b = \frac{B}{\beta^2\alpha^2 M}, \tag{2.9}$$

$$f_0 = \frac{F\beta}{\alpha^2 M}, \tag{2.10}$$

we rewrite the cosine function as:

$$\cos\Big(\frac{\Omega}{\alpha}t + \Phi\Big) = \cos\Big(\frac{\Omega}{\alpha}t - \frac{\Omega}{\alpha}\Big(-\frac{\alpha}{\Omega}\Phi\Big)\Big), \tag{2.11}$$

we put, $\omega = \Omega/\alpha, \quad t_0 = -(\alpha/-\Omega)\Phi$. Finally, substituting all the scaled coefficients:

$$\ddot{x} + \gamma\dot{x} - ax + bx^3 = f_0\cos(\omega(t - t_0)), \tag{2.12}$$

The term $-ax + bx^3$ represents the nonlinear stiffness force (stiffness is the degree to which an object resists deformation caused by an applied force), where a is the linear stiffness parameter and b is the non-linear cubic stiffness parameter. Depending on the signs on the two parameters a and b, different models can be presented by the Duffing equation. They are listed as follows:

- If $a < 0$ and $b > 0$: the equation (2.12) corresponds to Duffing oscillator with hardening stiffness where the hardening spring is represented by: $k = a - bx^2$. In Figure 2.1 we present the potential corresponding to this case.
- If $a < 0$ and $b < 0$: the spring is said to be soft, thus we have a Duffing oscillator with softening stiffness where the potential

  $$U(x) = -\frac{ax^2}{2} + \frac{bx^4}{4} = \frac{|a|}{2}x^2 - \frac{|b|}{4}x^4, \tag{2.13}$$

  corresponds to this case is described as softening Figure 2.2:

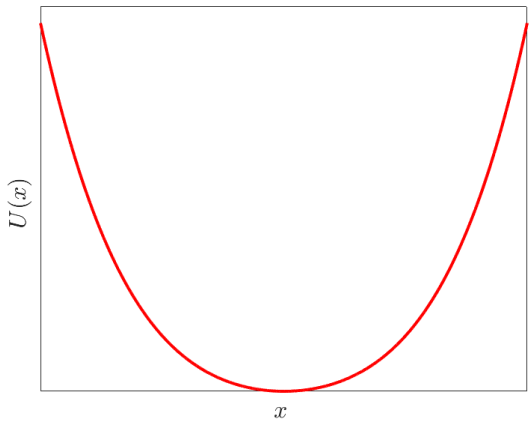


Figure 2.1: Potential of Duffing oscillator: $U(x) = -\frac{a}{2}x^2 + \frac{b}{4}b^4$, $a < 0$ and $b > 0$ with hardening stiffness $k = a - bx^2$ under random excitation.

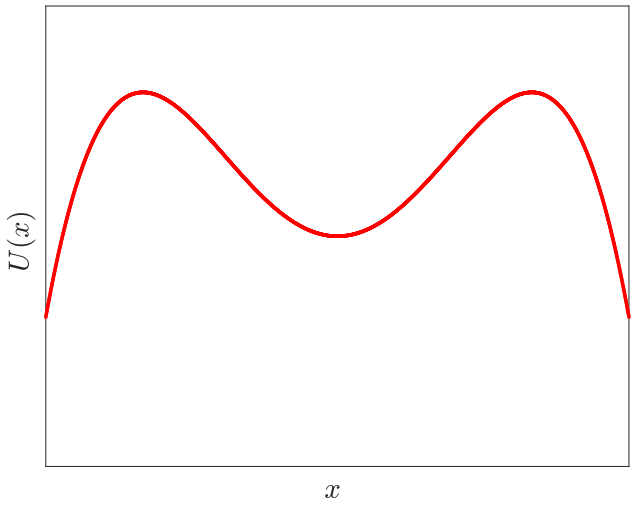


Figure 2.2: Potential well: $U(x) = -\frac{ax^2}{2} + \frac{bx^4}{4}$, $a < 0$ and $b < 0$.

- If $a > 0$ and $b = 0$ the Duffing equation describes a damped and driven simple harmonic oscillator.
- If $a > 0$ and $b > 0$: the equation (2.12) describes a double twin wells potential [84] that can be modelled by a ball rolling up and down the potential wells, with the ball slowly losing energy due to the friction that comes from the damping term as shown in Figure 2.3.

  This case also provides the simplest possible model for the forced vibrations of a cantilever beam in the non-uniform field of two permanent magnets [81].

  In Figure 2.4, the movement of the two magnets that comes from the oscillations of the cantilever beam, creates a time-varying magnetic field where displacement of this beam x is the variable of the system. The elastic force that resists deformation is represented by the linear stiffness term ax while the nonlinear term bx^3 accounts for the cubic

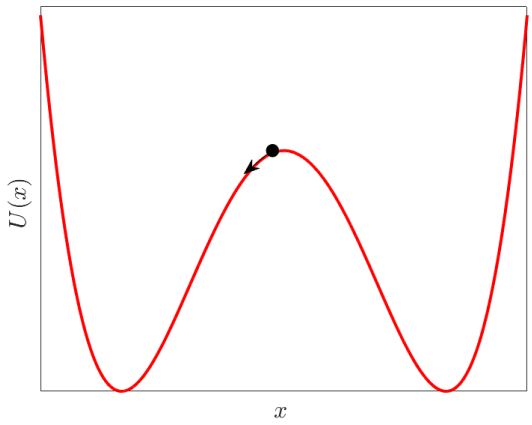


Figure 2.3: Modelling of double twin wells potential Duffing equation: $U(x) = -\frac{ax^2}{2} + \frac{bx^4}{4}$, $a > 0$ and $b > 0$.

relationship between displacement and force, introducing nonlinearity.

The cantilever beam responds to the forces exerted by the magnets and the external excitation force $f_0 \cos(\omega(t - t_0))$. This can lead to significant oscillations and show distinct behaviours in the beam's motion.

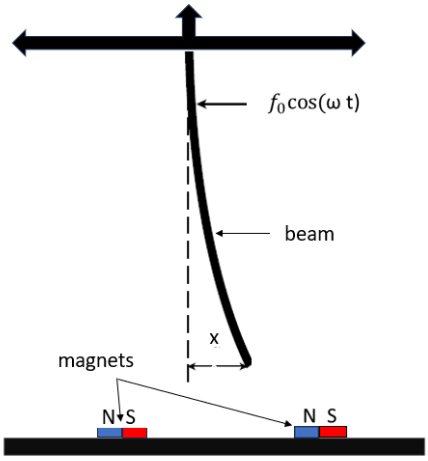


Figure 2.4: Cantilever beam in the nonuniform field of two permanent magnets.

Solving the Duffing equation describes how the mechanical oscillator responds to different forces and how its motion evolves over time.

Depending on the parameters $(a, b, \gamma, f_0, \omega)$ and the initial conditions, the oscillator can exhibit a wide range of behaviours, including periodic motion, resonance, chaotic behaviour, and more.

Setting $a = 1$, $b = 1$ simplifies the equation without loss of generality by choosing: $\alpha = \sqrt{\frac{A}{M}}$,

$\beta = \sqrt{\frac{B}{AM^2}}$. This makes it easier to analyse and understand the behaviour of the system and we may choose $t_0 = 0$, without loss of generality, also. The equation (2.12) becomes:

$$\ddot{x} + \gamma\dot{x} - x + x^3 = f_0 \cos(\omega t). \tag{2.14}$$

In this form, the parameters of the system are γ, f_0, ω. In all simulations of the Duffing model, both classical and fractional, we fix the driving frequency ω as 1.

2.1 Undamped unforced Duffing equation

When $\gamma = 0, f_0 = 0$, the problem can be studied analytically. The undamped unforced Duffing equation is given by:

$$\ddot{x} - x + x^3 = 0, \tag{2.15}$$

thus, the potential of the system, when no periodic force or damping is present, is:

$$U(x) = -\frac{x^2}{2} + \frac{x^4}{4}. \tag{2.16}$$

In this case, the potential exhibits a double-well structure characterised by two minima located at $x = +1$ and $x = -1$, along with a local maximum at the origin $x = 0$ as shown in Figure 2.5:

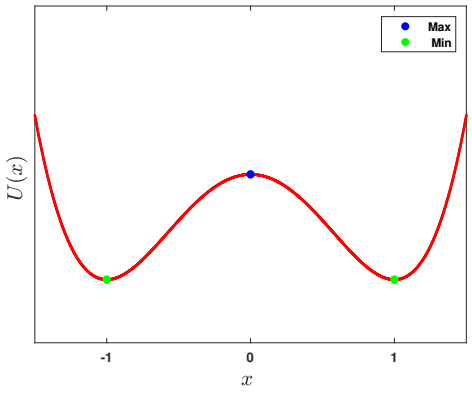


Figure 2.5: Potential function $U(x)$ given by (2.16).

This case was the first model of oscillation of the beam described by the Duffing equation, without external force and damping.

The equivalent first order system of (2.15) is:

$$\begin{cases} \dot{x} = y, \\ \dot{y} = x - x^3. \end{cases} \tag{2.17}$$

This system has three fixed points:

- $(x, y) = (0, 0)$ is a unstable fixed point.

- $(x, y) = (\pm 1, 0)$ are two stable fixed points (two centers).

The equation (2.15) is an integrable Hamiltonian system with the Hamiltonian function:

$$H(x, y) = \frac{1}{2}y^2 - \frac{1}{2}x^2 + \frac{1}{4}x^4 = E. \tag{2.18}$$

where the term $\frac{1}{2}y^2$ is the kinetic energy (mass has been scaled to be 1) and $U(x)$ (2.16) as potential energy, then (2.18) is the total energy E of the system. This energy remains constant along the solutions corresponding to the level curves (2.18). In this case, there are:

- a saddle at the origin $(0, 0)$,
- two centers at $(\pm 1, 0)$,
- two homoclinic orbits given by:

$$\begin{aligned} \Gamma_0^{\pm} : q_0^{\pm}(t) &= \pm\left(\sqrt{2}\text{sech}(t), -\sqrt{2}\text{sech}(t)\tanh(t)\right) \\ &= \pm\left(\frac{\sqrt{2}}{\cosh(t)}, -\sqrt{2}\frac{\sinh(t)}{\cosh^2(t)}\right). \end{aligned} \tag{2.19}$$

As shown in Figure 2.6 [133].

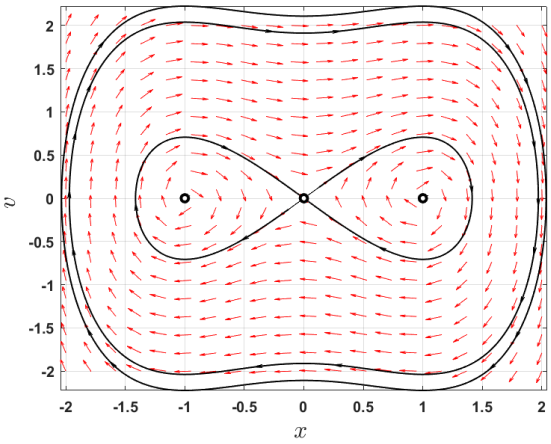


Figure 2.6: Orbits of the unforced Duffing oscillator.

2.2 Damped unforced Duffing equation

The damped unforced Duffing equation is described by the following equation:

$$\ddot{x} + \gamma\dot{x} - x + x^3 = 0. \tag{2.20}$$

Thus, the damped, unforced, Duffing system is:

$$\begin{cases} \dot{x} = y, \\ \dot{y} = x - x^3 - \gamma\dot{x}, \quad \gamma > 0. \end{cases} \tag{2.21}$$

The system (2.21) is no longer conservative and the energy function (2.18) in this case is not constant:

$$\frac{dH}{dt}(x,y) = -\gamma y^2 \leq 0. \tag{2.22}$$

The total energy is diminished as time increases and there are no closed orbits: all solutions tend to one of the three fixed points, either $(0,0)$ or one of the two well bottoms $(\pm 1, 0)$.

■ **Equilibrium points and its stability** : The fixed points remain the same as in the previous case. The Jacobi matrix of (2.21) is:

$$J = \begin{pmatrix} 0 & 1 \\ 1-3x^2 & -\gamma \end{pmatrix}. \tag{2.23}$$

The analysis of the eigenvalues of the Jacobi matrix (2.23) provides insight into the stability of its equilibria.

– The matrix associated to $(0,0)$ using (2.23) is:

$$J_{(0,0)} = \begin{pmatrix} 0 & 1 \\ 1 & -\gamma \end{pmatrix}. \tag{2.24}$$

Thus, the fixed point $(0,0)$ has two eigenvalues:

$$\begin{cases} \lambda_1 = -\frac{\gamma}{2} + \frac{\gamma}{2}\sqrt{1+\frac{4}{\gamma^2}}, \\ \lambda_2 = -\frac{\gamma}{2} - \frac{\gamma}{2}\sqrt{1+\frac{4}{\gamma^2}}. \end{cases} \tag{2.25}$$

Since $\sqrt{1+\frac{4}{\gamma^2}} > 1$, we have two eigenvalues (2.25) with different signs $\lambda_1 > 0$, $\lambda_2 < 0$ and hence the origin is a saddle equilibrium point.

– The matrix associated to $(\pm 1, 0)$ using (2.23) is:

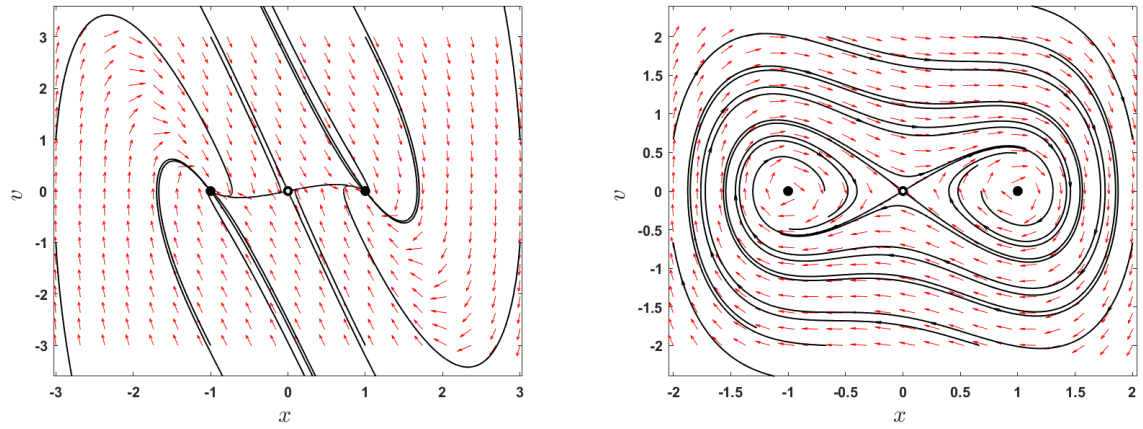
$$J_{(\pm 1,0)} = \begin{pmatrix} 0 & 1 \\ -2 & -\gamma \end{pmatrix}. \tag{2.26}$$

Thus, the two fixed points $(\pm 1, 0)$ have the same eigenvalues which are:

$$\lambda_{1,2} = -\frac{\gamma}{2} \pm \frac{\gamma}{2}\sqrt{1-\frac{8}{\gamma^2}}. \tag{2.27}$$

∗ If $\gamma^2 > 8$, the two equilibrium points $(\pm 1, 0)$ are stable nodes as shown in Figure 2.7(a).

∗ If $\gamma^2 < 8$, the two equilibrium points $(\pm 1, 0)$ are stable spiral points as shown in Figure 2.7(b) (stable foci).



(a) Stable nodes

(b) Stable spiral points

Figure 2.7: Vector field of undamped, unforced, Duffing equation.

2.3 Damped forced Duffing equation

The Duffing equation, when exposed to an external force $F = f_0 \cos(\omega t)$, exhibits nonlinear oscillations marked by chaotic regimes. The damped forced Duffing equation is:

$$\ddot{x} + \gamma\dot{x} - x + x^3 = f_0 \cos(\omega t). \tag{2.28}$$

The corresponding Cauchy problem with the initial conditions:

$$\begin{cases} x(0) = x_0, \\ \dot{x}(0) = v_0, \end{cases} \tag{2.29}$$

is well-posed and has a unique solution.

This equation is often used to model complex physical systems that present nonlinear behaviour and can exhibit interesting dynamics such as chaotic motion as a result of complex interactions between different components of the system. The damping tends to resist the motion of the system and leads to a gradual decrease in the amplitude of oscillations and the external force can influence the motion of the system by adding energy to it periodically.

Depending on the values of the amplitude f_0, the system shows various behaviours. To visualise them, we have represented the orbit in the xv-plane which we regard as our effective phase space. Additionally, we could construct a stroboscopic map that we have generated at the intervals of period $\frac{2\pi}{\omega}$ in time t, providing solutions at multiples of this period, corresponding to the external forcing's period. Using this map will make it much easier to analyse the behaviours of solutions.

For small amplitudes f_0, all trajectories converge towards one of the two fixed points $(\pm 1, 0)$, forming attracting orbits with a period $T = 2\pi/\omega$. In Figure 2.8, we present the phase space that converges towards $(+1, 0)$, for $f_0 = 0.001, \gamma = 0.25, x_0 = v_0 = 0$.

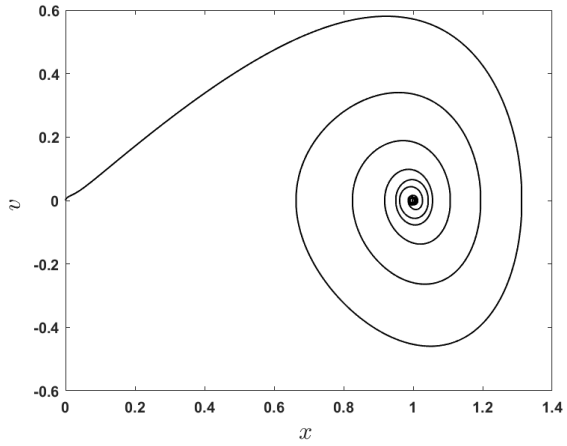


Figure 2.8: Trajectories attracted to the the fixed point $(1, 0)$ for small values of f_0: $f_0 = 0.001, \gamma = 0.25, x_0 = v_0 = 0$.

The Duffing equation presents a strange attractor for sufficiently large values of f_0. In Figure 2.9, we represent the strange attractor of the classical Duffing equation.

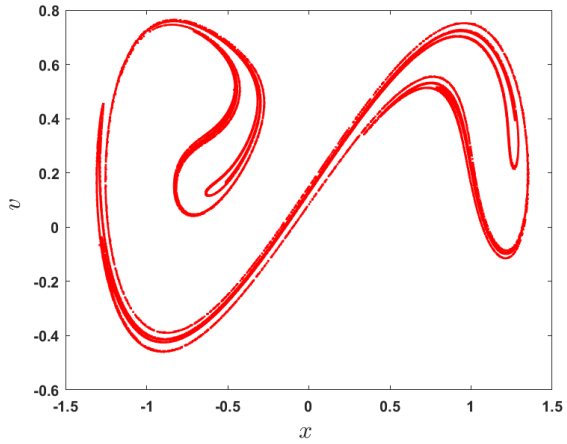


Figure 2.9: Strange attractor of classical Duffing equation for $f_0 = 0.3$.

2.4 Numerical solution of classical Duffing equation

Numerical methods offer a powerful approach to resolving complex dynamics. They allow researchers to simulate and analyse various phenomena such as bifurcations, periodic solutions, chaotic attractors, and sensitivity to initial conditions. The Duffing equation exhibits rich and complex dynamical behaviours. It is approximated using various numerical methods [46, 86, 82]. We list some of them to show this variety: Runge-Kutta of order 4 method [106], elliptic balance method [24], the Adomian decomposition method [139] and the differential transform method is explained in [122].

Straus Vázquez method (SV method) is a conservative, finite difference scheme. Initially, it was designed for solving nonlinear Klein–Gordon equations. This numerical method is second-order accurate in both space and time [119]. The ideas from the Strauss-Vázquez method have been expanded to be useful in different situations. In [50], Jiménez et al. described the numerical scheme used to simulate the following motion equation:

$$m\frac{d^2x}{dt^2} = -\frac{dU(x)}{dx}, \tag{2.30}$$

which conserve a discrete counterpart of the Hamiltonian:

$$H(x,y) = \frac{y^2}{2m} + U(x), \quad \text{with} \quad y = m\frac{dx}{dt} \quad and \quad \frac{dy}{dx} = -\frac{dU(x)}{dx}. \tag{2.31}$$

The numerical scheme of the motion equation using the SV method is:

$$m\frac{x_{n+1} - 2x_n + x_{n-1}}{\triangle t^2} = -\frac{U(x_{n+1}) - U(x_{n-1})}{x_{n+1} - x_{n-1}}. \tag{2.32}$$

This alternative numerical approach can approximate dissipative systems by treating them as conservative systems experiencing dissipation.

They approximate the motion equation (2.30) adding a dissipation term $g(x)\dot{x}$. Putting: $F(x) = -\frac{dU(x)}{dx}$ and $g(x) = \frac{dG}{dx}$, the numerical scheme in this case is:

$$m\frac{x_{n+1} - 2x_n + x_{n-1}}{\triangle t^2} = -\frac{U(x_{n+1}) - U(x_{n-1})}{x_{n+1} - x_{n-1}} + \frac{G(x_{n+1}) - G(x_{n-1})}{2\triangle t} \tag{2.33}$$

Jiménez et al. [49] applied this scheme (2.33) to approximate the classical Duffing equation (2.28).

Its variation law is given by:

$$\begin{aligned} \frac{dH(x,y)}{dt} &= \frac{d}{dt}\left(\frac{1}{2}y^2 + \frac{1}{2}x^2 + \frac{1}{4}x^4 - f_0 x\cos(\omega t)\right) \\ &= \dot{x}\left(\ddot{x} - x + x^3 - f_0\cos(\omega t)\right) + f_0\omega x\sin(\omega t) \\ &= \gamma\dot{x}^2 + f_0\omega x\sin(\omega t). \end{aligned} \tag{2.34}$$

Under all these considerations, the Strauss-Vázquez scheme that corresponds to (2.28) is the following:

$$m\left(\frac{x_{n+1} - 2x_n + x_{n-1}}{\triangle t^2}\right) + \gamma\frac{x_{n+1} - x_{n-1}}{2\triangle t} + \frac{U(x_{n+1}) - U(x_{n-1})}{x_{n+1} - x_{n-1}} = f_0\frac{\cos(\omega t_{n+1}) + \cos(\omega t_{n-1})}{2}, \tag{2.35}$$

where U is the potential (2.16) and $t_n = t_0 + n\triangle t$.

Comparing different methods, including the Gauss methods of orders 4 and 6, produced good results. This led to the conclusion that the SV method effectively describes the system's

behaviour. They presented limited periodic solutions and a strange attractor that shares similarities with the classical case [49].

The forced Duffing equation exhibits a different type of motion depending on its parameters. All parameters are held constant while varying only the amplitude f_0, that considered as our control parameter.

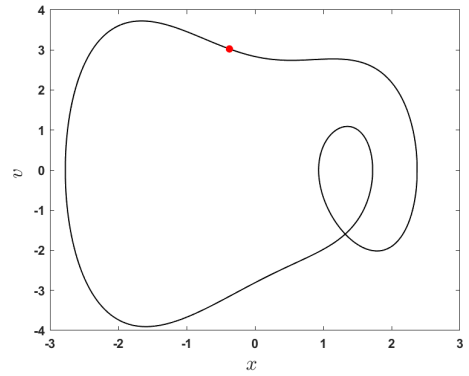
These behaviours include periodic motion with different periods T and chaotic motion. They are presented by looking at the phase space and the stroboscopic map. The period T is the frequency $2\pi/\omega$ of the external force. For a periodic orbit, the stroboscopic map is a single dot, when the period is doubled there is a double dot and the process goes on.

In Figure 2.10, we present several periodic attractors of period T, with different values of f_0, using the parameters $x_0 = 0.5$, $v_0 = 0.2$, $\gamma = 0.25$, and $\omega = 1$. The phase space is shown as a black curve, while the red dots represent the points on the stroboscopic map.

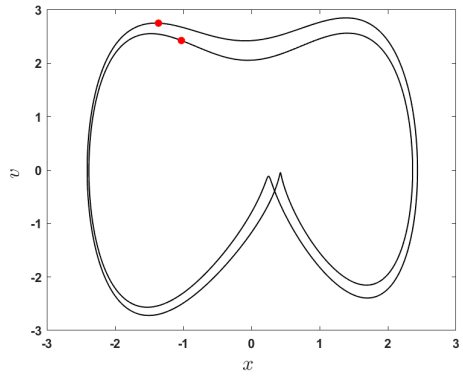
One of the defining features of chaos is the presence of strange attractors. In Figure 2.11, we present multiple stroboscopic maps of strange attractors achieved using varying f_0 values. The outcomes, whether periodic or chaotic, vary depending on the chosen parameter values [22, 52, 121]. Chaos manifests through the emergence of strange attractors as parameter values are varied where the destabilization of the periodic orbits gives rise to a tangled web of trajectories in phase space, the system transitions from ordered to chaotic behaviour and presents a strange attractor.

Identifying the critical parameter values at which chaos emerges is crucial for understanding the system's behaviour and predicting its long-term evolution. The Melnikov method is a good technique for determining the onset of chaos in the Duffing equation. The Melnikov method delineates the boundary between regular and chaotic regimes, indicating that chaos arises only when parameter values meet the condition [36, 39, 40]:

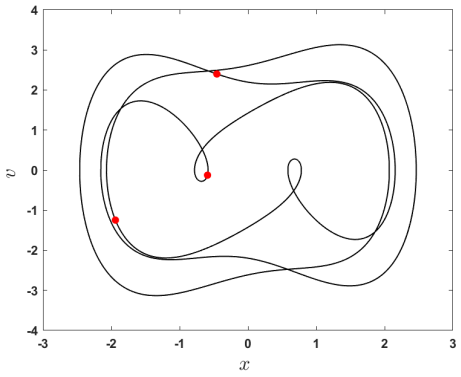
$$\frac{f_0}{\gamma} > \frac{4}{3}\frac{\cos(\pi\omega/2)}{\sqrt{2}\pi\omega}. \tag{2.36}$$



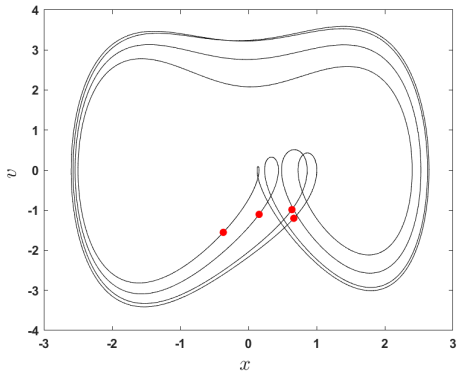
(a) Periodic attractor T for $f_0 = 3.46$



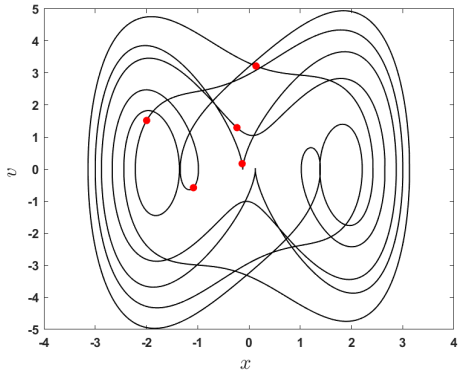
(b) Periodic attractor $2T$ for $f_0 = 2.7$



(c) Periodic attractor $3T$ for $f_0 = 1.87$

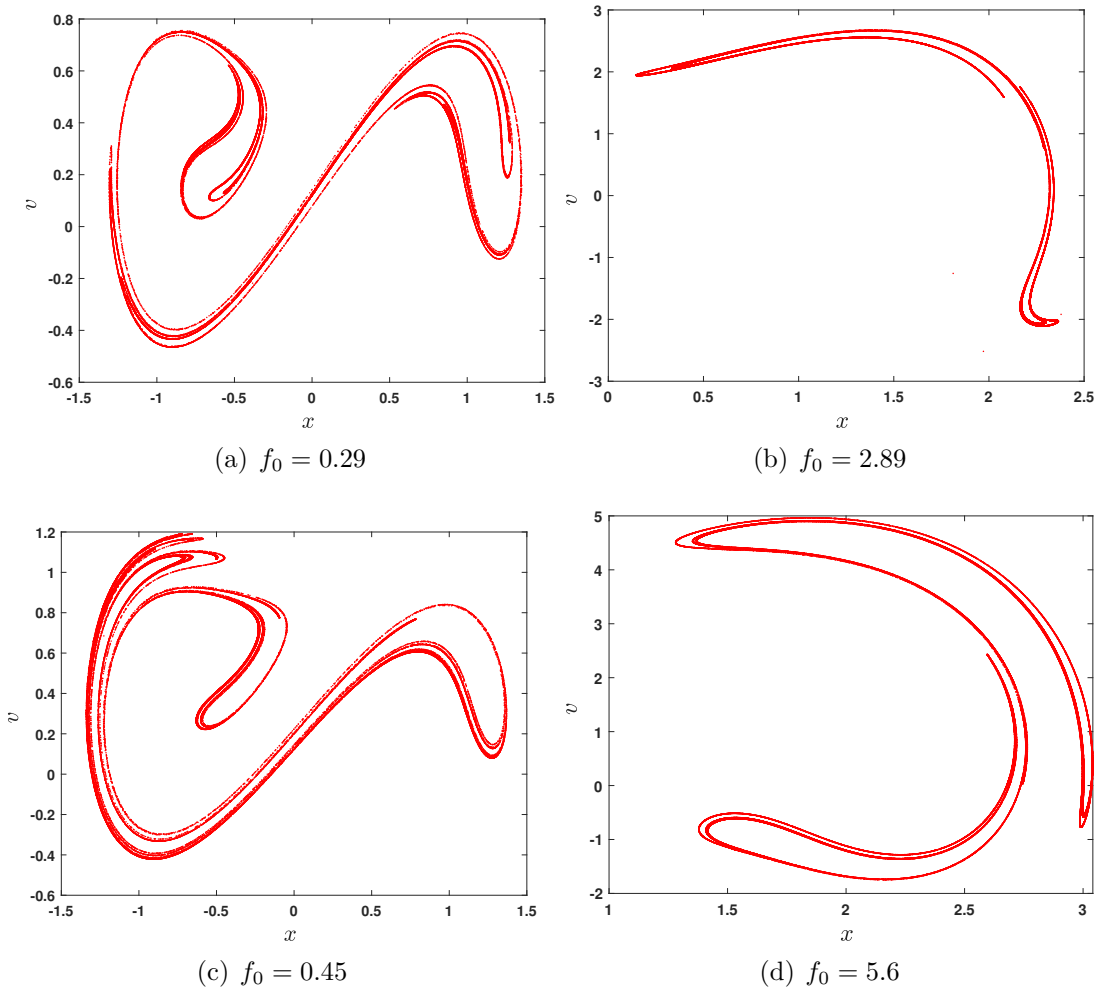


(d) Periodic attractor $4T$ for $f_0 = 3.25$



(e) Periodic attractor $5T$ for $f_0 = 5.66$

Figure 2.10: Orbits in phase space and stroboscopic map (red points) for different periodic attractors for $x_0 = 0.5.$, $v_0 = 0.2$



(a) $f_0 = 0.29$ (b) $f_0 = 2.89$

(c) $f_0 = 0.45$ (d) $f_0 = 5.6$

Figure 2.11: Strange attractors for different values of f_0.

Chapter 3

Fractional Duffing equation and its numerical simulation

3.1 Introduction

Fractional calculus introduces the idea of taking derivatives and integrals of non-integer orders, which adds a new level of complexity and generality to the study of functions and their properties. It can model complex behaviours that cannot be easily described by integer-order calculus. It has applications in various fields such as physics, engineering, biology, economics, and more. It has been demonstrated that modelling some physical systems using fractional calculus is more accurate than using integer calculus. This is because the behaviour of many physical phenomena depends on the previous time history. It emerges in the mathematical world as the study of integral and derivative operators of non-integer orders on domains of real or complex functions.

3.1.1 State of the art

Many researchers have studied variant forms of fractional Duffing equation, associated with either different fractional derivatives or different replacements of the integer order derivatives [43, 115, 9].

In the study of the chaos in this equation, various numerical methods have been used to approximate it [49, 30, 120]. For instance, the Adams–Bashforth–Moulton predictor-corrector method approximates the fractional derivative [120]. The fourth-order Runge–Kutta and tenth-order CFE-Euler methods are also employed to simulate the fractional order Duffing equation that exhibits various behaviours [9] also a combined numerical method based on two different approaches: the SV method and the Diethelm method which is presented in [49].

The fractional order has a significant impact on the behaviour of the system. Many authors conducted a parameter study of its influence in the range $[0, 1]$, revealing how it affects the transition from a regular solution to a chaotic one [120, 30, 71].

The other parameters also have a crucial role in the behaviour of the system, the damping

coefficient [13, 14] and the amplitude coefficient [30].

The different behaviours exhibited by the system can be identified through analysis of the solution using the phase space, stroboscopic map plots and the bifurcation diagram [9, 14].

The effect of using anharmonic external perturbations looking for geometrical resonances has been studied in [49].

Understanding the dynamics of the system involves characterizing chaos in the fractional Duffing equation. This can be achieved by observing the emergence of a strange attractor, which can be visualized through methods such as the stroboscopic map or phase space analysis.

The threshold of chaos is a key factor in determining when the fractional Duffing equation transitions into chaotic behaviour. It can be precised by studying the bifurcation diagrams which revealed critical thresholds for the onset of chaos [71] or using the Melnikov method [125, 85, 135].

Recent studies have explored the chaotic behaviour of the fractional Duffing equation, focusing on calculating the maximum Lyapunov exponent from time series data [135]. This measure offers valuable insights into the system's sensitivity to initial conditions and chaotic behaviour; however, it provides only a partial understanding of the system's dynamics.

Approximating all Lyapunov exponents (LCEs) using the Jacobi matrix can offer a comprehensive understanding of the system and provide a basis for comparing results obtained from time series analysis. Jiménez et al. [51] provided an approximation of all LCEs of the fractional Duffing equation in the range $\alpha \in (0, 1)$.

Our research introduces a similar approach to approximate all Lyapunov exponents of the system. We use a new numerical method (SV + Odibat method) to approximate the solution, which results in improved approximations. Moreover, we extend this study to include the range $\alpha \in (1, 2)$.

This comprehensive method offers a more complete characterization of the system's chaotic behaviour and sensitivity to initial conditions.

By extending the Melnikov method and combining it with some numerical techniques, we accurately estimate the onset of chaos in the range $\alpha \in (0, 2)$.

In the existing studies [135, 71], regular solutions in the fractional Duffing equation are often characterised as periodic; however, our analysis reveals this is not the case. Through our analysis, we demonstrate that periodic solutions do not exist in the fractional Duffing equation.

3.2 The Considered problem

In the first chapter, we introduced the Duffing equation, a classic representation of a chaotic system. This equation exhibits various behaviours depending on the specific parameter values it assumes. This mathematical model is a second-order nonlinear differential equation with dissipation and time-dependent forcing. It can be considered as an alternative view of a

perturbed Hamiltonian or Lagrangian system [36].

Duffing's equation can be extended into a fractional differential equation through various forms. This extension can be based either on the second-order differential equation or the system of two simultaneous first-order equations. In this process, it is possible to replace some or all of the standard derivatives with fractional derivatives.

Here we are concerned with the forced Duffing oscillator with fractional-order damping and negative linear stiffness which models the same physical device of the classical case but with a viscoelastic dissipation. It is given by:

$$\ddot{x} + \gamma({}_{t_0}D_t^{\alpha}x)(t) - x + x^3 = f_0\cos(\omega t). \tag{3.1}$$

One notable advantage of this equation is that it possesses a smooth solution, at the very least a C^2 continuous solution, which can be guaranteed to exist [56, 48, 51].

While various authors have already observed chaotic behaviour in fractional Duffing equations, our primary objective is to analyse and describe this behaviour using two different techniques. To achieve that, we approximate the Lyapunov exponents and extend the Melnikov method [36, 39] to the damped fractional Duffing equation (3.1) for specific values of the fractional order α.

This analysis relies on utilizing the approximate solution of the fractional equation, estimated by a new numerical method. Furthermore, we define the dimension of the phase space of the fractional equation and study the periodicity of its solutions. And, we aim to uncover phenomena in the solutions that have not been encountered in the models presented and studied before.

3.2.1 Phase space of fractional Duffing equation

In classical dynamical systems, the phase space is the set in which all possible states of the system are represented. Each point uniquely characterises the state: different states correspond to different points and each coordinate of the point represents a variable of the system. The dimension of the phase space corresponds to the number of parameters determining that state. If the system is sufficiently regular such that the initial value problem is well posed, each point in phase space corresponds to a unique solution starting there at the initial time.

It can also be viewed as the number of initial conditions necessary to determine uniquely the solution. The dimension also corresponds to the number of data necessary to prolong a solution after a given time.

In the classical Duffing equation (2.28), the vector of initial conditions (x_0, v_0) is a point in phase space xv that represents, then, the initial state. The solution $(x(t), v(t))$ represents the subsequent states and the set $\{(x(t), v(t))|t \in [t_0, t_1]\}$, is a trajectory between two given times t_0 and t_1. We may prolong a solution using the last state $(x(t_1), v(t_1))$ as an initial condition, which is, in fact, just an initial value problem but at a different time. Thus, different initial data can be compared and solutions starting at different times can be considered.

Let us consider the case of the fractional Duffing system. The expression of the Caputo derivative fixes the initial time. The initial conditions that ensure the existence and the unicity of the solution starting at that given time are just the same as in the classical case. But to prolong a solution $(x(t), v(t))$ after a given time $t_1 > t_0$, all intermediate values between t_0 and t_1 must be known:

$$(x(t), v(t)),\ \forall t \in [t_0, t_1]. \tag{3.2}$$

On the other hand, only two values are necessary to start the solution to (3.1) at time $t_0 = 0$. We may, thus, wonder whether the phase space is initially of finite dimension and becomes of infinite dimension afterwards.

To fix the idea, let us consider the following initial value problem:

$$\begin{cases} \ddot{x} + \gamma({}_{t_1}D_t^{\alpha})x(t) - x + x^3 = f_0\cos(\omega t), \\ x(t_1) = a\,, \quad \dot{x}(t_1) = b\,. \end{cases} \tag{3.3}$$

We perform the change of variables $t = s + t_1$ and $\tau = \sigma + t_1$ and applying them to the Caputo fractional derivative ${}_{t_1}D_t^{\alpha}x(t)$ with $\lceil\alpha\rceil = n$, $n \in \mathbb{N}$:

$$\begin{aligned} {}_{t_1}D_t^{\alpha}x(t) &= \frac{1}{\Gamma(n-\alpha)}\int_{t_1}^{t}\frac{\frac{\partial^n}{\partial\tau^n}x(\tau)}{(t-\tau)^{\alpha+1-n}}\,d\tau \\ &= \frac{1}{\Gamma(n-\alpha)}\int_{0}^{t-t_1}\frac{\frac{\partial^n}{\partial\sigma^n}x(\sigma+t_1)}{(t_1+s-\sigma-t_1)^{\alpha+1-n}}\,d\sigma, \\ &= \frac{1}{\Gamma(n-\alpha)}\int_{0}^{s}\frac{\frac{\partial^n}{\partial\sigma^n}x(\sigma+t_1)}{(s-\sigma)^{\alpha+1-n}}\,d\sigma, \\ &= {}_0D_t^{\alpha}x(s+t_1) = {}_0D_s^{\alpha}y(s), \end{aligned} \tag{3.4}$$

with $y(s) = x(s + t_1)$.

With this, we may rewrite (3.3) as:

$$\begin{cases} y'' + \gamma_0 D_s^{\alpha}y(s) - y + y^3 = f_0\cos(\omega s + \phi_0), \quad \phi_0 = \omega t_1\,, \\ y(0) = a\,, \quad y'(0) = b\,, \end{cases} \tag{3.5}$$

where the prime stands for derivation with respect to s. We see that we obtain the same system as (3.3) starting at $t_0 = 0$, and with an initial time-phase ϕ_0 (phase shift).

Even when we start the solution of the fractional equation at time t_1 different from the initial time t_0, we end with a fractional system started at time $t = 0$ but with a phase shift. Thus, we may consider that any solution that starts at a later time is, in fact, a solution that started at $t_0 = 0$ but with a phase ϕ_0 which is dependent on the starting time selected.

Hence, we can state any solution at $t_0 = 0$ by three parameters: x_0, v_0, ϕ_0. We conclude that our phase space has three dimensions corresponding to the number of parameters determining that state. Since the phase is constant, we can consider the phase space to have, effectively, two dimensions.

3.2.2 Periodicity of solution

In the classical Duffing equation, periodic solutions play a significant role in understanding the system's behaviour. However, the fractional Duffing equation differs in that it does not exhibit periodic solutions. This equation instead leads to unique dynamics, providing insights into the system's behaviour beyond the classical scenario.

Let us check the periodicity of the initial value problem (3.3), we suppose that (3.1) has a periodic solution with period $T = \frac{2\pi}{\omega}k$, $k \in \mathbb{Z}$:

$$\forall\, t \geq 0, \quad x(t) = x(t+T), \tag{3.6}$$

the assumption (3.6) is valid also for (3.3), $\forall\, t_1 > t \geq 0$, thus:

$$\begin{aligned} &\ddot{x}(t+T) + \gamma({}_{t_1}D_t^{\alpha})x(t+T) - x(t+T) + x^3(t+T) = f_0 \cos\Big(\omega(t+T)\Big) \qquad (3.7)\\ \iff \qquad &\ddot{x}(t) + \gamma({}_{t_1}D_t^{\alpha})x(t+T) - x(t) + x^3(t) = f_0 \cos(\omega t). \end{aligned}$$

If we assume (3.6), all the terms in (3.7) are periodic with the possible exception of the fractional derivative.

Let us suppose that it is periodic with period T:

$$\forall\, t \geq 0, \quad {}_{t_1}D_t^{\alpha}x(t) = {}_{t_1}D_t^{\alpha}x(t+T). \tag{3.8}$$

This gives:

$$I_1 = \int_{t_1}^{t} \frac{\frac{\partial^n}{\partial\tau^n}x(\tau)}{(t-\tau)^{\alpha+1-n}}\, d\tau = \int_{t_1}^{t+T} \frac{\frac{\partial^n}{\partial\tau^n}x(\tau)}{(t+T-\tau)^{\alpha+1-n}}\, d\tau, \quad n = \lceil\alpha\rceil. \tag{3.9}$$

Let us put $s = \tau - T$, we obtain:

$$I_1 = \int_{t_1}^{t+T} \frac{\frac{\partial^n}{\partial\tau^n}x(\tau)}{(t+T-\tau)^{\alpha+1-n}} d\tau \;=\; \int_{t_1-T}^{t} \frac{\frac{\partial^n}{\partial s^n}x(s+T)}{(t-s)^{\alpha+1-n}}\, ds. \tag{3.10}$$

We put, now, $\mu = s - t_1$ to find:

$$\begin{aligned} I_1 &= \int_{-T}^{t-t_1} \frac{\frac{\partial^n}{\partial\mu^n}x(\mu+t_1)}{(t-t_1-\mu)^{\alpha+1-n}}\, d\mu,\\ &= \int_{-T}^{0} \frac{\frac{\partial^n}{\partial\mu^n}x(\mu+t_1)}{(t-t_1-\mu)^{\alpha+1-n}}\, d\mu + \int_{0}^{t-t_1} \frac{\frac{\partial^n}{\partial\mu^n}x(\mu+t_1)}{(t-t_1-\mu)^{\alpha+1-n}}\, d\mu\\ &= I_2 + I_3. \end{aligned} \tag{3.11}$$

For I_3, let us put $\tau = \mu + t_1$:

$$I_3 = \int_0^{t-t_1} \frac{\frac{\partial^n}{\partial \mu^n} x(\mu + t_1)}{(t - t_1 - \mu)^{\alpha+1-n}} \, d\mu = \int_{t_1}^{t} \frac{\frac{\partial^n}{\partial l^n} x(\tau)}{(t-\tau)^{\alpha+1-n}} \, d\tau = I_1. \tag{3.12}$$

Thus, from (3.11) and (3.12), we obtain:

$$I_2 = \int_{-T}^{0} \frac{\frac{\partial^n}{\partial \mu^n} x(\mu + t_1)}{(t - t_1 - \mu)^{\alpha+1-n}} \, d\mu = 0. \tag{3.13}$$

From (3.4), we have $x(t_1 + \mu) = y(\mu)$, thus (3.13) becomes:

$$I_2 = \int_{-T}^{0} \frac{\frac{\partial^n}{\partial \mu^n} y(\mu)}{(t - \mu)^{\alpha+1-n}} \, d\mu, \tag{3.14}$$

and, since $s = \mu + T$, (3.14) becomes:

$$I_2 = \int_{0}^{T} \frac{\frac{\partial^n}{\partial s^n} y(s - T)}{(t - s + T)^{\alpha+1-n}} \, ds. \tag{3.15}$$

The assumption about the periodicity of x, also implies the periodicity of y. This gives:

$$I_2 = \int_{0}^{T} \frac{\frac{\partial^n}{\partial s^n} y(s - T)}{(t - s + T)^{\alpha+1-n}} \, ds = {}_0D_t^{\alpha} y(T) = 0. \tag{3.16}$$

Thus, using (1.62)

$$I_2 = 0 \iff y(T) = \sum_{j=0}^{n-1} \frac{b_j}{j!} (T)^j, \quad n = \lceil \alpha \rceil. \tag{3.17}$$

Such a polynomial can not be T-periodic ($y(T) = y(2T) = \cdots$) unless it is a constant. Consequently, there are no T-periodic solutions to the initial value problem (3.3).

3.3 Numerical methods for the fractional Duffing equation

To compute the solutions of the system, we have chosen two numerical methods that approximate differently the fractional derivative. A combined SV + Diethelm method and a combined SV + Odibat method. In both cases, an SV approach is used to represent the non-fractional terms, while the Caputo derivative is represented by either Diethelm (1.65) [17] or Odibat approximation (1.68) [87]. The two numerical methods are outlined below, and

a comprehensive explanation, step-by-step, of the way to obtain its scheme with a detailed description of each method's implementation.

Let us express the equation (3.1) in a slightly more general form:

$$\ddot{x} + \gamma D_t^\alpha x(t) - x + x^3 = f_0 \cos(\omega t),\ \alpha \in (0,1) \cup (1,2) \tag{3.18}$$

where we used now the simplified notation, $D_t^\alpha x(t)$, instead of $({}_{t_0}D_t^\alpha x)(t)$.

The problem of the existence and unicity of the solution of (3.18) has been considered in [56], as we mentioned before, therefore, we assume that the equation (3.18) with initial conditions:

$$x(t_0) = x_0, \quad \dot{x}(t_0) = v_0, \quad t_0 = 0, \tag{3.19}$$

has a unique solution for any problem where the two initial conditions are known [51].

3.3.1 SV + Diethelm method for $\lceil\alpha\rceil = 1$ and $\lceil\alpha\rceil = 2$

For $\lceil\alpha\rceil = 1$

In the case $\lceil\alpha\rceil = 1$ we have used the same method as in [51]. It is limited to values of $\alpha \in (0,1)$ and has a truncation error $\mathcal{O}(\triangle t^{2-\alpha})$. We consider a discrete time-mesh of step-size $\triangle t$, with $t_n = t_0 + n\triangle t$, and represent by x_n the numerical approximation to the solution x at time t_n. Diethelm's representation of the Caputo fractional derivative is given by [17]:

$$D_t^\alpha x(t_n) = \frac{1}{\triangle t^\alpha \Gamma(2-\alpha)} \sum_{k=0}^{n} c_{k,n} \left(x_{n-k} - x_0\right) + \mathcal{O}(\triangle t^{2-\alpha}), \tag{3.20}$$

where the coefficients $c_{k,n}$ are (1.67).

Since the term for $k = n$ in the sum is zero, we obtain:

$$D_t^\alpha x = \frac{1}{h^\alpha \Gamma(2-\alpha)} \left(x_n - x_0 + \sum_{k=1}^{n-1} c_{k,n} \left(x_{n-k} - x_0\right) \right). \tag{3.21}$$

The discrete scheme of (3.18) using (3.21) and (2.35) is:

$$\begin{aligned} \frac{x_{n+1} - 2x_n + x_{n-1}}{\triangle t^2} &+ \frac{\gamma}{\triangle t^\alpha \Gamma(2-\alpha)} \left(x_n - x_0 + \sum_{k=1}^{n-1} c_{k,n} \Big(x_{n-k} - x_0\Big) \right) \\ &- \frac{x_{n+1} + x_{n-1}}{2} + \frac{x_{n+1}^3 + x_{n+1}^2 x_{n-1} + x_{n+1} x_{n-1}^2 + x_{n-1}^3}{4} \\ &= f_0 \frac{\cos(\omega t_{n+1}) + \cos(\omega t_{n-1})}{2}. \end{aligned} \tag{3.22}$$

This procedure is not self-starting since we must, initially, know both x_0 and x_1. The initial value x_0 is directly obtained from the initial data (3.19). The other is computed, for instance, using a Taylor expansion of $x(t)$ around t_0, particularized at $t = t_1 = \triangle t$, with truncation error $\mathcal{O}(\triangle t^4)$:

$$x(t_1) = x_1 = x_0 + \triangle t v_0 + \frac{\triangle t^2}{2!} \ddot{x}_0 + \frac{\triangle t^3}{3!} \dddot{x}_0. \tag{3.23}$$

To determine $\dddot{x}_0$ we may assume that the initial data satisfy the equation. Differentiating equation (3.18) at time zero we obtain:

$$\begin{cases} \dot{x}_0 = v_0, \\ \ddot{x}_0 = x_0 - x_0^3 + f_0, \\ \dddot{x}_0 = v_0 - 3x_0^2 v_0. \end{cases} \tag{3.24}$$

The regularity in $x(t)$ that supposes the existence of $\ddot{x}_0$, implies also that all the fractional derivatives involved are zero at $t = 0$ (see [56]). In any case, we can consider x_1 exact up to $\mathcal{O}(\triangle t^3)$: using (3.23) is, at any rate, a possible choice since we are not trying to solve for specific values of the initial data.

We define the value of the velocity at time-step $n > 0$, using a discrete representation of the second-order derivative given by:

$$v_n = \frac{x_{n+1} - x_{n-1}}{2\triangle t}, \tag{3.25}$$

which has an $\mathcal{O}(\triangle^2)$ error. The details of this can be found in [49].

For $\lceil \alpha \rceil = 2$

Diethelm's approximation (3.21) is limited to the case $\lceil \alpha \rceil = 1$. We may extend it to the case $\lceil \alpha \rceil = 2$ transforming Eq.(3.18) into a system such that all fractional derivatives involved have orders that fall within the specified range $(0, 1)$. We use the property of the Caputo derivative (1.57) and introduce $v = D^1 x$, $D^{\alpha-1} v = z$, such that we have:

$$\begin{cases} D^1 x = v, \\ D^{\alpha-1} v = z, \\ D^1 v = -\gamma z + x - x^3 + f_0 \cos(\omega t). \end{cases} \tag{3.26}$$

We obtain the following fractional equation:

$$\ddot{x} + \gamma D_t^{\beta} v(t) - x + x^3 = f_0 \cos(\omega t), \quad \beta = \alpha - 1, \tag{3.27}$$

with initial values

$$x(0) = x_0, \quad v(0) = v_0. \tag{3.28}$$

Now, $\beta \in (0, 1)$, and we may apply the previous approach, with the benefit that the coefficients are the same as before.

The numerical scheme that corresponds to (3.27) is:

$$\begin{aligned} \frac{x_{n+1} - 2x_n + x_{n-1}}{\triangle t^2} = &- \frac{\gamma}{\triangle t^{\beta} \Gamma(2-\beta)} \left(v_n - x_0 + \sum_{k=1}^{n-1} c_{k,n} \Big(v_{n-k} - v_0 \Big) \right) \\ &+ \frac{x_{n+1} + x_{n-1}}{2} - \frac{x_{n+1}^3 + x_{n+1}^2 x_{n-1} + x_{n+1} x_{n-1}^2 + x_{n-1}^3}{4} \\ &+ f_0 \frac{\cos(\omega t_{n+1}) + \cos(\omega t_{n-1})}{2}. \end{aligned} \tag{3.29}$$

The discretization of the first equation in (3.26) is quite relevant and may give rise to an unstable method. For instance:

$$\frac{x_{n+1} - x_{n-1}}{2\triangle t} = \frac{v_{n+1} + v_{n-1}}{2}, \tag{3.30}$$

has a behaviour similar to that of the leap-frog method for partial differential equations and shows a splitting of the solution among alternating values that is unstable. A stable representation is obtained using the backwards finite difference of order 2:

$$v_n = \frac{3x_n - 4x_{n-1} + x_{n-2}}{2\triangle t}, \tag{3.31}$$

which has a local truncation error $\mathcal{O}(\triangle t^2)$.

To start the method we need now, besides x_0 and v_0, both x_1 and v_1. For the first one we use (3.23) and (3.24), as before, for the latter one we use a similar construction:

$$v_1 = v_0 + \triangle \dot{v}_0 + \frac{\triangle t^2}{2!}\ddot{v}_0 + \frac{\triangle t^3}{3!}\dddot{v}_0. \tag{3.32}$$

We obtain $\ddot{v}_0$ and $\dddot{v}_0$ differentiating the second equation of system (3.26) at time zero, assuming once again that it satisfies the equation:

$$\begin{cases} \dot{v}_0 = x_0 - x_0^3 + f_0, \\ \ddot{v}_0 = v_0 - 3x_0^2 v_0, \\ \dddot{v}_0 = (1 - 3x_0^2)\dot{v}_0 - 6x_0 v_0^2 - \omega^2 f_0. \end{cases} \tag{3.33}$$

3.3.2 SV + Odibat method for $\lceil \alpha \rceil = 1$ and $\lceil \alpha \rceil = 2$

Equations involving fractional derivatives introduce computational challenges due to their non-local nature. It is therefore recommended to explore and use different numerical methods and compare their results for consistency. In our case, the previous SV + Diethelm method and a new method (SV + Odibat). These two distinct numerical methods are employed to assess the overall consistency of the simulations for this problem.

In the previous section, we introduced a numerical method for solving the fractional Duffing equation. Now in this section, we introduce a new numerical approach to approximate the solution of this equation. It is based on approximating the Caputo fractional derivative using the Odibat method, resulting in a lower truncation error order, $\mathcal{O}(\triangle t^2)$ instead of $\mathcal{O}(\triangle t^{2-\alpha})$ of Diethelm's method.

The primary idea behind this second method is to approximate the fractional derivative term of the Duffing equation with the Odibat algorithm given by (1.68), where $m - 1 < \alpha \leq m$, $\lceil \alpha \rceil = m$, [87].

Now, we transform the continuous variables into a discrete representation. We take the discrete representation of the fractional derivative at a given discrete time value t_k. Starting

from initial time $t_0 = 0$. It is given by:

$$\begin{aligned}(D_t^\alpha x)(t_k) &= \frac{\triangle t^{m-\alpha}}{\Gamma(m+2-\alpha)}\Big[\Big((k-1)^{m-\alpha+1} - (k-m+\alpha-1)k^{m-\alpha}\Big)x^{(m)}(0) \\ &+ \sum_{j=1}^{k-1}\Big((k-j+1)^{m-\alpha+1} - 2(k-j)^{m-\alpha+1} + (k-j-1)^{m-\alpha+1}\Big)x^{(m)}(t_j) \\ &+ x^{(m)}(t_k)\Big]; \quad m = \lceil\alpha\rceil \in \mathbb{N}, \end{aligned} \tag{3.34}$$

where $x^{(m)}$ represents the derivative of x of (integer) order m. The local truncation error is of the order $\mathcal{O}(\triangle t^2)$ [87], where $\triangle t$ represents the discrete mesh size.

We simplify the notation by defining the following coefficients:

$$\begin{cases} C_{k,0}(\alpha,m) = (k-1)^{m-\alpha+1} - (k-m+\alpha-1)k^{m-\alpha}, \\ C_{k,j}(\alpha,m) = (k-j+1)^{m-\alpha+1} - 2(k-j)^{m-\alpha+1} + (k-j-1)^{m-\alpha+1}, j = 1,...,k-1, \\ C_{k,k}(\alpha,m) = 1. \end{cases} \tag{3.35}$$

This last coefficient needs not to be defined but in this way, it is easier to compare the method with the standard representation than one may find, for instance, in [3]. Besides, since m depends on α, it would not be necessary to explicit the dependence of the coefficients on it but we maintain it here for the sake of clarity.

We have to keep in mind that $j \leq k-1$ because, otherwise, the coefficients become singular. As a curiosity:

$$C_{1,0}(\alpha,m) = m - \alpha.$$

Compared to the Diethelm method, the coefficients depend now on $k-j$ instead of just k.

To avoid using the derivatives of x, Odibat substitutes them by finite difference formulas, obtaining:

$$\begin{aligned}(D^\alpha x)(t_k) &= \frac{\triangle t^{-\alpha}}{\Gamma(m+2-\alpha)}\Big[C_{k,0}(\alpha,m)\,\triangle_m(0) + \sum_{j=1}^{k-1} C_{k,j}(\alpha,m)\,\triangle_m(t_j) \\ &+ \triangle_m(t_k)\Big]; \quad m = \lceil\alpha\rceil \in \mathbb{N}, \end{aligned} \tag{3.36}$$

The $\triangle_m$ functions are those approximations to the derivatives by finite differences (except for the power of $\triangle t$ in the denominator) and correspond to:

$$\triangle_1(t) = \frac{x(t+\triangle t) - x(t-\triangle t)}{2}, \tag{3.37}$$

$$\triangle_2(t) = x(t+\triangle t) - 2x(t) + x(t-\triangle t), \tag{3.38}$$

in general, for $m = 2n, \quad n \in \mathbb{N}$:

$$\triangle_{2n}(t) = \sum_{l=0}^{2n}(-1)^l \frac{(2n)!}{l!(2n-l)!}x\Big(t + (n-l)\triangle t\Big), \tag{3.39}$$

and, for $m = 2n+1, \quad n \in \mathbb{N}$:

$$\triangle_{2n+1}(t) = \sum_{l=0}^{2n+1} (-1)^l \frac{(2n+1)!}{l!(2n+1-l)!} \frac{1}{2}\Big[x\Big(t+(n-l)\triangle t\Big) + x\Big(t+(n+1-l)\triangle t\Big)\Big]. \quad (3.40)$$

Nevertheless, this approximation is not necessarily interesting in all the cases:

1. At $t = 0$ this necessitates the use of values on the left side of zero, that are not known or are not defined. On the other hand, $x^{(m)}(0)$ is known, in principle, since it is provided by the initial data in the case $m = 1$ and its value can be determined in the case $m = 2$ from (3.18), if we accept that the initial data satisfies the equation.
2. For the intermediate values (for $m = 1$ as well as for $m = 2$), it is indeed convenient to replace the derivative by its finite difference approximation since its value is not known.

For $\lceil \alpha \rceil = 1$

To implement this method, we represent the fractional derivative in (3.18) by the approximation of Odibat at time t_n and the SV approach for the rest of the terms, the discrete equation is:

$$\begin{aligned} \frac{x_{n+1} - 2x_n + x_{n-1}}{\triangle t^2} &+ \gamma(D_t^\alpha x_n) - \frac{x_{n+1} + x_{n-1}}{2} + \frac{x_{n+1}^3 + x_{n+1}^2 x_{n-1} + x_{n+1} x_{n-1}^2 + x_{n-1}^3}{4} \\ &= f_0 \frac{\cos(\omega t_{n+1}) + \cos(\omega t_{n-1})}{2}. \end{aligned} \quad (3.41)$$

The Odibat approximation of Caputo fractional derivative $D_t^\alpha x_n$ for the discrete case is given by:

$$\begin{aligned} D_t^\alpha x_n = \frac{\triangle t^{1-\alpha}}{\Gamma(3-\alpha)} & \frac{x_{n+1} - x_{n-1}}{2\triangle t} \\ & + \frac{\triangle t^{1-\alpha}}{\Gamma(3-\alpha)} \left(C_{n,0}(\alpha,1)\dot{x}_0 + \sum_{j=1}^{n-1} C_{n,j}(\alpha,1) \frac{x_{j+1} - x_{j-1}}{2\triangle t} \right). \end{aligned} \quad (3.42)$$

We substitute (3.42) in (3.41) to find:

$$\begin{aligned} & \frac{x_{n+1} - 2x_n + x_{n-1}}{\triangle t^2} - \frac{x_{n+1} + x_{n-1}}{2} \\ & \quad + \frac{\gamma \triangle t^{1-\alpha}}{\Gamma(3-\alpha)} \left(C_{n,0}(\alpha,1)\dot{x}_0 + \sum_{j=1}^{n-1} C_{n,j}(\alpha,1) \frac{x_{j+1} - x_{j-1}}{2\triangle t} + \frac{x_{n+1} - x_{n-1}}{2\triangle t} \right) \\ & \quad + \frac{x_{n+1}^3 + x_{n+1}^2 x_{n-1} + x_{n+1} x_{n-1}^2 + x_{n-1}^3}{4} = f_0 \frac{\cos(\omega t_{n+1}) + \cos(\omega t_{n-1})}{2}, \end{aligned} \quad (3.43)$$

with coefficients $C_{n,j}(\alpha, 1)$:

$$\begin{cases} C_{n,0}(\alpha,1) = (n-1)^{2-\alpha} - (n-2+\alpha)n^{1-\alpha}, \\ C_{n,j}(\alpha,1) = (n-j)^{2-\alpha} \left[\left(1 - \frac{1}{n-j}\right)^{2-\alpha} - 2 + \left(1 - \frac{1}{n-j}\right)^{2-\alpha} \right], \\ j = 1, \ldots, n-1. \end{cases} \quad (3.44)$$

To facilitate algorithm construction, we slightly modify and simplify this expression for implementation in computer programs, such as MATLAB.

We write all in the same hand side, multiply by $\triangle t^2$ and collect the terms in x_{n+1} as in the following formula:

$$\begin{aligned}\left[1+\frac{\gamma\triangle t^{2-\alpha}}{2\Gamma(3-\alpha)}-\frac{\triangle t^2}{2}\right]x_{n+1} &+ \frac{\triangle t^2}{4}\left(x_{n+1}^3+x_{n+1}^2x_{n-1}+x_{n+1}x_{n-1}^2\right)\\ &- 2x_n+\left[1-\frac{\gamma\triangle t^{2-\alpha}}{2\Gamma(3-\alpha)}-\frac{\triangle t^2}{2}\right]x_{n-1}+\frac{h^2}{4}x_{n-1}^3\\ &+ \frac{\gamma\triangle t^{3-\alpha}}{\Gamma(3-\alpha)}\left[C_{n,0}(\alpha,1)\dot{x_0}+\sum_{j=1}^{n-1}C_{n,j}(\alpha,1)\frac{x_{j+1}-x_{j-1}}{2\triangle t}\right]\\ &- \frac{\triangle t^2 f_0}{2}\Big(\cos(\omega t_{n+1})+\cos(\omega t_{n-1})\Big)=0, \end{aligned} \tag{3.45}$$

With all these considerations, we can implement the method and run the simulation.

For $\lceil\alpha\rceil = 2$

In this section, we will present the numerical scheme of the SV + Odibat method for $1<\alpha<2$. The Caputo fractional derivative $(D_t^\alpha x)_n$ is approximated at time t_n by:

$$\begin{aligned}D_t^\alpha x_n = &\frac{\triangle t^{2-\alpha}}{\Gamma(4-\alpha)}\frac{x_{n+1}-2x_n+x_{n-1}}{\triangle t^2}\\ &+\frac{\triangle t^{2-\alpha}}{\Gamma(4-\alpha)}\left(C_{n,0}(\alpha,2)\ddot{x}_0+\sum_{j=1}^{n-1}C_{n,j}(\alpha,2)\frac{x_{j+1}-2x_j+x_{j-1}}{\triangle t^2}\right).\end{aligned} \tag{3.46}$$

We substitute (3.46) in (3.41) to find:

$$\begin{aligned}&\frac{x_{n+1}-2x_n+x_{n-1}}{\triangle t^2}-\frac{x_{n+1}+x_{n-1}}{2}+\frac{\gamma\triangle t^{2-\alpha}}{\Gamma(4-\alpha)}\frac{x_{n+1}-2x_n+x_{n-1}}{\triangle t^2}\\ &\quad+\frac{\gamma\triangle t^{2-\alpha}}{\Gamma(4-\alpha)}\left(C_{n,0}(\alpha,2)\ddot{x}_0+\sum_{j=1}^{n-1}C_{n,j}(\alpha,2)\frac{x_{j+1}-2x_j+x_{j-1}}{\triangle t^2}\right)\\ &\quad+\frac{x_{n+1}^3+x_{n+1}^2x_{n-1}+x_{n+1}x_{n-1}^2+x_{n-1}^3}{4}=f_0\frac{\cos(\omega t_{n+1})+\cos(\omega t_{n-1})}{2}.\end{aligned} \tag{3.47}$$

The coefficients correspond in this case to:

$$\begin{cases} C_{n,0}(\alpha,2)=(n-1)^{3-\alpha}-(n-3+\alpha)n^{2-\alpha}\\ C_{n,j}(\alpha,2)=(n-j)^{3-\alpha}\Big[\Big(1-\frac{1}{n-j}\Big)^{3-\alpha}-2+\Big(1-\frac{1}{n-j}\Big)^{3-\alpha}\Big],\\ j=1,\dots,n-1. \end{cases} \tag{3.48}$$

As in the previous case, we need to determine x_1 using the Taylor expansion given by (3.23). We are going to simplify the numerical scheme (3.46) to make it easier to implement in the computer program. Like before, we will multiply by $\triangle t^2$ and organize the terms accordingly. This yields:

$$\left[1+\frac{\gamma\triangle t^{2-\alpha}}{\Gamma(4-\alpha)}-\frac{\triangle t^2}{2}\right]x_{n+1}+\frac{\triangle t^2}{4}\left(x_{n+1}^3+x_{n+1}^2x_{n-1}+x_{n+1}x_{n-1}^2\right)$$
$$-2\left[1+\frac{\gamma\triangle t^{2-\alpha}}{\Gamma(4-\alpha)}\right]x_n+\left[1+\frac{\gamma\triangle t^{2-\alpha}}{\Gamma(4-\alpha)}-\frac{\triangle t^2}{2}\right]x_{n-1}+\frac{\triangle t^2}{4}x_{n-1}^3$$
$$+\frac{\gamma\triangle t^{4-\alpha}}{\Gamma(4-\alpha)}\left[C_{n,0}(\alpha,2)(x_0-x_0^3+f_0)+\sum_{j=1}^{n-1}C_{n,j}(\alpha,2)\frac{x_{j+1}-2x_j+x_{j-1}}{\triangle t^2}\right]$$
$$-\frac{\triangle t^2 f_0}{2}\Big(\cos(\omega t_{n+1})+\cos(\omega t_{n-1})\Big)=0. \quad (3.49)$$

Even though they share similarities, equations (3.45) and (3.49) have enough differences to require separate implementations in two different programs.

3.4 Numerical results

We have solved numerically the fractional equations in the range $(0<\alpha<1)$ and $(1<\alpha<2)$ using both methods presented in Section 3.3.

3.4.1 Phenomenology of solutions

As mentioned before, the xv-plane is our effective phase space. We will visualize our results there.

The orbits acquired are portrayed within this plane. In addition, we use the stroboscopic map of period $T=2\pi/w$ in time, which gives the solution at time multiples of that period.

In some cases, we present only the x component of the solution and the restricted stroboscopic map corresponding to that. We present either the solutions or their stroboscopic maps in a (false) 3D-projection.

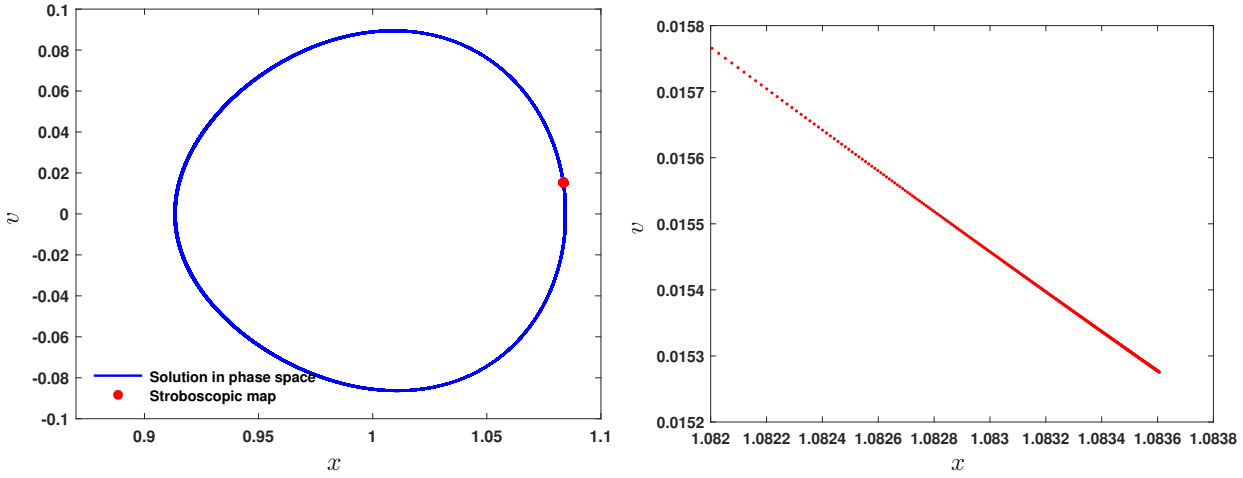
The numerical simulations are intended to investigate the effect of the amplitude f_0 and the order of the fractional derivative α, with the frequency ω and the damping coefficient γ taking constant values, $\omega=1, \gamma=0.25$, and compare it with some classical cases.

The system is very rich, it can exhibit very different behaviours. To showcase the most important of them in our study, we have considered different values for f_0 and α to present these distinct solutions. We enumerate in what follows the main features.

★ **Regular solutions**

There are regular solutions where the orbits in the phase plane appear to tend rapidly to a closed curve. When the stroboscopic map is plotted, we see that the points tend to a fixed point (period T) or a discrete set of a few fixed points (higher periodicity with multiples of T). Although the fractional equation cannot have periodic solutions, as we have demonstrated above, regular solutions tend to have a closed curve.

This is a very important point that differentiates between fractional-order and integer-order derivatives. In the classical case, the attracting periodic curve is a solution. But in this case, the attractor in the regular case appears to be a periodic curve which is not a solution. We show in Figure 3.1 a regular solution that tends towards a T-periodic curve, with the points in the stroboscopic map tending towards a unique fixed point in the phase plane xv.

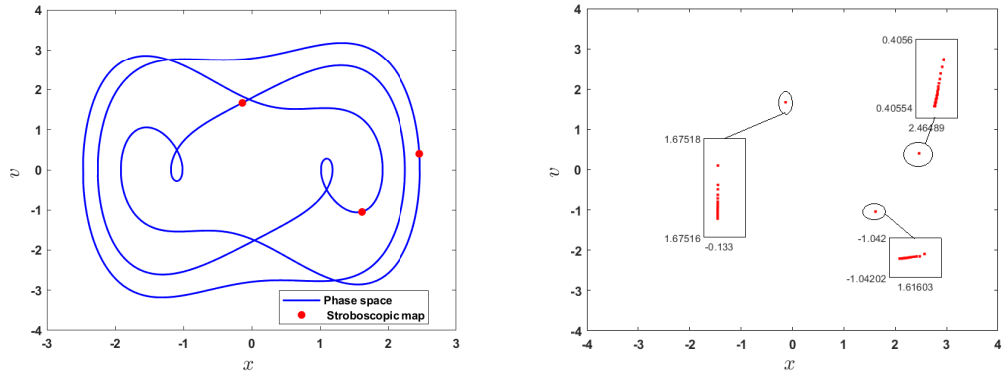


(a) Representation in phase space of solution that tends towards a periodic limit case

(b) Stroboscopic map as a sequence of points that tends to be a single one as time extends

Figure 3.1: Phase space and stroboscopic map for a regular solution that tends towards a T-periodic curve with $\alpha = 0.5$, $f_0 = 0.1$, $x_0 = v_0 = 0$.

In Figure 3.2, we present a regular solution that tends towards a $3T$-periodic curve. We see clearly how the three sets of points in the stroboscopic map tend to have three fixed points as time increases.



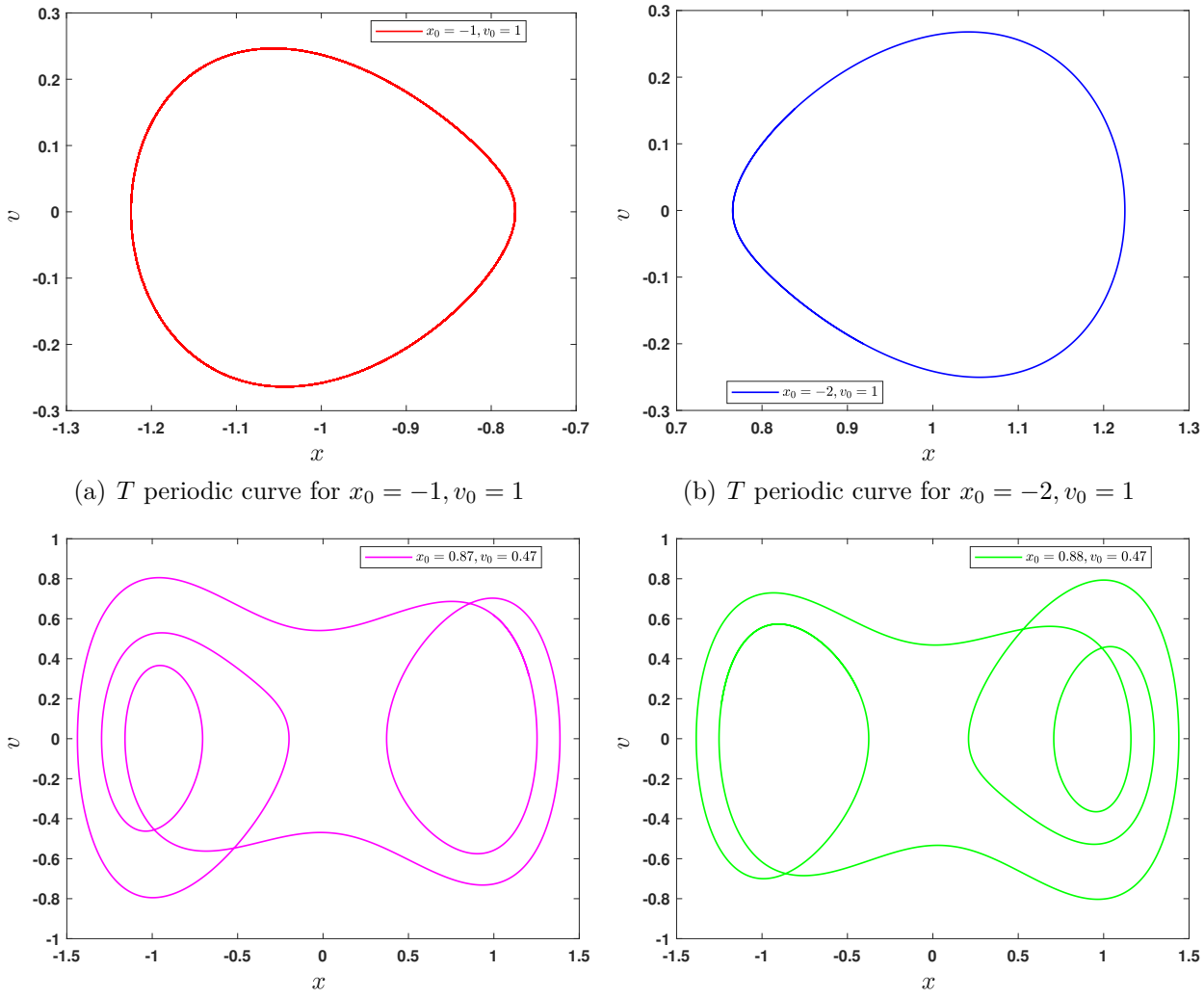
(a) Representation in phase space of solution that tends towards a $3T$ periodic limit case

(b) Stroboscopic map as a sequence of points that tends to a limit set of three points as time extends

Figure 3.2: Phase space and stroboscopic map of a regular solution tends towards a $3T$-periodic curve with $\alpha = 0.8$, $f_0 = 2$, $x_0 = v_0 = 0$.

It is interesting to note that the regular attractor is not, in general, unique. For fixed values of all the parameters, depending on the initial conditions the solutions can exhibit diverse behaviours and converge towards distinct closed curves. This phenomenon underscores the system's sensitivity to its starting state and the importance of considering a wide range of initial conditions when studying the dynamics. Consequently, even small deviations in the initial conditions can lead to significantly different outcomes.

This sensitivity to the initial conditions, that is to be expected in a chaotic regime, is here present in the case of regular solutions. In Figure 3.3 we show four regular attractors, with some different periodicities, for fixed values of the parameters but different initial conditions.



(a) T periodic curve for $x_0 = -1, v_0 = 1$

(b) T periodic curve for $x_0 = -2, v_0 = 1$

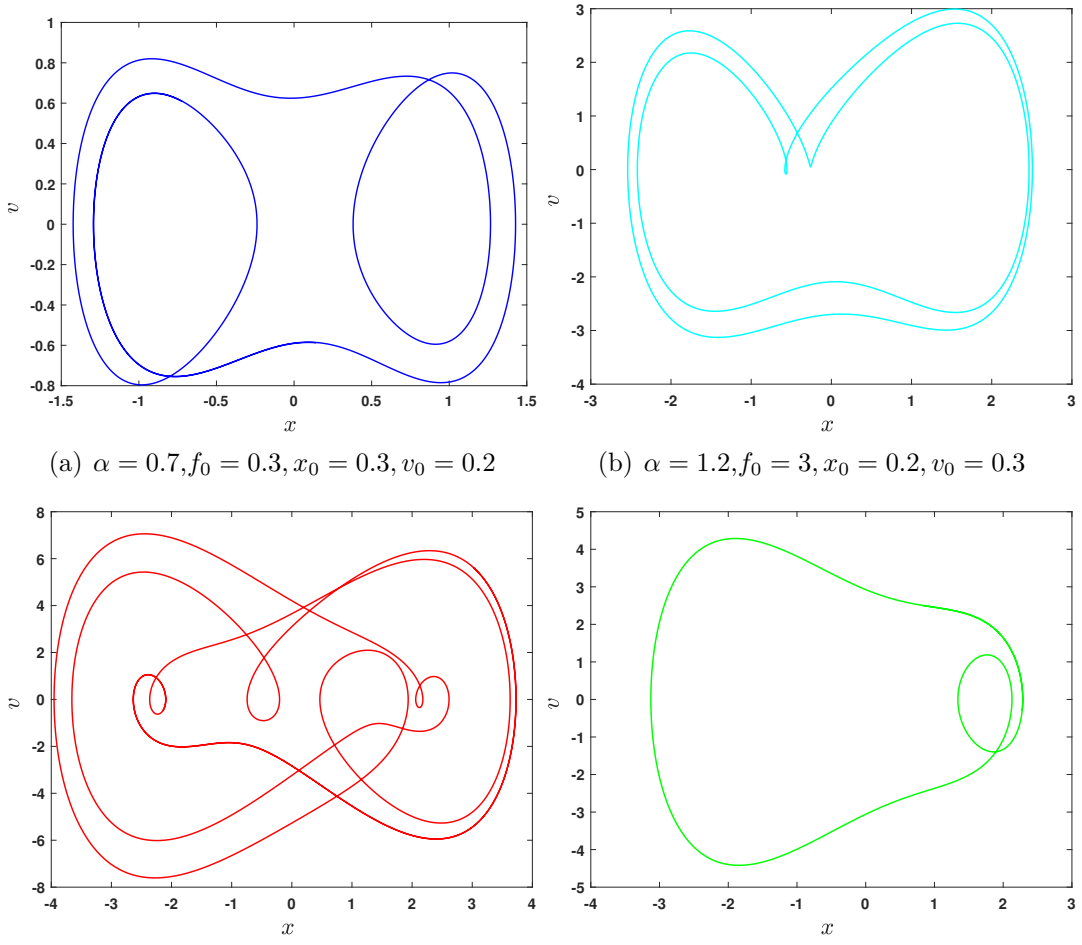
(c) $4T$ periodic curve for $x_0 = 0.87, v_0 = 0.47$

(d) $4T$ periodic curve for $x_0 = 0.88, v_0 = 0.47$

Figure 3.3: Multiplicity of limit cycles in the regular regime: for different initial conditions with the same set of parameters: $\alpha = 0.6$, $f_0 = 0.2409$.

For different values of parameters and different initial conditions, in Figure 3.4 we

present different periodic curves with distinct periods.



(a) $\alpha = 0.7, f_0 = 0.3, x_0 = 0.3, v_0 = 0.2$

(b) $\alpha = 1.2, f_0 = 3, x_0 = 0.2, v_0 = 0.3$

(c) $\alpha = 1.7, f_0 = 11, x_0 = -0.1, v_0 = 0.1$

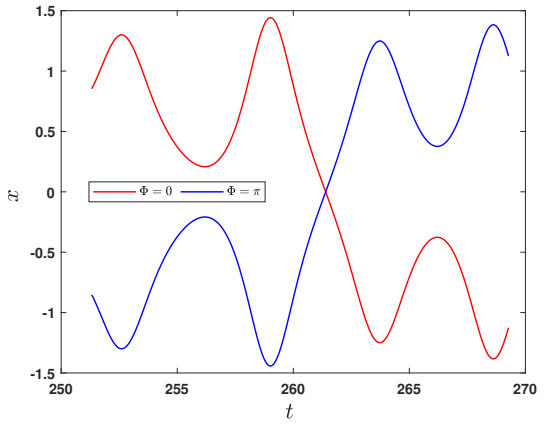
(d) $\alpha = 1.9, f_0 = 5, x_0 = 0, v_0 = 0$

Figure 3.4: Regular attractors of the fractional Duffing equation for several values of α.

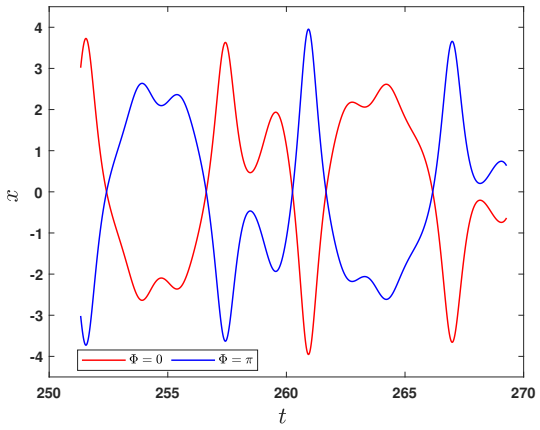
When we look at Figures 3.3(c) and 3.3(d), we observe that they exhibit symmetry. In the classical Duffing equation, regular attractors manifest as periodic curves in the phase plane that are symmetric with respect to the transformations $x \to -x$ and $v \to -v$. A similar pattern seems to emerge in the fractional scenario. Equation (3.18) can be rewritten as follows:

$$\begin{aligned} -\ddot{x} + \gamma(D_t^\alpha(-x))(t) + x - x^3 &= f_0 \cos(\omega t) \\ \Leftrightarrow \ddot{x} + \gamma(D_t^\alpha x)(t) - x + x^3 = -f_0 \cos(\omega t) &= f_0 \cos(\omega(t+\Phi)), \quad \Phi = \frac{\pi}{\omega}, \end{aligned} \tag{3.50}$$

the transformation maintains the equation's invariance but results in a phase shift in the cosine term. The equation thus contains a phase factor $\Phi = \frac{\pi}{\omega}$. Let us apply this transformation to the two sets of parameters that correspond to the Figures: 3.3(d) and 3.4(c). In Figure 3.5, we present the solution versus time to see the symmetry obtained after the transformation.



(a) Solutions for $\alpha = 0.6, f_0 = 0.2409$: Red curve with $x_0 = 0.88, v_0 = 0.47$, $\Phi = 0$; andblue curve with $x_0 = -0.88$, $v_0 = -0.47$, $\Phi = \pi/\omega$ (after transformation).



(b) Solutions for $\alpha = 1.7, f_0 = 11$: Red curve with $x_0 = -0.1, v_0 = 0.1$, $\Phi = 0$; and blue curve with $x_0 = +0.1, v_0 = -0.1$, $\Phi = \pi/\omega$ (after transformation).

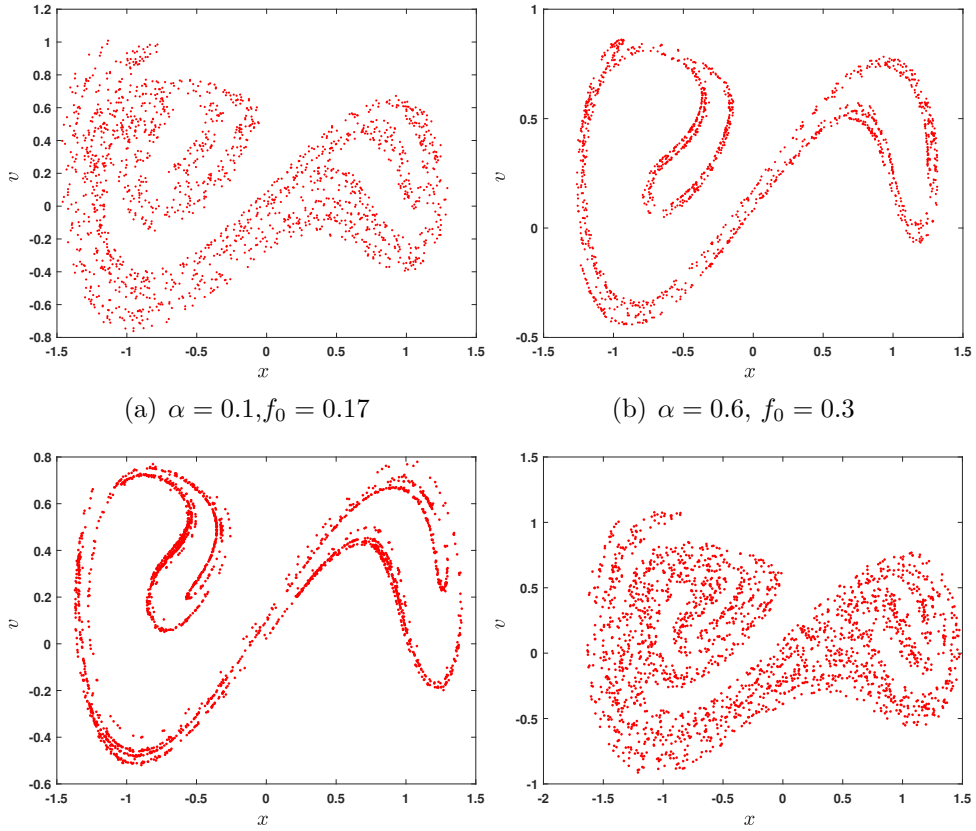
Figure 3.5: Comparison of fractional Duffing equation solutions: with phase $\phi = 0$ and phase-shifted solution ($\phi = \pi$)

This transformation reveals the symmetry of the solutions, as we observed. When a regular attractor emerges for a specific parameter set, it indicates the presence of a corresponding symmetric attractor. This symmetric attractor can be obtained using the transformation mentioned earlier, or it might already exist for a different set of parameters.

★ Chaotic solutions

There are chaotic solutions, clearly identified by presenting a quick convergence to a strange attractor in the stroboscopic map, similar to the one obtained in the classical

model for the same values of the parameters. We present several examples of the strange attractor in Figure 3.6 for different values of α and f_0.



(a) $\alpha = 0.1, f_0 = 0.17$ (b) $\alpha = 0.6,\ f_0 = 0.3$

(c) $\alpha = 1.3, f_0 = 0.3$ (d) $\alpha = 1.9, f_0 = 0.2$

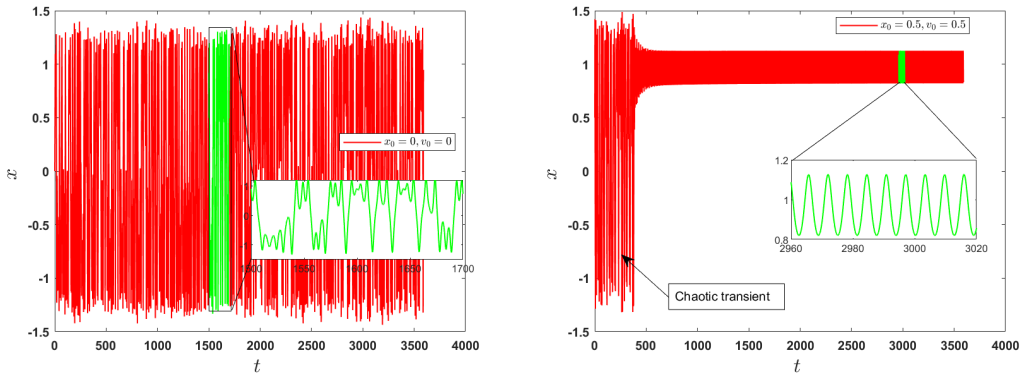
Figure 3.6: Strange attractors of the fractional Duffing equation for several values of α.

As we mentioned before, solutions with the same parameters have the potential to converge towards distinct attractors. This happens also when chaotic solutions are present. For some values of the parameters, and depending on the initial conditions, there is a coexistence of regular solutions that tend to different regular attractors and chaotic solutions that tend to a unique strange attractor. We illustrate this in Figure 3.7, where we only show the x-component of the solution, the behaviour of v being similar.

★ Long chaotic transient

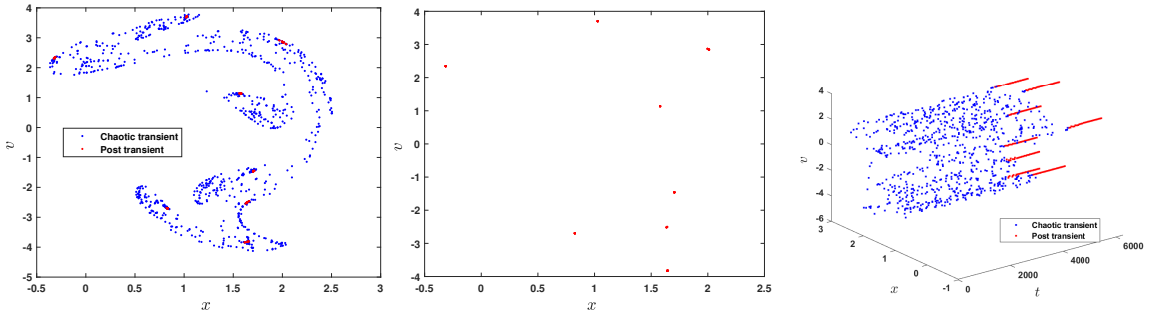
There is a range of regular solutions that present a long chaotic transient: for some time, quite long in some cases, the stroboscopic map shows a "cloud" of points that resembles a strange attractor but after that, the solution clearly tends towards a periodic curve. In Figure 3.8(a), we illustrate this with a solution that, after a very long transient (the blue point), tends to a closed curve of period $8T$ in the phase plane with the points in the stroboscopic map tending towards to a limit set of 8 points as shown in Figure 3.8(b).

For a clearer view of this behaviour in Figure 3.8(c), we present the evolution of the



(a) Chaotic solution for $x_0 = 0$, $v_0 = 0$ (b) Regular solution for $x_0 = 0.5$, $v_0 = 0.5$

Figure 3.7: Time series for chaotic and regular solutions for $\alpha = 0.1$, $f_0 = 0.16$ for two different initial conditions. In (b) the solution tends to a regular attractor after a chaotic transient.



(a) Stroboscopic map for a solution with a long chaotic transient (b) Stroboscopic map from $t = 5020.2651 : 6283.1853$ (c) Stroboscopic map and time for a solution with a long chaotic transient, $\alpha = 0.3$, $f_0 = 3$, $x_0 = 1.23$, $v_0 = 1.21$.

Figure 3.8: The solution regularised after a long chaotic transient and tends towards a closed curve of period $8T$ (and a limit set of 8 points in the stroboscopic map), $\alpha = 0.3$, $f_0 = 3$, $x_0 = 1.23$, $v_0 = 1.21$.

points in false 3D projection adding, thus, the time evolution.

This behaviour also appears to be very sensitive to the initial conditions: two solutions starting from close initial data may present transients of very different lengths as shown in Figure 3.9 for $\alpha = 0.25$, $f_0 = 0.229$.

We notice a chaotic transient for the initial conditions $x_0 = 0.001$, $v_0 = 0.0098$ (red points) but once we add the small quantity $\epsilon = (2\pi/700)^8$ to the previous initial condition as a perturbation the transient is extended in the order of 10^5 time steps (black points).

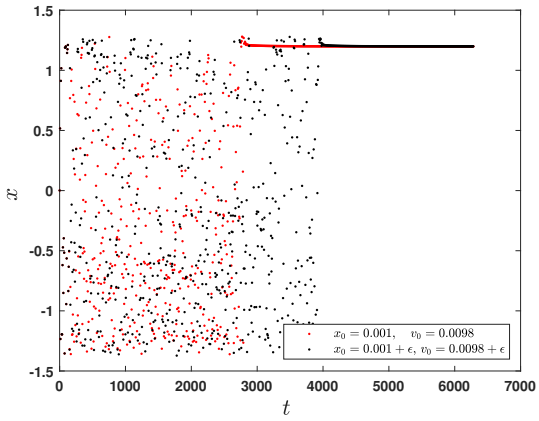


Figure 3.9: Stroboscopic map of different chaotic transients for $\alpha = 0.25$, $f_0 = 0.229$ shows that two solutions with nearby initial conditions, display transients of different lengths.

The chaotic transient can even present an intermittent behaviour, with a chaotic regime alternating several times with a regular one, and eventually reaching a regular phase that can be different to the previous regular ones. We illustrate this in Figure 3.10.

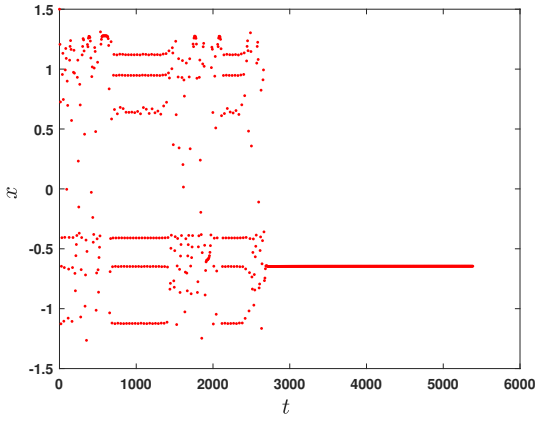
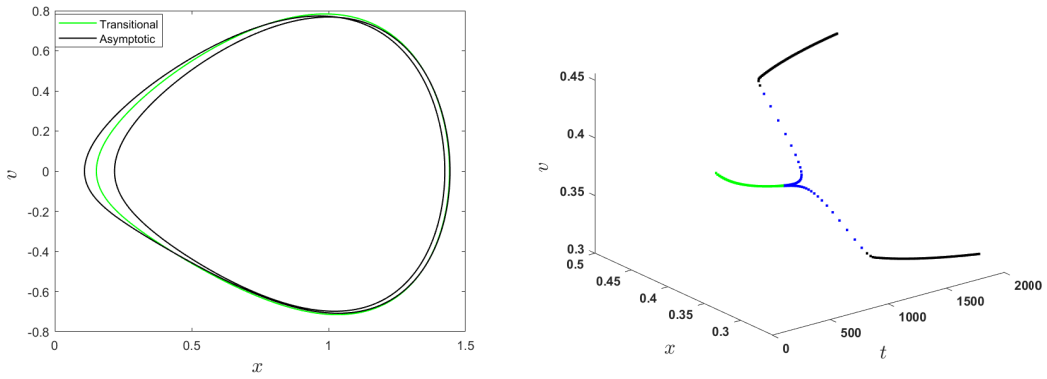


Figure 3.10: Stroboscopic map with intermittent chaotic transient for $\alpha = 1.1$, $f_0 = 0.25$.

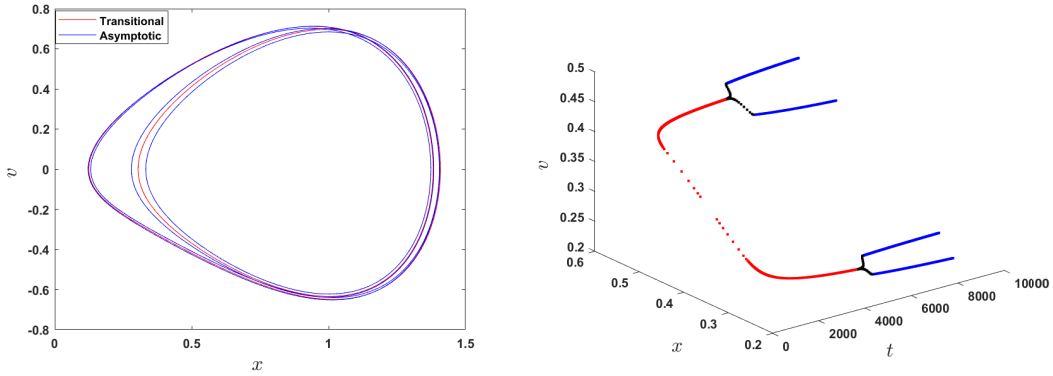
★ Solutions switching from regular attractors

We have just mentioned above the case of solutions presenting a chaotic transient that regularizes, afterwards, somehow switching from approaching a chaotic attractor to finally tending towards a regular one. Similarly, we have observed solutions switching from regular attractors: solutions that start close to a regular, periodic, curve but after some time evolve towards a different one. The stroboscopic map in such cases shows what resembles a bifurcation in time. We illustrate this with two examples in Figure 3.11 and Figure 3.12.



(a) Phase space (b) Stroboscopic map and time

Figure 3.11: Phase space and Stroboscopic map of the transition from a T-periodic attractor to a $2T$ attractor, $\alpha = 1.1$, $f_0 = 0.2$, $x_0 = 0$, $v_0 = 0.5$.



(a) Phase space (b) Stroboscopic map and time

Figure 3.12: Phase space and Stroboscopic map of the transition from a $2T$-periodic attractor to a $4T$ attractor, $\alpha = 1.2$, $f_0 = 0.19$, $x_0 = 0.5$, $v_0 = 0.5$.

This switching between two regular attractors can also occur through a chaotic-like transition. We illustrate this in Figure 3.13, where the solution starts near a T-periodic curve to finally approach a $3T$ curve.

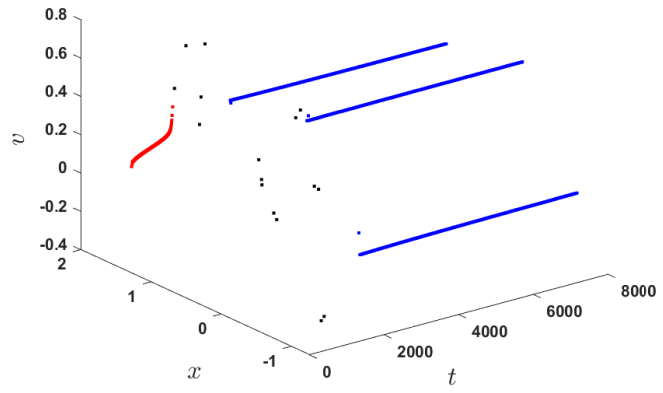


Figure 3.13: Phase space and Stroboscopic map of the transition from a T-periodic attractor to a 3T attractor via a chaotic-like transition for $\alpha = 1.1$, $f_0 = 0.2$, $x_0 = 0.5$, $v_0 = 0.5$.

Finally, the transition can also be from a regular attractor to a chaotic one, as shown in Figure 3.14. This last case is, somehow, the reverse situation of the long chaotic transient described in the previous point.

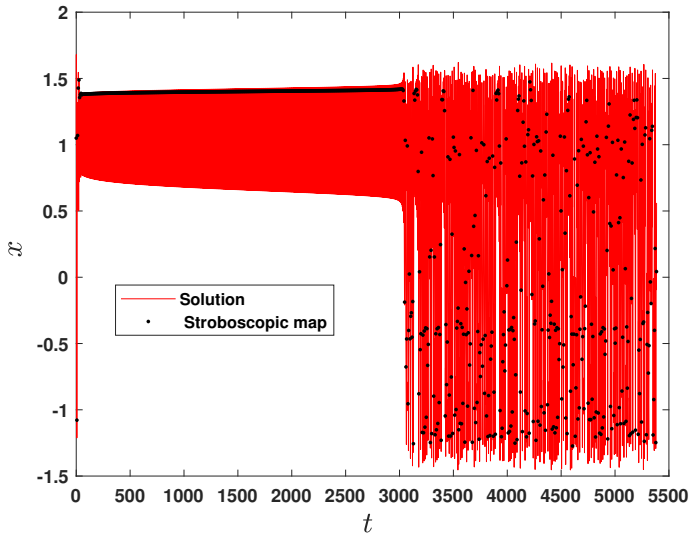


Figure 3.14: Switching from a regular attractor to a chaotic one, for $\alpha = 1.1$, $f_0 = 0.4$, $x_0 = 1.05$, $v_0 = 1.06$.

For another set of parameters, following this chaotic behaviour as we saw in Figure 3.14, a regular attractor with different periods may reappear. This regular attractor can transition to another regular attractor as time increases as shown in Figure 3.15.

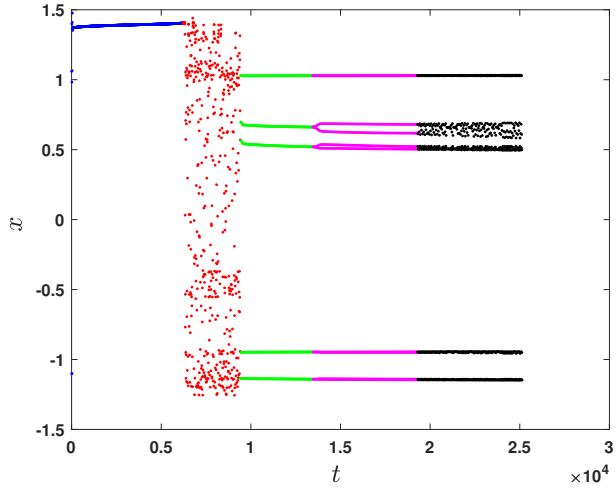


Figure 3.15: Switching from a regular $(T)-$chaotic$-$regular $(5T)-$regular $(7T)-$chaotic attractor, for $\alpha = 1.1$, $f_0 = 0.387$, $x_0 = 1.05$, $v_0 = 1.06$.

★ **Intermittent behaviours** Last, but not least, we have found intermittent behaviours in some chaotic solutions. The system exhibits a periodic pattern during extended time intervals. However, these laminar phases have distinct lengths interrupted by chaotic bursts, their occurrence seemingly random. Each burst has a distinct and finite duration before disappearing, leading to the initiation of a new laminar phase. This pattern cyclically repeats itself [78]. In some cases, the regular-like phases of the solution oscillate around just one of the centres of the underlying classical Hamiltonian system as in Figure 3.16.

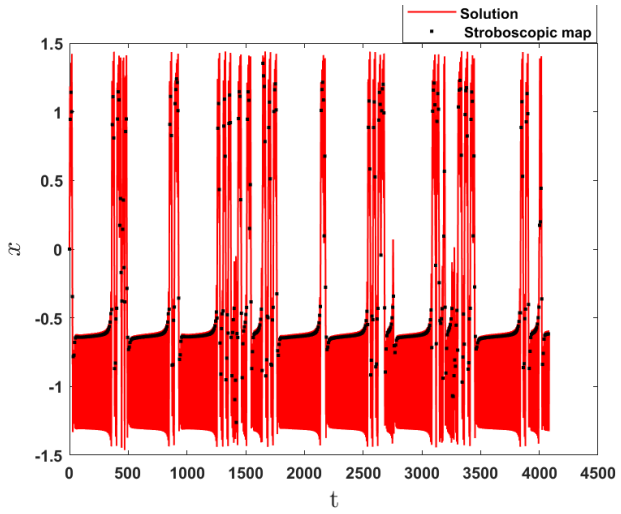


Figure 3.16: Intermittency with oscillations around one center $(-1, 0)$, for $\alpha = 1.25$, $f_0 = 0.2271$, $x_0 = 0.00101$, $v_0 = 0.002$.

In other cases, the regular-like phases can be around any of the two centres, passing from one to the other, occasionally, as in Figure 3.17.

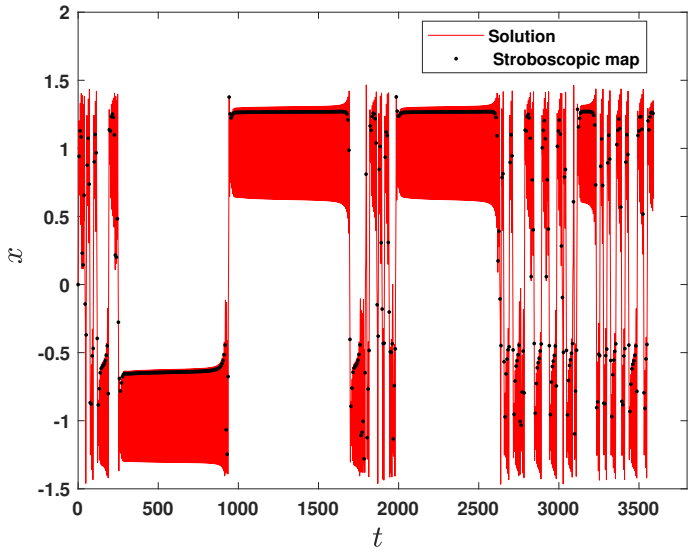


Figure 3.17: Intermittency with oscillations around any of the two centers $(\pm 1, 0)$, for $\alpha = 1.35$, $f_0 = 0.2119$, $x_0 = v_0 = 0$.

We have also found cases where the regular-like phases of the solution oscillate around both centres of the underlying classical Hamiltonian system. We present such a case in Figure 3.18.

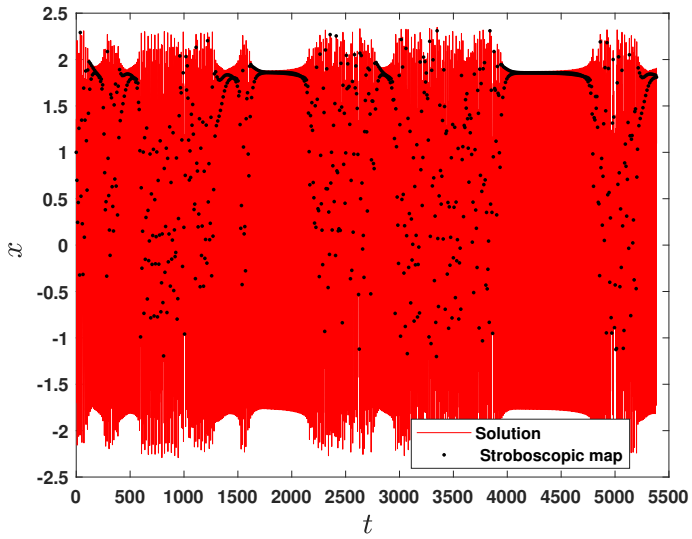


Figure 3.18: Intermittency with oscillations around the two centres, $\alpha = 0.1$, $f_0 = 0.778, x_0 = 1$, $v_2 = 0$.

Chapter 4

Characterizing chaos in the fractional Duffing equation

Detecting chaos can be achieved through either analytical analysis of the problem or numerical analysis of its data. One of the effective methods for evaluating chaotic behaviour is the measurement of Lyapunov characteristic exponents (LCEs), which assess the rate of exponential separation of solutions: a positive exponent indicates a local exponential separation of nearby orbits and it is associated with chaotic behaviour in bounded solutions.

Lyapunov exponents can provide qualitative and quantitative characteristics of dynamic behaviour. The analysis of the Lyapunov exponents has proven to be a useful tool for examining chaotic motions [109, 134].

4.1 Lyapunov characteristic exponents (LCEs)

Let us consider a general dynamical system of the form:

$$\begin{cases} \dot{x} = f(t,x), \\ x(0) = x_0, \quad x \in \mathbb{R}^n, \end{cases} \tag{4.1}$$

where we assume that the vector field $f(t,x)$ and $\frac{\partial}{\partial t}f(t,x)$, are continuous functions [5, 37]. Lyapunov exponents quantify the rate of divergence or convergence of nearby trajectories in phase space, in order to analyse how two close trajectories separate.

Let us consider two solutions, a reference solution $x(t)$ and, a "fiduciary [1]" one $y(t)$. We define the difference between them as:

$$\forall t, \quad \vec{\delta}(t) = \vec{x}(t) - \vec{y}(t), \tag{4.2}$$

Since we want to study close solutions, we consider $\|\vec{\delta}(0)\| << 1$.

[1] Fiduciary solution: is a slightly perturbed solution

The difference vector $\vec{\delta}$ can be approximated linearly from the linear problem:

$$\begin{cases} \dot{\vec{\delta}}(t) = J(t)\vec{\delta}(t), \\ \vec{\delta}(0) = \vec{\delta}_0. \end{cases} \tag{4.3}$$

where $J(t)$ is the Jacobi matrix at time t.

The solution of equation (4.3) can be written as:

$$\vec{\delta}(t) = M(t)\vec{\delta}_0, \tag{4.4}$$

with $M(t)$ the fundamental solution matrix of (4.3), whose evolution equation is:

$$\begin{cases} \dfrac{dM(t)}{dt} = J(t)M(t), \\ M(0) = M_0, \end{cases} \tag{4.5}$$

and the matrix M_0 is the initial condition of the matrix differential equation (4.5). To satisfy (4.4) M_0 should be the identity matrix I. The matrix $M(t)$ can be numerically approximated using numerical integration techniques (e.g., Runge-Kutta methods).

Definition 9 *Let $\mu_1, ..., \mu_N$ be the eigenvalues of the matrix $M(t)$ from* (4.5)*. The LCEs, λ_k, of the trajectory $x(t)$ are defined by:*

$$\lambda_k := \lim_{t\to\infty} \frac{1}{t} \ln |\mu_k(t)|. \tag{4.6}$$

We analyze this definition further, assuming that $z(t)$ are the eigenvector of $\mu_k(t)$, thus:

$$M(t)z = \mu_k z. \tag{4.7}$$

Using the vector norm, $|\mu_k(t)|$ can be expressed as:

$$|\mu_k(t)| = \frac{\|M(t)z\|}{\|z\|}. \tag{4.8}$$

From (4.4), $|\mu_k(t)|$ can be replaced by the quotient:

$$|\mu_k(t)| = \frac{\|\delta(t)\|}{\|\delta_0\|} = \frac{\|M(t)\delta_0\|}{\|\delta_0\|}. \tag{4.9}$$

Then, from (4.9), the expression (4.6) becomes:

$$\lambda_k := \lim_{t\to\infty} \frac{1}{t} \ln \frac{\|M(t)\delta_0\|}{\|\delta_0\|}. \tag{4.10}$$

The LCEs, λ_k, measure the expansion or contraction of the phase space locally around a given orbit, in the different directions of the phase space [113].

4.1.1 Computations of the LCEs

- If the equations cannot be solved analytically, rendering it impossible to know the solution analytically, then the evolution equation for the Jacobi matrix cannot be solved analytically. In such scenarios, turning to numerical simulations becomes essential. The evolution equation (4.5) for the Jacobi matrix can be discretized and also solved numerically. Equation (4.5) has to be integrated simultaneously with (4.1) because we need the numerical solution of (4.1) to obtain the matrix M [31].
- As an alternative to using the Jacobi matrix if we cannot linearise the system, the fiduciary orbit technique may approximate the maximum Lyapunov Characteristic Exponent, $\lambda_{\max}$, by calculating the separation increase between a reference solution and a slightly perturbed solution (fiduciary one) [10]. Even so, it is necessary to rescale the fiduciary solution every few steps to avoid numerical loss of precision due to an exponential separation or an exponential collapse.
- Finally, there is the case where the solution is known as a time series, without any other analytical reference. Instead of solving the evolution equation, the approach tracks trajectories in phase space derived from the time series. The separation rates are measured by tracking the divergence or convergence of neighbouring trajectories over time; this allows Lyapunov exponents to be computed [134, 109].

Analysis:
If the largest Lyapunov exponent is negative, nearby trajectories converge. The system is then considered to be non-chaotic. If there is at least one positive Lyapunov exponent, there is an exponential growth that is interpreted to correspond to an exponential divergence of nearby orbits and thus a sensitivity to initial conditions: two trajectories of the system starting close to each other will diverge after some time. The system is considered to be chaotic [115].

Additional properties: The sum of all LCEs for continuous time satisfies:

$$\sum_{n=1}^{N} \lambda_n = \lim_{t\to\infty} \frac{1}{t} \int_0^t \operatorname{trace}[J(x(s))]ds. \tag{4.11}$$

This property is relevant when the trace of the Jacobi matrix is a constant. For instance, in the case of Duffing's equation (2.28), the trace of its Jacobi matrix is $\operatorname{trace}(J) = -\gamma$, independently of (x, v) and, thus:

$$\sum_{n=1}^{2} \lambda_n = -\gamma. \tag{4.12}$$

Lyapunov dimension

To estimate the fractal dimension of the strange attractor in the plane xv, we may use the Lyapunov dimension proposed by Kaplan and Yorke in [53] that corresponds to:

$$D_L = j + \frac{\sum_{k=1}^{j} \lambda_j}{|\lambda_{j+1}|}, \tag{4.13}$$

where the Lyapunov exponents, λ_j, are assumed to be ordered:

$$\lambda_1 \leq \lambda_2 \leq \cdots \leq \lambda_j, \tag{4.14}$$

whith j the maximum index such that:

$$\sum_{k=1}^{j} \lambda_j \geq 0, \quad \sum_{k=1}^{j+1} \lambda_j < 0. \tag{4.15}$$

Chaos in fractional differential equations has mainly been considered by analogy to the more well-studied integer order ODE problems, whenever the solutions present a behaviour similar [2, 131, 9, 73, 43], for instance, a strange attractor.

Some authors have considered the signal approach which involves studying the time series or signals produced by the system's variables over time. The time-series approach uses the same idea as the fiduciary orbit technique: comparing two nearby orbits. But in this case, one cannot choose different initial data arbitrarily. To overcome this, given the data at some time t_0 (not necessarily the initial time), the whole time series is searched for a data, at some other time, say t_1, in which the values are very close to that at time t_0. Then the sequence starting at t_0 and that starting at t_1 are used to check how their differences grow or decay [134, 109].

In the case of a fractional system, it is generally not convenient to compare solutions starting at different times, since they are not equivalent to two solutions starting from close data at the same time.

Computing Lyapunov characteristic exponents remains a valuable method for assessing chaos in dynamical systems. In the context of fractional systems, Lyapunov exponents can still be computed, although with modifications to account for the fractional derivatives.

Besides that, another possibility to assess chaos in a dynamical system comes from the Melnikov method. Extending this method to fractional systems allows for the examination of chaotic phenomena induced by perturbations, providing insights into the system's stability and chaotic behaviour. While adapting the Melnikov method to fractional systems may require consideration of fractional derivatives, it offers a systematic approach for detecting chaos beyond what signal analysis alone can provide.

Our main focus in the next section is to employ the methods described in Section 4.1, including the linearization of the dynamical system and the fiduciary orbit technique, to investigate the fractional Duffing equation.

Therefore, this study explores the approximation of Lyapunov Characteristic Exponents (LCEs) in the fractional Duffing equation, considering two distinct cases based on the range of α, the order of the fractional term: $\lceil \alpha \rceil = 1$ and $\lceil \alpha \rceil = 2$.

4.2 LCEs for $\lceil \alpha \rceil = 1$

We aim to estimate all the LCEs using the linearization method by approximating the Jacobi matrix. We present, here, an adaptation of this method to compute all the LCEs [51]. We

analyse the linearized system for this case and build an effective Jacobi matrix.

4.2.1 Analytical Approximation

Building upon the previous analysis, section 4.1, we will now apply it to obtain an effective Jacobi matrix for the fractional Duffing equation (3.1).

To estimate the LCEs, let us consider two nearby solutions for (3.1): a reference solution (x, v) where $v = \dot{x}$ is the velocity and (y, u) which is close to the first solution, with $u = \dot{y}$. The difference between both solutions is governed by the system:

$$\begin{cases} \dot{x} - \dot{y} = v - u, \\ \dot{v} - \dot{u} = -U'(x) + U'(y) - \gamma D_t^{\alpha}(x - y), \quad 0 < \alpha < 1. \end{cases} \tag{4.16}$$

The dot notation indicates differentiation with respect to time t, while the prime notation indicates differentiation with respect to the solution variables x or y.

We define $\delta = x - y$ and $\eta = v - u$, the two perturbations of the reference solution (x, v) to the close one (y, u). After linearization, we obtain:

$$\begin{cases} \dot{\delta} = \eta, \\ \dot{\eta} = -U''(x)\delta - \gamma D_t^{\alpha}\delta. \end{cases} \tag{4.17}$$

We now substitute the Caputo fractional derivative (1.52) for $0 < \alpha < 1$ to obtain:

$$\begin{cases} \dot{\delta} = \eta, \\ \\ \dot{\eta} = -U''(x)\delta - \dfrac{\gamma}{\Gamma(1-\alpha)} \displaystyle\int_0^t \frac{\eta(\tau)}{(t-\tau)^{\alpha}} d\tau, \quad 0 < \alpha < 1. \end{cases} \tag{4.18}$$

The two solutions are considered to be very close to each other. It supposes that they are practically identical over a specific initial time interval which we denote as $[0, t_1)$. After this specific time t_1, the solutions are assumed to be distinguishable:

$$\forall t \in [0, t_1), \quad \eta(t) \approx 0 \Longrightarrow \int_0^{t_1} \frac{\eta(\tau)}{(t-\tau)^{\alpha}} d\tau = 0 \tag{4.19}$$

Due to a continuity argument functions with small perturbations possess small fractional derivatives. We may consider that the integral in (4.18) provides a small contribution. Thus, in good approximation, we have:

$$\int_0^t \frac{\eta(\tau)}{(t-\tau)^{\alpha}} d\tau = \int_0^{t_1} \frac{\eta(\tau)}{(t-\tau)^{\alpha}} d\tau + \int_{t_1}^t \frac{\eta(\tau)}{(t-\tau)^{\alpha}} d\tau \approx \int_{t_1}^t \frac{\eta(\tau)}{(t-\tau)^{\alpha}} d\tau, \quad 0 < \alpha < 1, \tag{4.20}$$

and, with this, we estimate (4.18) as:

$$\begin{cases} \dot{\delta} = \eta, \\ \\ \dot{\eta} = -U''(x)\delta - \dfrac{\gamma}{\Gamma(1-\alpha)} \displaystyle\int_{t_1}^t \frac{\eta(\tau)}{(t-\tau)^{\alpha}} d\tau, \quad 0 < \alpha < 1. \end{cases} \tag{4.21}$$

Using the Taylor expansion of $\eta(\tau)$ around t gives:

$$\eta(\tau) = \eta(t) + (\tau - t)\dot{\eta}(t) + \frac{(\tau - t)^2}{2}\ddot{\eta}(t) + \mathcal{O}\Big((\tau - t)^3\Big) \tag{4.22}$$

After substitution in (4.21) and integration in τ, the linearized system becomes:

$$\begin{cases} \dot{\delta} = \eta, \\ \dot{\eta} = \dfrac{-U''(x)}{C}\delta - \gamma\dfrac{\triangle t^{1-\alpha}}{C\Gamma(2-\alpha)}\eta, \end{cases} \tag{4.23}$$

with $\triangle t = t - t_1$, discarding higher order terms in $\triangle t$.

The coefficient C is:

$$C = 1 - \frac{\gamma\triangle t^{2-\alpha}(1-\alpha)}{\Gamma(3-\alpha)}, \quad 0 < \alpha < 1. \tag{4.24}$$

The corresponding Jacobi matrix for system (4.23), J_1, is:

$$J_1 = \begin{pmatrix} 0 & 1 \\ \frac{-U''(x)}{C} & -\gamma\frac{\triangle t^{1-\alpha}}{C\Gamma(2-\alpha)} \end{pmatrix}. \tag{4.25}$$

Using the Jacobi matrix (4.25), both LCEs, λ_1, λ_2, for this case can be obtained. Further details are provided in [51].

Since (4.25) has a constant trace, (4.11) holds and the sum of both LCEs satisfies:

$$\lambda_1 + \lambda_2 = \text{trace}(J_1) = -\frac{\gamma\triangle t^{1-\alpha}}{C\Gamma(2-\alpha)}, \quad 0 < \alpha < 1. \tag{4.26}$$

To check the conservation given by (4.26), we use the relative error:

$$\xi_1 = \frac{|\lambda_1 + \lambda_2 - \text{trace}(J_1)|}{\text{trace}(J_1)}. \tag{4.27}$$

Having obtained both LCEs, we are now able to compute the Lyapunov Dimension D_L. In this case, where $j = 1$, D_L as expressed in equation (4.13) simplifies to:

$$D_L = 1 + \frac{\lambda_1}{|\lambda_2|}. \tag{4.28}$$

4.2.2 Numerical Results

We consider (4.25) to be the effective Jacobi matrix for the linearized fractional system for this case and we use it to estimate the two LCEs of the system, λ_1 and λ_2, with $\lambda_1 > \lambda_2$.

We have also computed the maximum LCE, $\lambda_{\max}$, with the fiduciary orbit method as an alternative independent estimation of λ_1.

In the study conducted by Jiménez et al. [51], the authors used the SV + Diethelm method to approximate the Lyapunov Characteristic Exponents (LCEs). Initially, we replicated their findings, and then, we applied a different approach (SV + Odibat method) in order to identify any discrepancies.

In Figure 4.1, we represent both LCEs, λ_1 and λ_2, and $\lambda_{\max}$, for the chaotic solutions with α has the same values of the paper [51].

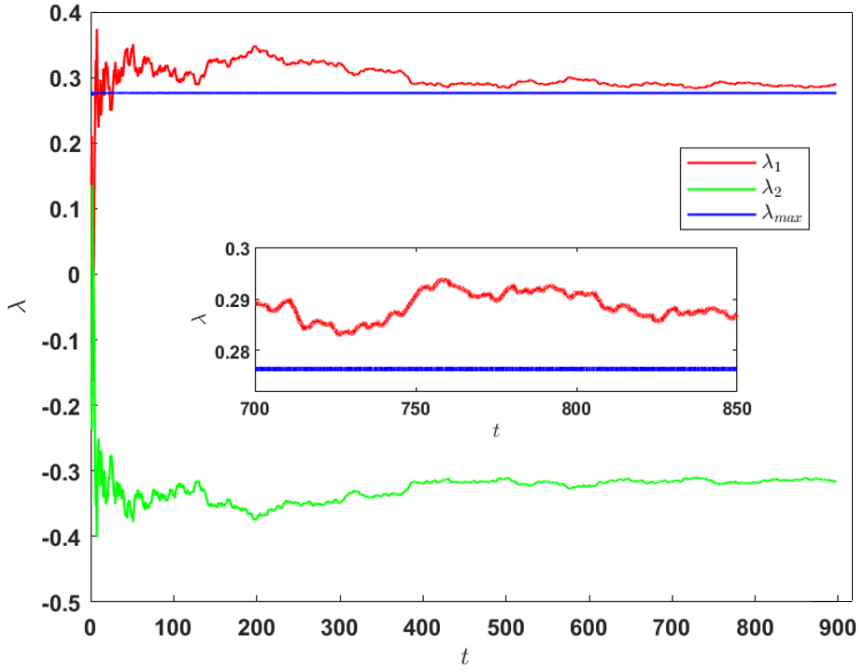


Figure 4.1: Estimates of the LCEs for the fractional Duffing's equation, chaotic solution with $\alpha = 0.8$, $f_0 = 0.3$, $x_0 = 0.8, v_0 = 0$ (SV + Diethelm method).

In [51], a small quantitative gap was observed between the estimation of the values of the maximum LCE obtained by the two methods.

We have used now the new numerical method SV + Odibat to approximate the LCEs for both regular and chaotic regimes and obtained a quantitative gap much smaller. We understand that this is due to our numerical method SV + Odibat method being more accurate.

In Figure 4.2, we present both LCEs, λ_1 and λ_2, and $\lambda_{\max}$, for the same parameter taken in the previous work. In Figure 4.2 both LCEs, λ_1 and $\lambda_{\max}$, are positive corresponding to a chaotic solution.

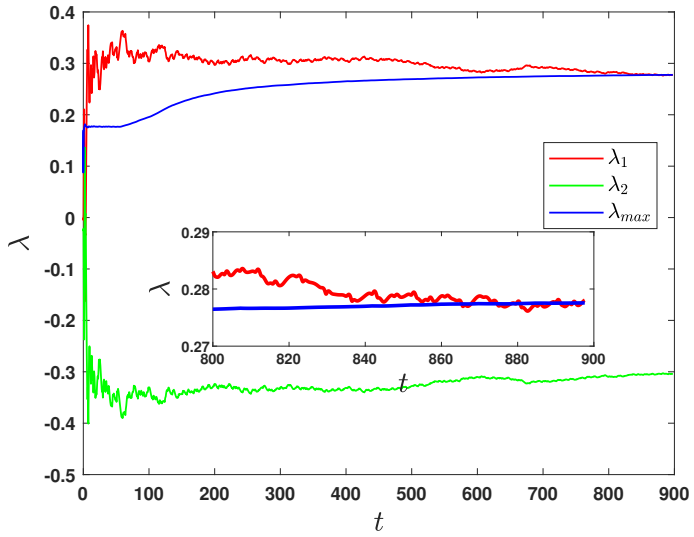


Figure 4.2: Estimation of LCEs shows the agreement between the positive Lyapunov exponent λ_1 and $\lambda_{\max}$: chaotic solution for $\alpha = 0.5$, $f_0 = 0.3$, $x_0 = 0.8$, $v_0 = 0$ (SV + Odibat method).

and in Figure 4.3 both of them are negative which is an indication of a regular solution.

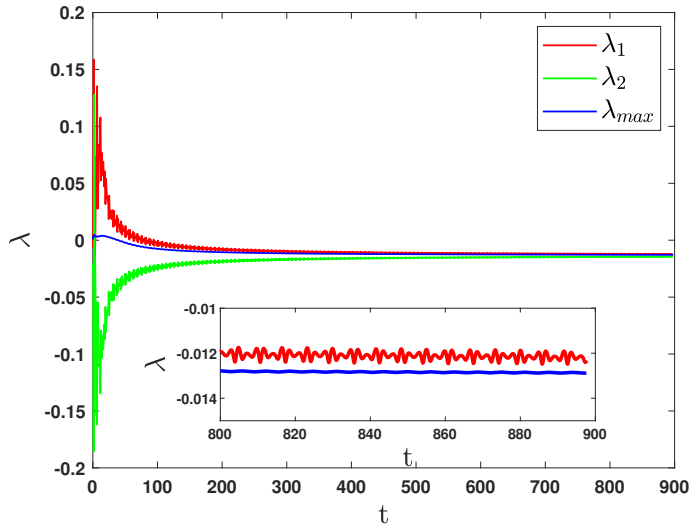


Figure 4.3: Estimation of LCEs shows the agreement between the positive Lyapunov exponent λ_1 and $\lambda_{\max}$: regular solution for $\alpha = 0.5, f_0 = 0.15$, $x_0 = 0.8$, $v_0 = 0$ (SV + Odibat method).

Besides, as an indication of possible computing errors, we have checked the conservation law (4.26) and found always a good agreement, the relative errors being smaller than 10^{-5}. In Figure 4.4, we present the relative error in the case $0 < \alpha < 1$ with $\alpha = 0.5, x_0 = 0.8, v_0 = 0$ for time step $\triangle t = 2\pi/700$ for both cases of chaotic and regular solutions.

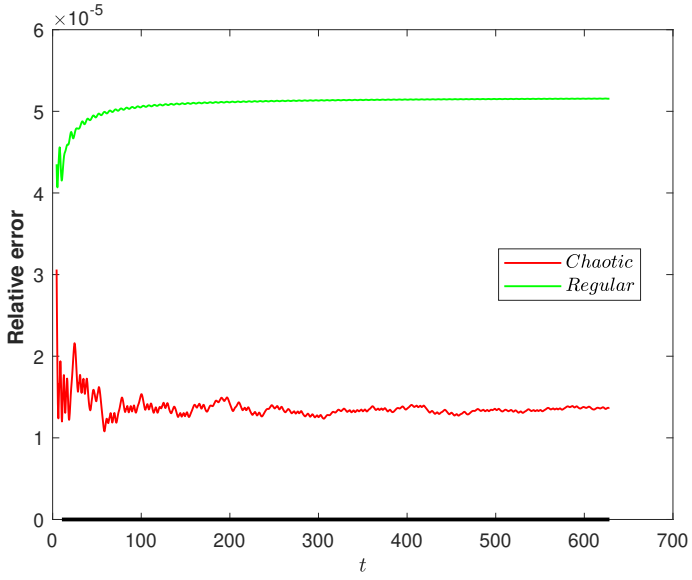


Figure 4.4: Accuracy of the conservation law (4.26) for $\alpha = 0.5$.

4.3 LCEs for $\lceil \alpha \rceil = 2$

Following a similar approach as in the preceding case to obtain the Jacobi matrix, we extend now the linear approximation to the case $\alpha \in (1, 2)$.

4.3.1 Analytical Approximation

The Caputo fractional derivative of δ corresponding to this case is:

$$D_t^\alpha \delta(t) = \frac{1}{\Gamma(2-\alpha)} \int_0^t \frac{\delta''(\tau)}{(t-\tau)^{\alpha-1}}\, d\tau, \quad 1 < \alpha < 2. \tag{4.29}$$

We substitute (4.29) in the linearized system (4.17):

$$\begin{cases} \dot{\delta} = \eta, \\ \dot{\eta} = -U''(x)\delta - \dfrac{\gamma}{\Gamma(2-\alpha)} \displaystyle\int_0^t \frac{\delta''(\tau)}{(t-\tau)^{\alpha-1}} d\tau, \quad 1 < \alpha < 2, \end{cases} \tag{4.30}$$

and use $\delta''(\tau) = \eta'(\tau)$ to obtain:

$$\begin{cases} \dot{\delta} = \eta, \\ \dot{\eta} = -U''(x)\delta - \dfrac{\gamma}{\Gamma(2-\alpha)} \displaystyle\int_0^t \frac{\eta'(\tau)}{(t-\tau)^{\alpha-1}} d\tau, \quad 1 < \alpha < 2. \end{cases} \tag{4.31}$$

For $\forall t \in [0, t_1)$, $\dot{\eta}(t) \approx 0$, the system (4.31) becomes:

$$\begin{cases} \dot{\delta} = \eta, \\ \dot{\eta} = -U''(x)\delta - \dfrac{\gamma}{\Gamma(2-\alpha)}\left[\displaystyle\int_0^{t_1} \frac{\eta'(\tau)}{(t-\tau)^{\alpha-1}}d\tau + \int_{t_1}^{t} \frac{\eta'(\tau)}{(t-\tau)^{\alpha-1}}d\tau\right] \\ \quad \approx -U''(x)\delta - \dfrac{\gamma}{\Gamma(2-\alpha)}\displaystyle\int_{t_1}^{t} \frac{\eta'(\tau)}{(t-\tau)^{\alpha-1}}d\tau, \quad 1<\alpha<2. \end{cases} \tag{4.32}$$

We insert $t = t_1 + \triangle t$ into equation (4.32):

$$\begin{cases} \dot{\delta} = \eta, \\ \dot{\eta} = -U''(x)\delta - \dfrac{\gamma}{\Gamma(2-\alpha)}\displaystyle\int_{t_1}^{t_1+\triangle t} \frac{\eta'(\tau)}{(t-\tau)^{\alpha-1}}d\tau, \quad 1<\alpha<2. \end{cases} \tag{4.33}$$

Using the Taylor expansion to approximate $\eta'(\tau)$ around t for time step $\triangle t$ small enough, we have:

$$\begin{aligned} \dot{\eta} &= -U''(x)\delta - \frac{\gamma}{\Gamma(2-\alpha)}\dot{\eta}(t)\int_{t_1}^{t_1+\triangle t}(t_1+\triangle t-\tau)^{1-\alpha}d\tau \\ &\quad + \frac{\gamma}{\Gamma(2-\alpha)}\ddot{\eta}(t)\int_{t_1}^{t_1+\triangle t}(t_1+\triangle t-\tau)^{2-\alpha}d\tau + ... \end{aligned} \tag{4.34}$$

After the integration, we obtain:

$$\dot{\eta} = -U''(x)\delta - \frac{\gamma\triangle t^{2-\alpha}}{\Gamma(3-\alpha)}\dot{\eta}(t) + \frac{\gamma(2-\alpha)\triangle t^{3-\alpha}}{\Gamma(4-\alpha)}\ddot{\eta}(t) + \mathcal{O}(\triangle t^{4-\alpha}). \tag{4.35}$$

In the previous expression, $\ddot{\eta}$ appears as well as $\dot{\eta}$, and we cannot "close" the equations. This distinguishes the current case from the previous one.

To solve this problem we need to express $\ddot{\eta}$ as a function of δ and $\dot{\eta}$. To achieve this we resort to approximating the second-order derivative by finite differences. Given the truncation error in our approximation of $\dot{\eta}$, a suitable approximation for $\ddot{\eta}$ is given by the three points backwards finite difference:

$$\ddot{\eta}(t) = \frac{\eta(t) - 2\eta(t-\triangle t) + \eta(t-2\triangle t)}{\triangle t^2} + \mathcal{O}(\triangle t). \tag{4.36}$$

As both solutions can be considered identical (up to numerical precision) over an interval of time $t \in [0, t_1)$, η is zero for all times in this interval, and we have:

$$\eta(t - n\triangle t) = 0, \quad \forall n \geq 2. \tag{4.37}$$

Using this assumption, the finite difference of $\ddot{\eta}$ (4.36) becomes:

$$\ddot{\eta}(t) = \frac{\eta(t) - 2\eta(t - \triangle t)}{\triangle t^2} + \mathcal{O}(\triangle t). \tag{4.38}$$

In order to express $\ddot{\eta}$ as a function of $\eta(t)$ and $\dot{\eta}(t)$, we need now to express $\eta(t - \triangle t)$ as a function of those variables. Once again we use a finite difference with a suitable truncation error. In this case a four-point formula:

$$\begin{aligned} \dot{\eta}(t) &= \frac{-2\eta(t - 3\triangle t) + 9\eta(t - 2\triangle t) - 18\eta(t - \triangle t) + 11\eta(t)}{6\triangle t} + \mathcal{O}(\triangle t^3) \\ &= \frac{-18\eta(t - \triangle t) + 11\eta(t)}{6\triangle t} + \mathcal{O}(\triangle t^3), \end{aligned} \tag{4.39}$$

that gives us:

$$\eta(t - \triangle t) = \frac{11}{18}\eta(t) - \frac{\triangle t}{3}\dot{\eta}(t) + \mathcal{O}(\triangle t^4). \tag{4.40}$$

With all this have:

$$\begin{aligned} \ddot{\eta}(t) &= \frac{\eta(t) - 2\eta(t - \triangle t)}{\triangle t^2} + \mathcal{O}(\triangle t) \\ &= \frac{1}{\triangle t^2}\eta(t) - \frac{2}{\triangle t^2}\left[\frac{11}{18}\eta(t) - \frac{\triangle t}{3}\dot{\eta}(t) + \mathcal{O}(\triangle t^4)\right] + \mathcal{O}(\triangle t) \\ &= \frac{-2}{9\triangle t^2}\eta(t) + \frac{2}{3\triangle t}\dot{\eta}(t) + \mathcal{O}(\triangle t), \end{aligned} \tag{4.41}$$

and, substituting into (4.35), we finally obtain:

$$\begin{aligned} \dot{\eta} &= -U''(x)\delta(t) - \frac{\gamma\triangle t^{2-\alpha}}{\Gamma(3-\alpha)}\dot{\eta}(t) + \frac{2\gamma(2-\alpha)\triangle t^{2-\alpha}}{3\Gamma(4-\alpha)}\dot{\eta}(t) \\ &\quad - \frac{2\gamma(2-\alpha)\triangle t^{1-\alpha}}{9\Gamma(4-\alpha)}\eta(t) + \mathcal{O}(\triangle t^{4-\alpha}). \end{aligned} \tag{4.42}$$

In order to use the same framework of the previous case, we rewrite (4.33) as:

$$\begin{cases} \dot{\delta} = \eta, \\ \dot{\eta} = \dfrac{-U''(x)}{C}\delta + \dfrac{B}{C}\eta, \quad 1 < \alpha < 2, \end{cases} \tag{4.43}$$

where the coefficients C and B are, in this case:

$$\begin{cases} C = 1 + \dfrac{\gamma(5-\alpha)\Delta t^{2-\alpha}}{3\Gamma(4-\alpha)}, \\ B = -\dfrac{2\gamma(2-\alpha)\triangle t^{1-\alpha}}{9\Gamma(4-\alpha)}. \end{cases} \tag{4.44}$$

The corresponding effective Jacobi matrix for system (4.43), J_2, is:

$$J_2 = \begin{pmatrix} 0 & 1 \\ \frac{-U''(x)}{C} & \frac{B}{C} \end{pmatrix}. \tag{4.45}$$

As the trace of the Jacobi matrix is constant in this case too, we have that it is equal to the sum of the two LCEs:

$$\lambda_1 + \lambda_2 = \text{trace}(J_2) = \frac{B}{C}, \quad 1 < \alpha < 2. \tag{4.46}$$

4.3.2 Numerical Results

In this section, we present the numerical results obtained concerning the LCEs for $1 < \alpha < 2$.

We compute the LCEs for three behaviours of solution: chaotic, regular and intermittency.

We rely on the Jacobi matrix (4.45) to simulate both LCEs and compare the largest one, λ_1, with the one approximated by the fiduciary method, $\lambda_{\max}$.

In Figure 4.5, we present both LCEs, λ_1, λ_2, and the maximum Lyapunov exponent, $\lambda_{\max}$, for a chaotic solution.

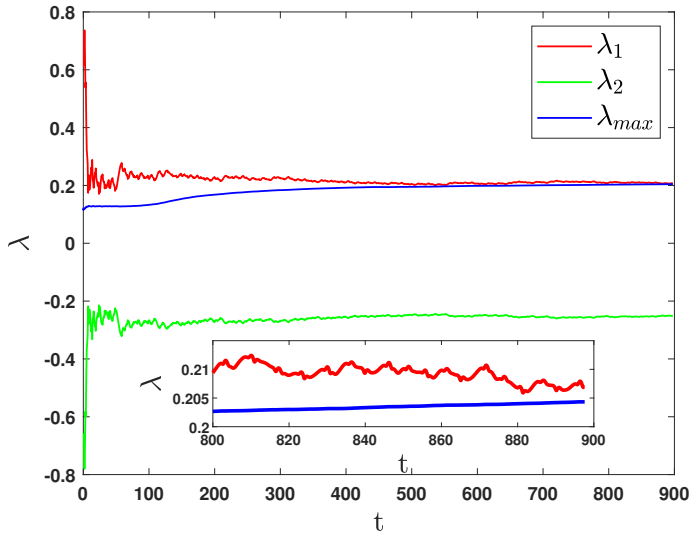


Figure 4.5: Estimation of Lyapunov Characteristic Exponents (LCEs) for a chaotic solution, for $\alpha = 1.1$, $x_0 = v_0 = 0, f_0 = 0.29$.

In Figure 4.6, we present both Lyapunov exponents λ_1, λ_2 and $\lambda_{\max}$ for a regular solution.

In both cases, chaotic as well as regular solutions, we find a good agreement between λ_1 and $\lambda_{\max}$.

To check the conservation law for this case (4.46), we present the relative error of the sum of the LCEs with respect to the trace of J_2 using $\triangle t = 2\pi/700$. We found it to be smaller than $5 \cdot 10^{-5}$.

$$\xi_2 = \left| \frac{|\lambda_1 + \lambda_2 - \text{trace}(J_2)|}{\text{trace}(J_2)} \right| < 5 \cdot 10^{-5}. \tag{4.47}$$

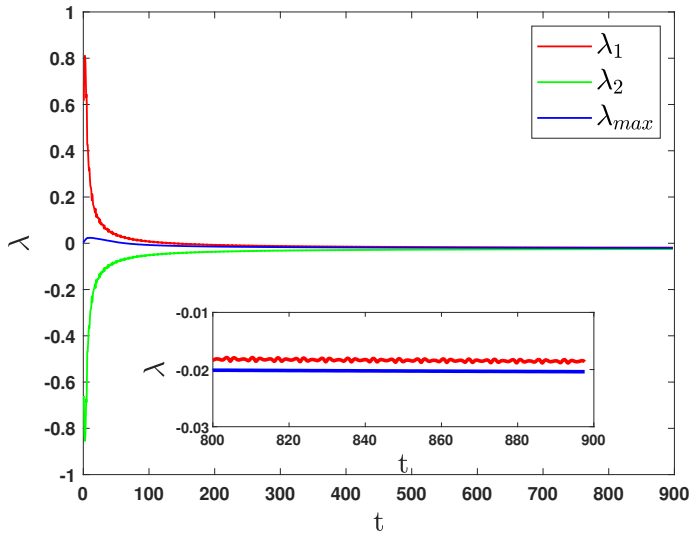


Figure 4.6: Estimation of Lyapunov Characteristic Exponents (LCEs) for a regular solution, $f_0 = 0.12$.

We present this in Figure 4.7.

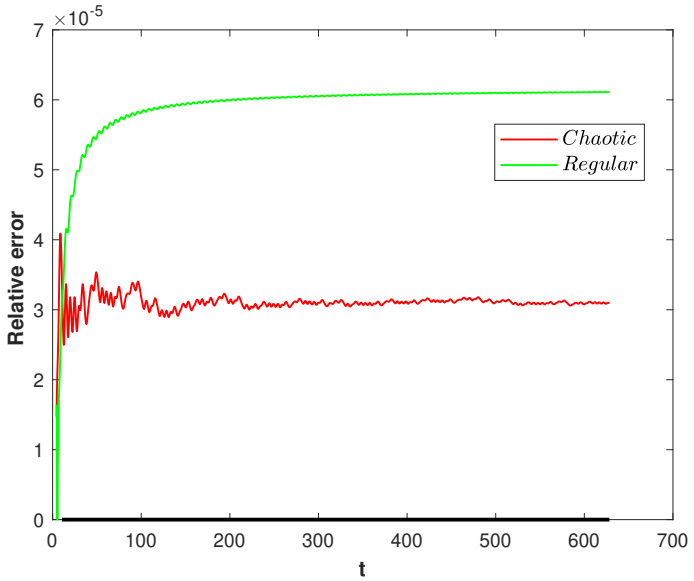
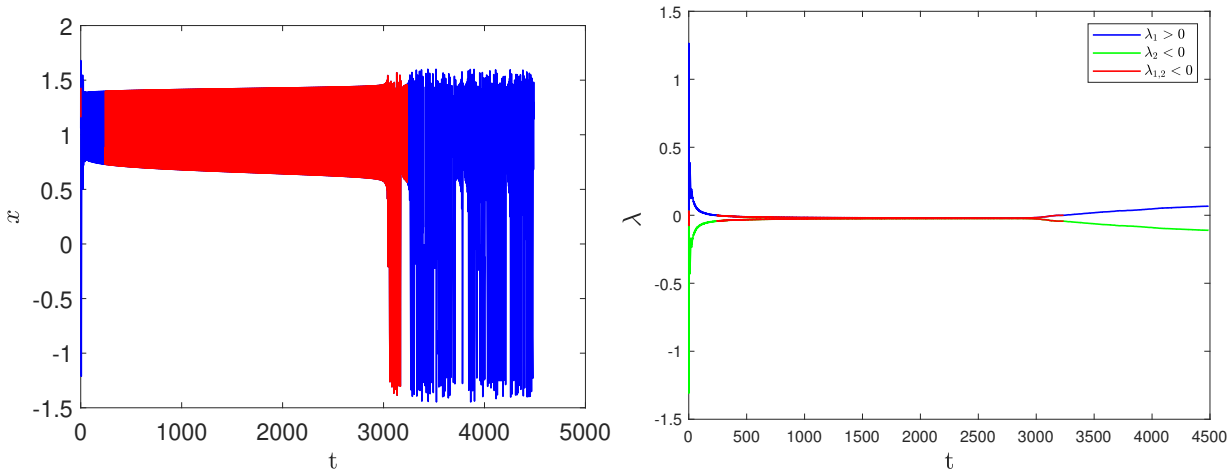


Figure 4.7: Accuracy of the conservation law (4.26) for $\alpha = 1.1$.

For the behaviour of a long regular regime followed by a chaotic one, the LCEs agree with the chaoticity of solutions. For intermittency with a long regular phase that ends in a chaotic behaviour, the exponents may tend to zero or even take a negative value but grow afterwards when the chaos is present, as in Figure 4.8.

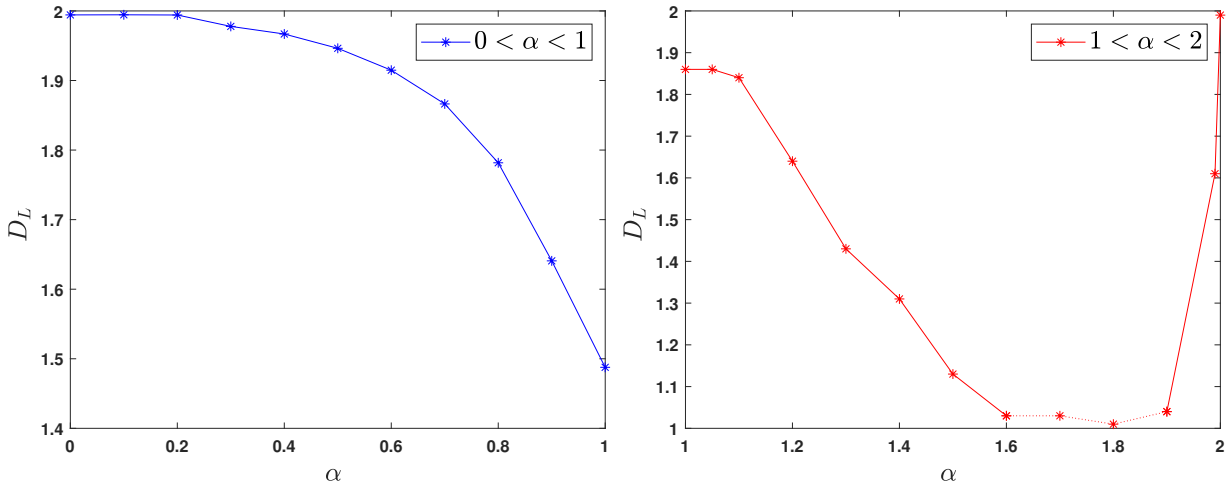


(a) Solution (b) Estimation of the LCEs

Figure 4.8: Estimation of the LCEs for a solution with a long regular phase, $\alpha = 1.1$, $f_0 = 0.4$, $x_0 = 1.05$, $v_0 = 1.06$.

For regular solutions with a long chaotic initial transient, the LCEs are computed only after this transient. Accordingly, the LCEs tend to have negative values as time increases.

Having estimated both Lyapunov exponents we can compute the Lyapunov dimension D_L given by (4.28). In Figure 4.9, we present D_L as a function of α for the threshold values.



(a) $0 < \alpha < 1$ (b) $1 < \alpha < 2$

Figure 4.9: Estimates of the Lyapunov dimension D_L versus α.

For values of $\alpha \in [1.6, 1.8]$, when the solution exhibits chaotic behaviour, the Lyapunov dimension approaches 1 rather than 2. The structure of the strange attractor in this range appears distinct from that of a Lyapunov dimension of 2. This observation is supported by Figure 4.9(b), where the dashed line represents this behaviour. However, for values of f_0

exceeding the threshold of chaos, the dynamics appear to behave as expected.

4.4 Extension of Melnikov method

Besides computing the Lyapunov Characteristic Exponents (LCEs) in the model studied as a tool to characterise chaos, as described in the preceding section, we aim to use another tool which is the extension of the Melnikov method to the fractional case.

This method is extensively employed for investigating chaos in dynamical systems. It is an analytic tool to ensure the existence of chaos in solutions of a dynamical system with specific critical points. We extend this approach to the fractional case.

4.4.1 Melnikov method for the classical Duffing equation

Melnikov began with the idea of considering a system described by a differential equation, in which one of its fixed points is a saddle point connected to itself by a homoclinic orbit. Based on such a system, the process of perturbing the system takes place with a time disturbance, which makes the stable and unstable manifolds of the fixed point intersect and this leads to the emergence of chaos [36, 133]. Given the system:

$$\begin{cases} \dot{X} = f(X) + \varepsilon g(t, X), \\ X \in \mathbb{R}^2, \\ t \in \mathbb{R} \end{cases} \tag{4.48}$$

where: $f \in C^2(\mathbb{R}^2)$ and $g \in C^2(\mathbb{R} \times \mathbb{R}^2)$ is periodic in t with period $T = \frac{2\pi}{\omega}$ and angular frequency ω. In the case of the classical Duffing equation, we rewrite (4.48) as a perturbed Hamiltonian system with Hamiltonian function $H(x, v)$:

$$\begin{cases} \dot{x} = \dfrac{\partial H}{\partial v}(x, v) + \varepsilon g_1(t, x, v), \\ \dot{v} = -\dfrac{\partial H}{\partial x}(x, v) + \varepsilon g_2(t, x, v) \end{cases} \tag{4.49}$$

Its vector form is:

$$\dot{q} = SDf(q) + \varepsilon g(t, q), \tag{4.50}$$

where:

- $q = (x, v)$.
- $Df = \left(\dfrac{\partial H}{\partial x}, \dfrac{\partial H}{\partial v} \right)$.
- $g = (g_1, g_2)$.
- $S = \begin{pmatrix} 0 & 1 \\ -1 & 0 \end{pmatrix}$.

There are some assumptions on (4.50). They are listed as follows:

- **Assumption 1**: for $\varepsilon = 0$, the unperturbed system $\dot{q} = SDf(q)$ has a hyperbolic fixed point p_0 connected to itself by a homoclinic orbit $q_0(t) = (x_0(t), v_0(t))$.
- **Assumption 2**: Let the homoclinic manifold $\Gamma_{p_0} = \{q \in \mathbb{R} \mid q = q_0(t), t \in \mathbb{R} \cup p_0\} = W^s(p_0) \cap W^u(p_0) \cap p_0$, with W^s the global stable manifold and W^u the global unstable manifold.

Under the previous assumptions the Melnikov function $M(t_0)$ is:

$$M(t_0) = \int_{-\infty}^{+\infty} e^{-\int_{-t_0}^{t} \nabla . f(q_0(s))ds} f\Big(q_0(t)\Big) \wedge g\Big(q_0(t, t+t_0)\Big)dt, \tag{4.51}$$

where $\wedge$ is the wedge product. Then, consider that $W^u(p_\varepsilon^{t_0})$ is the unstable Manifold and $W^s(p_\varepsilon^{t_0})$ is the stable Manifold of the system (4.50). Thus, the following theorem holds [36, 91]:

Theorem 1 *If $M(t_0)$ has simple zeros and is independent of ε, then, for $\varepsilon > 0$ small enough, $W^u(p_\varepsilon^{t_0})$ and $W^s(p_\varepsilon^{t_0})$ intersect transversely.*
If $M(t_0) > 0$ (or < 0) for all t_0 then:

$$W^u(p_\varepsilon^{t_0}) \cap W^s(p_\varepsilon^{t_0}) = \emptyset. \tag{4.52}$$

As $\varepsilon = 0$, $\nabla \cdot f = 0$, and the Melnikov function assumes a simpler form:

$$M(t_0) = \int_{-\infty}^{+\infty} f(q_0(t)) \wedge g(q_0(t, t+t_0))dt. \tag{4.53}$$

Hence, we are employing the Melnikov method to determine the threshold for chaos onset of the Duffing equation system.

Then, to compute the Melnikov function for (2.19), we rewrite it as the system (4.48) as follows:

$$\begin{cases} \dot{x} = v \\ \dot{v} = x - x^3 + \varepsilon(f_0 \cos(\omega t) - \gamma v) \end{cases} \tag{4.54}$$

Then, for $\varepsilon = 0$, we obtain the Hamiltonian system (2.17). Its Hamiltonian function is (2.18) and it has two homoclinic Orbits (2.19):

$$\begin{aligned} q_0^{\pm}(t) &= (X_0(t), V_0(t)) && (4.55) \\ &= \pm\Big(\sqrt{2}\text{sech}(t), -\sqrt{2}\text{sech}(t)\tanh(t))\Big) \\ &= \pm\left(\frac{\sqrt{2}}{\cosh(t)}, -\sqrt{2}\frac{\sinh(t)}{\cosh^2(t)}\right). && (4.56) \end{aligned}$$

Thus, the Melnikov function corresponds to the system (2.17) is given by (4.53). Substituting the two homoclinic orbits (4.56) in (4.53) gives the integral:

$$M(t_0, f_0, \gamma, \omega) = \int_{-\infty}^{+\infty} V_0(t) \left[f_0 \cos(\omega t + t_0) - \gamma V_0(t) \right] dt \tag{4.57}$$

$$= \sqrt{2} f_0 \int_{-\infty}^{+\infty} \operatorname{sech}(t) \tanh(t) \cos(\omega t) dt \tag{4.58}$$

$$-2\gamma \int_{-\infty}^{+\infty} \operatorname{sech}^2(t) \tanh^2(t) dt. \tag{4.59}$$

The Melnikov function for the Duffing equation is given by:

$$M(t_0, f_0, \gamma, \omega) = -\gamma \frac{4}{3} + f_0 \sqrt{2} \pi \omega \operatorname{sech}\left(\frac{\pi \omega}{2}\right) \sin(t_0 \omega). \tag{4.60}$$

It is sufficient to look at ω in terms of the ratio f_0/γ. This gives us the following threshold condition of the problem that we want to solve.

$$\frac{f_0}{\gamma} > \frac{4}{3} \frac{\cos(\pi \omega/2)}{\sqrt{2} \pi \omega}. \tag{4.61}$$

In the classical Duffing equation there is a competition between the amplitude of the external forcing f_0 and the coefficient of the dissipation γ. Melnikov method marks the boundary that separates the regular regime from the chaotic one [36]: chaos may appear only for values of the parameters that satisfy the condition (4.61).

4.4.2 Melnikov method for fractional Duffing equation

In [85], Niu, Jiangchuan, et al. investigate chaos detection in the Duffing system with fractional-order derivatives under external harmonic excitation, using the Melnikov method. They transform the system into a first-order approximate equivalent integer-order system using the harmonic balance method, enabling the application of the Melnikov method. Bifurcation and chaos analysis are investigated, supported by phase portraits.

Xing, Wuce, et al. [135] used the Melnikov method in the range $0 < \alpha < 1$. They investigated the fractional Duffing equation subjected to harmonic excitation, analysing how system coefficients impact the threshold value. Employing phase space and Poincaré maps, they illustrated the diverse behaviours observed within the system.

We aim to expand this method to investigate the onset of chaos of the fractional Duffing equation (3.1). To discern this onset, we employ two approaches to approximate the fractional integral that appears in the extended Melnikov function.

Extended Melnikov function for fractional Duffing equation

In the fractional model (3.1), we may look for different values of the parameters to see if a similar threshold exists.

The Melnikov function corresponds in this case to:

$$M(t_0, f_0, \gamma, \omega, \alpha) = \int_{-\infty}^{+\infty} V_0(t) \left[-\gamma D_t^\alpha X_0(t) + f_0 \cos(\omega t + t_0)\right] dt \tag{4.62}$$

$$= -\gamma \int_{-\infty}^{+\infty} V_0(t) D_t^\alpha X_0(t) dt + \int_{-\infty}^{+\infty} V_0(t) \left[\cos(\omega t + t_0)\right] dt,$$

$$\alpha \in (0,1) \cup (1,2). \tag{4.63}$$

We put:

$$K_\alpha = \int_{-\infty}^{+\infty} V_0(t) D_t^\alpha X_0(t) dt, \quad \alpha \in (0,1) \cup (1,2), \tag{4.64}$$

which is a fractional integral containing a fractional Caputo derivative of $X_0(t)$.

And, we assign the label K_2 to the second integral which retains its form (as in the classical case), in the fractional equation.

$$K_2 = \int_{-\infty}^{+\infty} V_0(t) \left[\cos(\omega t + t_0)\right] dt = \sqrt{2}\pi\omega \operatorname{sech}\left(\frac{\pi\omega}{2}\right) \sin(t_0\omega). \tag{4.65}$$

Thus:

$$M(t_0, f_0, \gamma, \omega, \alpha) = -\gamma K_\alpha + f_0 K_2. \tag{4.66}$$

In accordance with Melnikov theory [83], this gives rise to:

$$M(t_0, f_0, \gamma, \omega, \alpha) = -\gamma K_\alpha + f_0 K_2 = 0 \tag{4.67}$$

The necessary condition that should be obtained, corresponding to the onset of chaos in the fractional Duffing equation is:

$$\frac{f_0}{\gamma} > \frac{K_\alpha}{K_2}. \tag{4.68}$$

As no fractional-order derivative is present in K_2, it remains unchanged from the classical case. Thus, the problem is now to evaluate the fractional term (4.64). Splitting it into two integrals, thus:

$$K_\alpha = 2\int_0^{\infty} V_0(t) D_t^\alpha X_0(t) dt, \quad \alpha \in (0,1) \cup (1,2). \tag{4.69}$$

To approximate (4.69), we substitute in it, the Caputo derivative of the x-component $X_0(t)$ of (4.56):

$$\alpha \in (0,1): \qquad K_\alpha = \frac{2}{\Gamma(1-\alpha)} \int_0^\infty V_0(t) \left(\int_0^t \frac{V_0(s)}{(t-s)^\alpha}\, ds \right) dt, \tag{4.70}$$

$$\alpha \in (1,2): \qquad K_\alpha = \frac{2}{\Gamma(2-\alpha)} \int_0^\infty V_0(t) \left(\int_0^t \frac{V_0'(s)}{(t-s)^{\alpha-1}}\, ds \right) dt. \tag{4.71}$$

Let us verify whether the inner integral of $V_0(t)$ in (4.70) and $V_0'(t)$ in (4.71) can be approximated numerically. To achieve this, we will first examine their asymptotic behaviour after transforming them to exponential form:

$$V_0(t) = -\sqrt{2}\, \frac{\sinh(t)}{\cosh^2(t)} = -2\sqrt{2} e^{-t} \frac{1-e^{-2t}}{(1+e^{-2t})^2}, \tag{4.72}$$

$$V_0'(t) = \sqrt{2} \left(\frac{-1}{\cosh(t)} + \frac{2\sinh^2(t)}{\cosh^3(t)} \right) = 2\sqrt{2} e^{-t} \left(\frac{-1}{1-e^{-2t}} + \frac{2(1-e^{-2t})^2}{(1+e^{-2t})^3} \right). \tag{4.73}$$

The graphics of these two functions are presented in Figure 4.10.

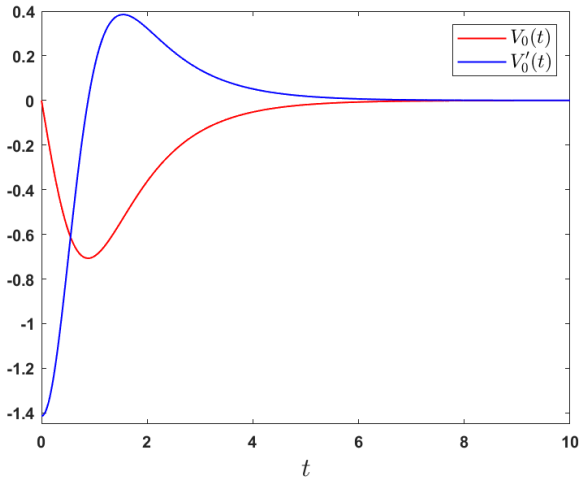


Figure 4.10: Graphics representations of the two functions V_0 (4.72) and V_0' (4.73).

Both of them have an interesting behaviour: their values are small after some time. The fractional integrals can be numerically computed, either directly or by truncation. The asymptotic behaviour as t grows is that of the exponential e^{-t}, for both functions as presented in Figure 4.11.

We may unify both expressions (4.70) and (4.71) into just one defining, as follows:

$$K_\alpha := \frac{2}{\Gamma(1-\beta)} \int_0^\infty V_0(t) \left(\int_0^t \frac{z(s)}{(t-s)^\beta}\, ds \right) dt, \quad \beta \in (0,1), \tag{4.74}$$

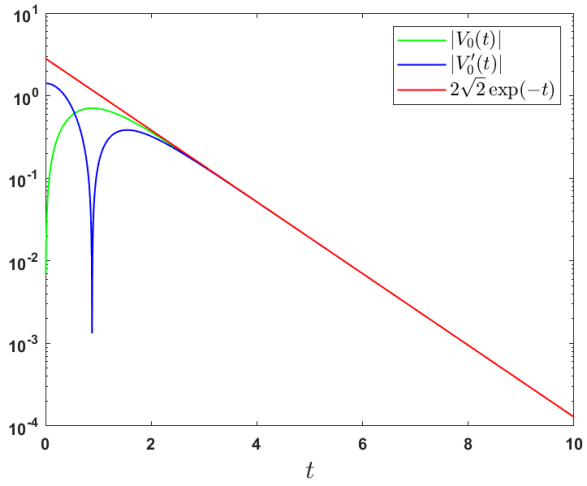


Figure 4.11: Functions x' and x'' in semi-logarithmic scale compared to the exponential.

with $z(s) := x^{(\lceil\alpha\rceil)}$. It has the following expression:

$$z(s) = \sqrt{8}(-1)^{\lceil\alpha\rceil}\exp^{-s}\left(\frac{\frac{-1}{1+e^{-2s}} - \left(\frac{-1}{1+e^{-2s}}\right)^{\lceil\alpha\rceil}}{\frac{-1}{1+e^{-2s}}} + 2^{\lfloor\alpha\rfloor}\frac{(1-e^{-2s})^{\lceil\alpha\rceil}}{(1+e^{-2s})^{\lceil\alpha\rceil+1}}\right), \quad (4.75)$$

and $\beta := \alpha + 1 - \lceil\alpha\rceil$.

4.4.3 Numerical integration methods chosen to approximate the fractional integral K_α

The idea developed in this section is to fix a numerical value for α and use suitable numerical methods to compute the integrals of K_α. As (4.74) is composed of two integrals, let us use the following notation:

- Let be I_s the integral in terms of s:

$$I_s(t) := \int_0^t \frac{z(s)}{(t-s)^\beta}\,ds \quad \beta \in (0,1), \quad (4.76)$$

Then, K_α becomes:

$$K_\alpha := \frac{2}{\Gamma(1-\beta)}\int_0^\infty V_0(t)I_s(t)dt, \quad \beta \in (0,1). \quad (4.77)$$

We will use two numerical integration methods for each integral in (4.77): to perform on one hand the integral in t and, on the other, the integral in s. We select:

- Gauss-Jacobi integration for the definite integral $I_s(t)$ (4.76),

- Gauss-Laguerre integration for the definite integral (4.77).

We present its general definitions in the following subsections.

Gauss-Laguerre quadrature

The Gauss-Laguerre quadrature [33] is a numerical integration method used to approximate a weighted integral of a function f over $[0, +\infty)$ of the form:

$$\int_0^\infty e^{-t} f(t)\, dt. \tag{4.78}$$

The generated formula with j nodes is expressed as:

$$\int_0^\infty e^{-t} f(t)\, dt = \sum_{i=1}^{j} w_i f(t_i) + E_j, \tag{4.79}$$

where:

- j is the number of nodes and weights used in the approximation (the degree of the quadrature),
- L_j is the Laguerre polynomial,
- t_i, $i = \{1, \ldots, j\}$, are the roots of Laguerre polynomial L_j,
- w_i are the quadrature weights, given by:

$$w_i = \frac{t_i}{(j+1)^2 [L_{j+1}(t_i)]^2}\,. \tag{4.80}$$

- Its error can be expressed as:

$$E_j = \frac{f^{(2j)}(\xi)}{(2j)!} \int_0^\infty x^j e^{-x}\, dx,\ \xi \in (0, +\infty). \tag{4.81}$$

There are non-trivial properties for the roots, the weights and the polynomials that allow to compute those values.

Since, in our case, the exponential appears naturally in both (4.72) and (4.73), this method can be well suited. In order to compute the integral, though, it is necessary to know the values of the other integral at all the chosen t_i values. This implies performing j evaluations of the second integral (4.76).

Gauss-Jacobi quadrature

Gauss-Jacobi quadrature is a numerical quadrature method rooted in Gaussian quadrature principles. This method is designed for integrals of the form:

$$\int_{-1}^{1} (1-v)^a (1+v)^b f(v)\, dv, \quad a, b > -1\,. \tag{4.82}$$

In our case, we will have to convert our integral from interval $[0, t]$ to the interval $[-1, 1]$. The quadrature formula is given by:

$$\int_{-1}^{1}(1-v)^a(1+v)^b f(v)\,dv = \sum_{k=1}^{n}\lambda_k f(v_k) + E_n. \tag{4.83}$$

The values v_k are the roots of the Jacobi polynomial of order n, $P_n^{(a,b)}$. They can be calculated by applying the explicit form of the Rodríguez formula [6]:

$$P_n^{(a,b)} \;=\; 2^{-n}\sum_{k=0}^{n}\binom{n+a}{k}\binom{n+b}{n-k}(x-1)^{n-k}(x+1)^k. \tag{4.84}$$

Its first order derivative $P_n'^{(a,b)}$ has the following formula:

$$\frac{d}{dx}\left[P_n^{(a,b)}(x)\right] \;=\; \frac{1}{2}(n+a+b+1)P_{n-1}^{(a+1,b+1)}. \tag{4.85}$$

The weights λ_k are given by:

$$\lambda_k = -\frac{2n+a+b+2}{n+a+b+1}\,\frac{\Gamma(n+a+1)\Gamma(n+b+1)}{(n+1)!\,\Gamma(n+a+b+1)}\,\frac{2^{a+b}}{P_n^{(a,b)\prime}(v_k)P_{n+1}^{(a,b)}(v_k)}\,. \tag{4.86}$$

The error term is:

$$E_n = \frac{\Gamma(n+a+1)\Gamma(n+b+1)\Gamma(n+a+b+1)}{(2n+a+b+1)[\Gamma(2n+a+b+1)]^2}\frac{2^{2+a+b+1}}{(2n)!}f^{(2n)}(\xi),\ \xi\in]-1,+1[. \tag{4.87}$$

Implementation in our case

We use Gauss-Jacobi quadrature to approximate the integral given in equation (4.76). First, we transform it to an integral over $[-1, 1]$, defining the new variables:

$$v = \frac{2}{t}s - 1\,,\quad s = \frac{t}{2}(v+1),\quad ds = \frac{t}{2}\,dv\,. \tag{4.88}$$

Using (4.88) in (4.76) gives:

$$I_s(t) = \frac{t}{2}\int_{-1}^{1}\frac{y\left(\frac{t}{2}(v+1)\right)}{\left[t-\frac{t}{2}(v+1)\right]^{\beta}}\,dv,\quad \beta\in(0,1). \tag{4.89}$$

Then:

$$I_s(t) = \left(\frac{t}{2}\right)^{1-\beta}\int_{-1}^{1}(1-v)^{-\beta}y\Big(s(v)\Big)\,dv\,. \tag{4.90}$$

After writing (4.76) as an integral over $[-1,1]$, we identify now the parameters with those in the Gauss-Jacobi quadrature formula (4.83). Then, we obtain:

$$a = -\beta \in (-1,0), \quad b = 0, \tag{4.91}$$

the two parameters (4.91) satisfy the conditions of Gauss-Jacobi quadrature, and, thus,

$$I_s(t) \approx \left(\frac{t}{2}\right)^{1-\beta} \sum_{k=1}^{n} \lambda_k y\Big(s(v_k)\Big). \tag{4.92}$$

In this case, the values λ_k are the roots of the Jacobi polynomial $P_n^{(-\beta,0)}$ of order n.

We need now the values of the roots and of the weights associated with this Jacobi polynomial for the n values that we choose. Now, we substitute $V_0(t)$ from (4.56) in the integral (4.77) to obtain:

$$\begin{aligned} K_\alpha &= \frac{2}{\Gamma(1-\beta)} \int_0^\infty V_0(t) I_s(t) dt \\ &= \frac{2}{\Gamma(1-\beta)} \int_0^\infty \left[-2\sqrt{2} e^{-t} \frac{1-e^{-2t}}{(1+e^{-2t})^2} \right] I_s(t) dt \\ &= \int_0^\infty e^{-t} \left[\frac{-4\sqrt{2}}{\Gamma(1-\beta)} \frac{1-e^{-2t}}{(1+e^{-2t})^2} I_s(t) \right] dt \\ &= \int_0^\infty e^{-t} f(t) dt, \quad \beta \in (0,1), \end{aligned} \tag{4.93}$$

where:

$$f(t) = \frac{-4\sqrt{2}}{\Gamma(1-\beta)} \frac{1-e^{-2t}}{(1+e^{-2t})^2} I_s(t). \tag{4.94}$$

With this, we can apply the Gauss-Laguerre quadrature to (4.93).

This has to be done for every value $t = t_i$, with $i = 1, \ldots, j$, and j the order of the Gauss-Laguerre integration.

Once the values $I_s(t_i)$, $i = 1, \ldots, j$, are known, and given (4.72) and (4.73), the double integral, K_α, given by (4.77), is approximated as:

$$\begin{aligned} K_\alpha &\approx -\frac{4\sqrt{2}}{\Gamma(1-\beta)} \sum_{i=1}^{j} w_i \frac{1-e^{-2t_i}}{(1+e^{-2t_i})^2} I_s(t_i) \\ &= -\frac{4\sqrt{2}}{\Gamma(1-\beta)} \sum_{i=1}^{j} w_i \frac{1-e^{-2t_i}}{(1+e^{-2t_i})^2} \left(\frac{t_i}{2}\right)^{1-\beta} \left(\sum_{k=1}^{n} \lambda_k y\Big(s(v_k)\Big) \right). \end{aligned} \tag{4.95}$$

The coefficients w_i and the roots t_i are independent of β but this is not the case for the λ_k's, and for the v_k's: they must be determined for each value of β that is considered. They also depend on t_i. The scheme of dependences would be something like this table, once a value of β is chosen:

For fixed j and n		
t_1, w_1	β	$v_1, \ldots, v_n; \lambda_1, \ldots, \lambda_n$
t_2, w_2		$v_1, \ldots, v_n; \lambda_1, \ldots, \lambda_n$
$\vdots$		$\vdots$
t_j, w_j		$v_1, \ldots, v_n; \lambda_1, \ldots, \lambda_n$

Table 4.1: Dependency scheme illustrating the calculation of K_α using coefficients ω_i, roots t_i, and functions v_k, λ_k based on the chosen value of β

4.4.4 Numerical and analytic onset of chaos

After computing K_α (4.95) for various values of α ranging from 0 to 2. We can now approximate (4.68). In Figure 4.12, We present the threshold of chaos obtained numerically. This threshold is established based on the fractional Melnikov function.

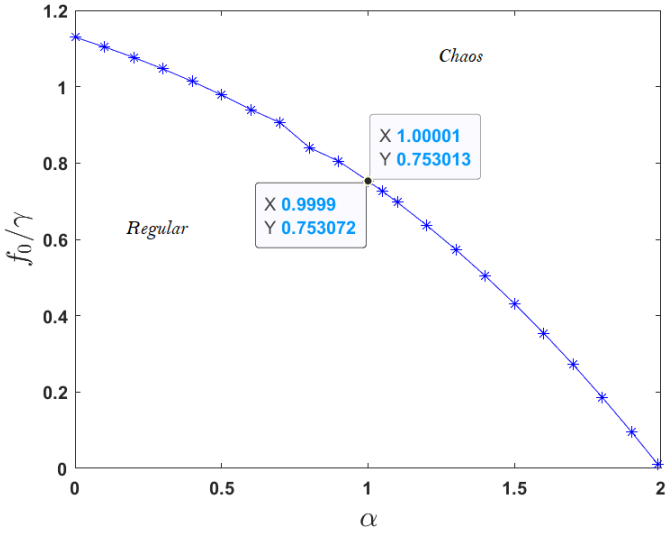


Figure 4.12: Chaos threshold Obtained by the Melnikov extension for $0 < \alpha < 2$.

In Figure 4.12, we represent the numerical results of the threshold obtained, the steps of producing this onset of chaos seem relevant and correct. We note that for the values of α near 1, we recover the same classical analytic threshold. We need now to compare it with the numerical threshold obtained from the behaviour of the solution.

From all our computations we have obtained a numerical estimation of the threshold separating the regular regime from that where chaotic solutions are found, depending on the values of α and f_0, keeping γ fixed. In Figure 4.13, we present the resulting curve of α versus f_0/γ.

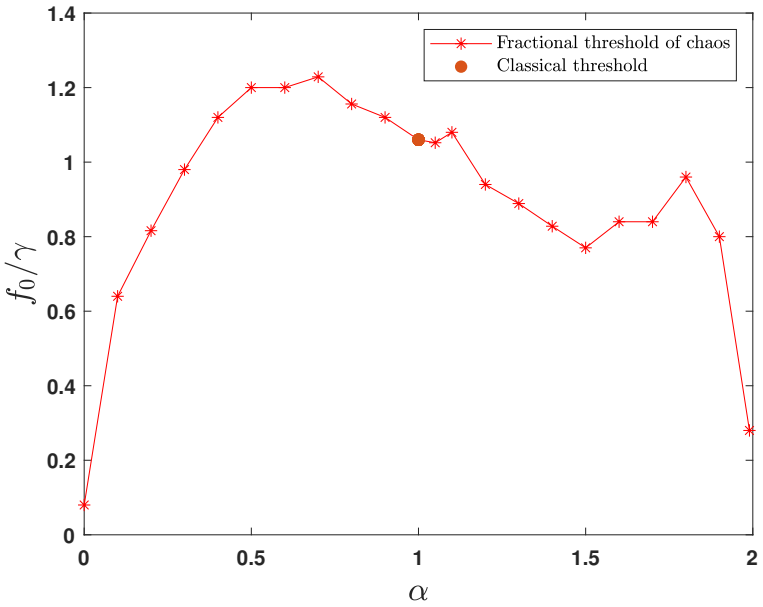


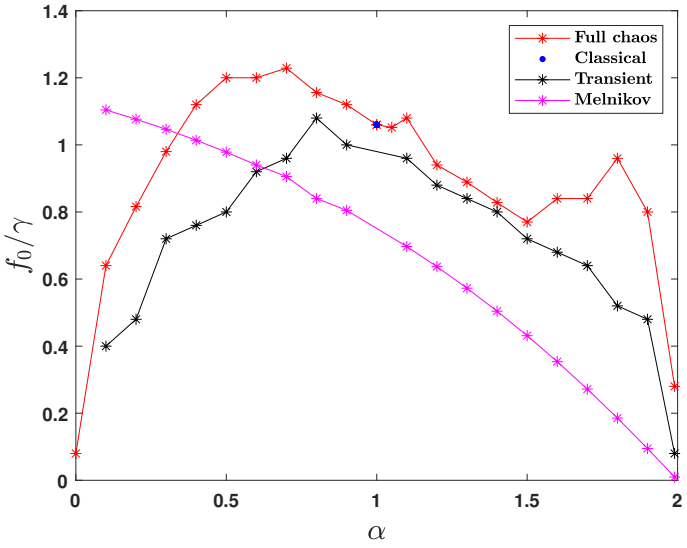
Figure 4.13: Numerical threshold for chaos.

The results presented in Figure 4.13 correspond to full chaos.

If we define the chaos threshold solely based on the presence of prolonged chaotic transients, we observe that the onset of chaos for different values of f_0 occurs at smaller magnitudes compared to when chaos is fully established.

Figure 4.14 illustrates the relationship between α and f_0/γ for three distinct scenarios of chaos onset:

- In the case of chaotic transients alone (represented by the black curve), the numerical threshold closely approximates the theoretical one.
- For situations of full chaos or intermittency (illustrated by the red curve), the chaos threshold is determined only when the solution exhibits complete chaos or intermittency.
- The pink curve represents the numerical outcomes obtained from the Melnikov extension.



(a)

Figure 4.14: Comparison of theoretical and numerical chaos thresholds Derived from the Melnikov extension method

In the classical Duffing equation, the analytic value of the threshold of chaos given by (4.61) appears for $f_0/\gamma \approx 0.75$ [36]. Numerically, the value of the threshold appears to be at $f_0/\gamma = 1.06$ as shown in Figure 4.13 (the curve of the classical case), which satisfies the Melnikov criteria but is significatively above.

In the fractional case, we recover the numerical value of the threshold of the classical case for the values of α near 1, as shown in Figure 4.13.

Observations indicate that the system behaves differently at its limits ($\alpha \to 0^+$ and $\alpha \to 1^-$) compared to the classical case. This discrepancy becomes evident when comparing the numerical threshold with the analytic one, as there is a rough correspondence within the range of $0.5 < \alpha < 1.5$. However, this correspondence is lost for the extreme values. Consequently, it can be concluded that the applicability of the Melnikov function is limited to the vicinity of the classical case, and it may not be suitable for the remaining range.

4.5 Limiting cases

The fractional equation has three distinct non-fractional limiting cases. They correspond to the three integer values of α:

- $\alpha = 1$.
- $\alpha = 0$.
- $\alpha = 2$.

Since the dependence on α is continuous, the behaviour of the fractional model tends to

that of the limiting cases as α tends to an integer. The central case, $\alpha = 1$, corresponds to the classical Duffing Equation. The remaining two values correspond, basically, to the same model, as we will see below.

To understand the behaviour of the solution of fractional equation (3.1) in the limits and illustrate its distinct behaviours, we require a comprehensive examination of the fractional equation at these limits.

We must then compare it with the classical case of the non-fractional equation, specifically the undamped forced Duffing equation. In this classical scenario, there is no dissipation in the system, rendering γ no longer a damping parameter.

4.5.1 Non-fractional equation: undamped forced Duffing equation

In the limit $\alpha \to 0^+$, the fractional derivative gives the identity operator [56]:

$$D_t^{0^+} x(t) = x(t), \tag{4.96}$$

and we have the equation:

$$\ddot{x} + (\gamma - 1)x + x^3 = f_0 \cos(\omega t). \tag{4.97}$$

In the limit $\alpha \to 2^-$, the fractional derivative corresponds to the second order derivative [56]:

$$D_t^{2^-} x(t) = \ddot{x}(t), \tag{4.98}$$

this gives the following:

$$(1 + \gamma)\ddot{x} - x + x^3 = f_0 \cos(\omega t). \tag{4.99}$$

Provided $\gamma - 1 < 0$, both equations (4.97) and (4.99) correspond to a conservative system perturbed by a periodic driving force. The difference between them is only in the value of some of the coefficients. Thus, the fractional model ends up, in both these extreme limits, modelling the same qualitative system. Let us present its general features.

Let be the general undamped forced Duffing equation with a positive nonlinear term:

$$m\ddot{x} - ax + x^3 = f_0 \cos(\omega t), \tag{4.100}$$

where m and a are two positive constants. Thus, the undamped forced Duffing system is:

$$\begin{cases} \dot{x} = v, \\ m\dot{v} = ax - x^3 + f_0 \cos(\omega t). \end{cases} \tag{4.101}$$

It corresponds to time-dependent a Hamiltonian system whose Hamiltonian function is:

$$H(x, y) = \frac{1}{2m}\dot{x}^2 - \frac{a}{2}x^2 + \frac{x^4}{4} - f_0 x \cos(\omega t). \tag{4.102}$$

The unforced system corresponds to:

$$\begin{cases} \dot{x} = v, \\ m\dot{v} = ax - x^3, \end{cases} \tag{4.103}$$

and has three critical points: two centers, located at $(+\sqrt{a}, 0)$ and $(-\sqrt{a}, 0)$, and a saddle point at the origin. The unstable equilibrium point $(0, 0)$ is connected to itself by two homoclinic orbits [36]. This is, basically, the same Hamiltonian (2.18) on which the classical Duffing equation is built.

The presence of the forcing term introduces a period that competes with the internal periods of the unperturbed Hamiltonian system. This mechanism allows chaotic solutions to exist. Nevertheless, it is possible to show that solutions in the plane xv are bounded between regular curves such that for large initial values the chaotic behaviour is suppressed [19].

The regular and the chaotic regions of the phase space can be visualized using the stroboscopic map with the period of the external force, $T = 2\pi/\omega$. For the numerical simulations, we use the Strauss-Vázquez approach [50]:

$$m\left(\frac{x_{n+1} - 2x_n + x_{n-1}}{\triangle t^2}\right) + \frac{U(x_{n+1}) - U(x_{n-1})}{x_{n+1} - x_{n-1}} = f_0 \frac{\cos(\omega t_{n+1}) + \cos(\omega t_{n-1})}{2}, \tag{4.104}$$

where U is the potential (2.13). This method gives an exact discrete counterpart of the variation law of the Hamiltonian (4.102).

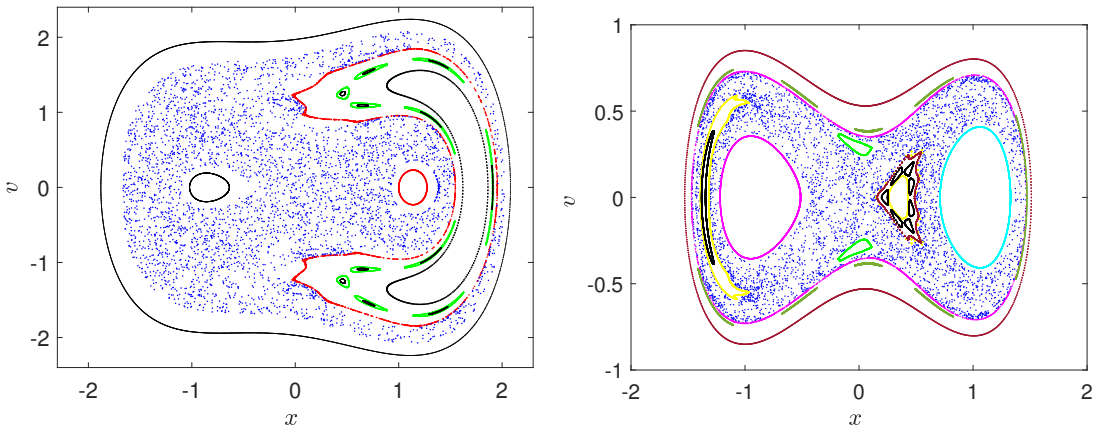
In the cases of fractional limits, we encounter two scenarios of the undamped forced Duffing equation, denoted as (4.97) and (4.99), both of which follow the general form (4.100) but have distinct sets of coefficients.

Exploring various combinations of γ and f_0 in each scenario reveals a confined central chaotic region, possibly containing internal structures resembling regularity islands.
Beyond this central region, the system consistently exhibits regular behaviour. However, due to variations in the coefficients between the two limits, the solution may not display the same attractor but the qualitative behaviour is the same.

With ω set to 1, we keep the parameters f_0 and γ variable. As we adjust γ, ranging between 0 and 1, we examine the system's behaviour. Notably, for values of γ approaching 0, the system exhibits similar chaotic attractors, resulting in the coefficients of (4.97) and (4.99) being closely aligned.

We illustrate the behaviour of the system with some different cases.

- In Figure 4.15 we present two examples for $\gamma = 0.01, f_0 = 0.13$ and $\gamma = 0.25, f_0 = 0.03$, and for both sets of parameters, the behaviour is similar in both cases.

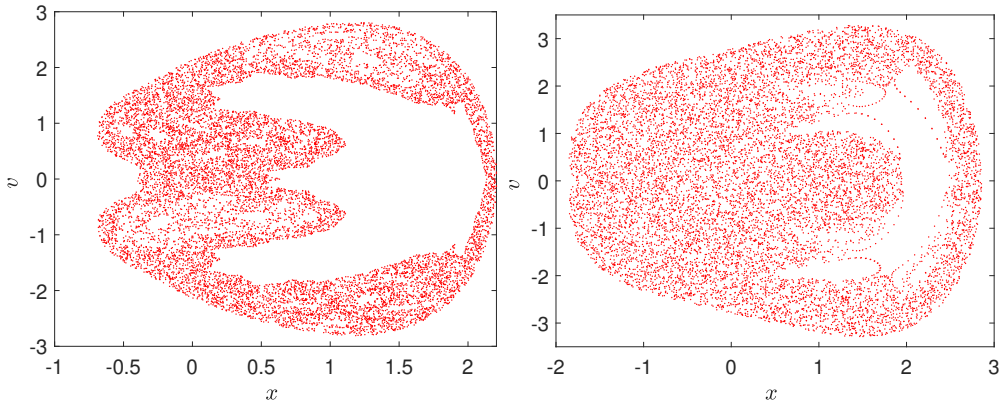


(a) $f_0 = 0.13$, $m = 1.01$, $a = 1$ (b) $f_0 = 0.03$, $m = 1.25$, $a = 1$

Figure 4.15: Stroboscopic maps for Equation (4.100). Different colors correspond to different initial conditions.

As γ values approach 1, unique attractors emerge at each limit. To illustrate this phenomenon, we provide two distinct examples featuring different f_0 values. Specifically, we focus on the case where $\gamma = 0.9$ (near 1) and the initial conditions are $x_0 = v_0 = 0$.

- In Figure 4.16, for $f_0 = 1$:

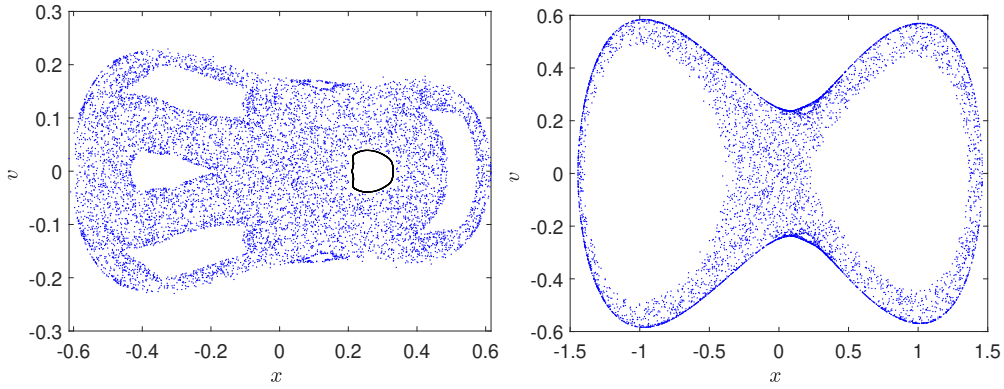


(a) $f_0 = 1, m = 1, a = 0.1$ correspond to (4.97) (b) $f_0 = 1$, $m = 1.9$, $a = 1$, correspond to (4.99)

Figure 4.16: Stroboscopic maps for equation (4.100) for value of $f_0 = 1$, shows a different chaotic attractors.

Although the parameters and the initial conditions are the same, the behaviour of the strange attractor is quite different.

- In Figure 4.17, for $f_0 = 0.03$:



(a) $f_0 = 0.03$, $m = 1$, $a = 0.1$ correspond to (4.97)

(b) $f_0 = 0.03$, $m = 1.9$, $a = 1$ correspond to (4.99)

Figure 4.17: Stroboscopic maps for Equation (4.100) for $f_0 = 0.03$, shows a different chaotic attractors.

It is important to note that the chaos in the solutions of equation (4.100) is quite different from that exhibited by the classical Duffing's equation. This is mainly because no dissipation is present. The absence of damping in the undamped forced Duffing equation (4.100), can lead to the emergence of islands of stability within chaotic regions, where trajectories exhibit regular or periodic behaviour amidst the surrounding chaos.

The trace of the Jacobi matrix of the system is now always zero and the Lyapunov exponents have the same value with opposed signs. If we extend the Lyapunov dimension as defined by (4.28), the value for chaotic solutions is always 2. These features are closer to that of chaos in Hamiltonian systems.

The boundedness of the chaotic part, and the solutions in general, can be seen in Figure 4.15, Figure 4.16 and Figure 4.17 where we show the central chaotic region that corresponds to small initial data and the regular behaviour of solutions with large initial data, for four different settings of the parameters and several initial values.

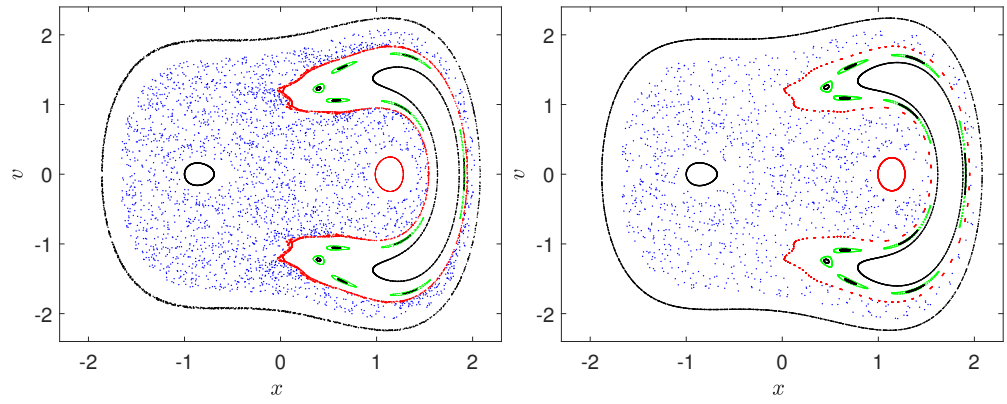
4.5.2 Fractional Duffing equation near the limits

Now, let us illustrate the behaviour of the fractional system for values of α nearing the limit cases by varying both parameters γ and f_0.

We have considered the typical regime ($\gamma - 1 < 0$) where both m and a are positive. We discard the case where ($\gamma - 1 > 0$) which is featureless since the system has a single critical point at the origin $(0, 0)$ that is a centre. We present some solutions for different combinations of parameters and compare them with the classical cases mentioned above, Subsection 4.5.1.

- In Figure 4.18 for $f_0 = 0.13$, $\gamma = 0.01$, $\omega = 1$:

  The similarity to the classical case, when choosing the same parameters and the same initial conditions as in Figure 4.15(a), is striking. For large initial conditions, all solutions

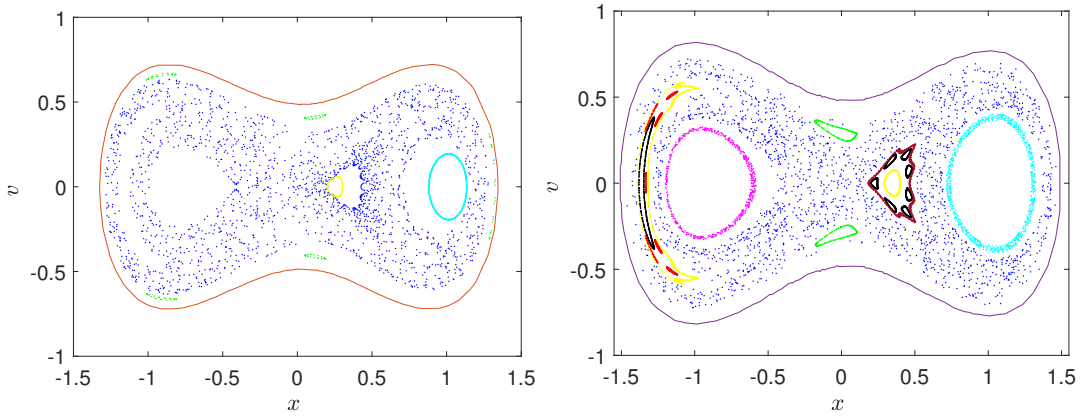


(a) $\alpha = 0.00001$ (b) $\alpha = 1.999999$

Figure 4.18: Stroboscopic maps for both limits with $f_0 = 0.13$, $\gamma = 0.01$, $\omega = 1$ shows the similarity to the classical case (Figure 4.15(a)).

are regular.

- In Figure 4.19 for $f_0 = 0.03$, $\gamma = 0.25$, $\omega = 1$:

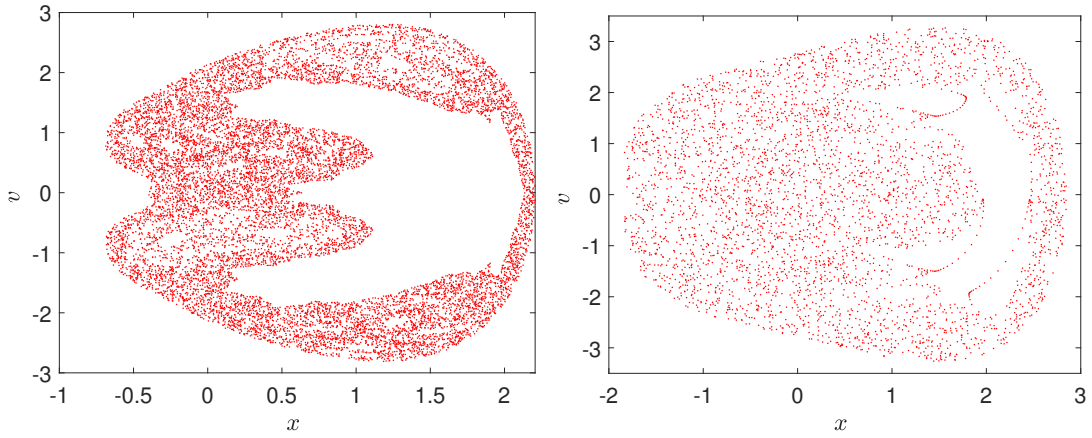


(a) $\alpha = 0.0001$ (b) $\alpha = 1.9999$

Figure 4.19: Stroboscopic maps for α near to 1 and 2 for $f_0 = 0.03$, $\gamma = 0.25$, $\omega = 1$.

Although the similarity with the classical case is not as striking as previously, it is clear that the structure is the same.

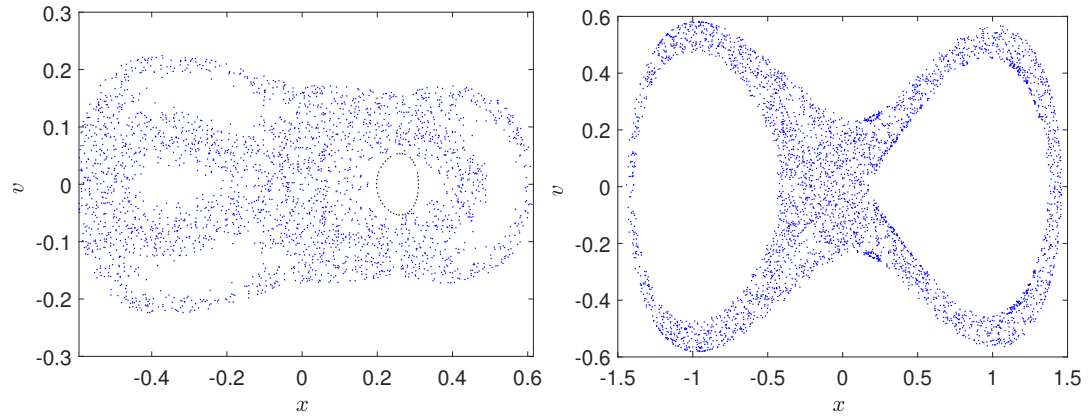
- In Figure 4.20 we present the strange attrator for $f_0 = 1, \gamma = 0.9$ for both limits as $\alpha = 1e - 07$ and $\alpha = 1.999999$ which are very similar to the classical case Figure 4.16(a) and Figure 4.16(b) respectively.



(a) $\alpha = 1e-07$ (b) $\alpha = 1.999999$

Figure 4.20: Stroboscopic maps for α near to 1 and 2 for $f_0 = 1$, $\gamma = 0.9$, $\omega = 1$, $x_0 = v_0 = 0$.

- In Figure 4.21 for $f_0 = 0.03, \gamma = 0.9, x_0 = v_0 = 0$, for both limits as $\alpha = 1e-07$ and $\alpha = 1.999999$:

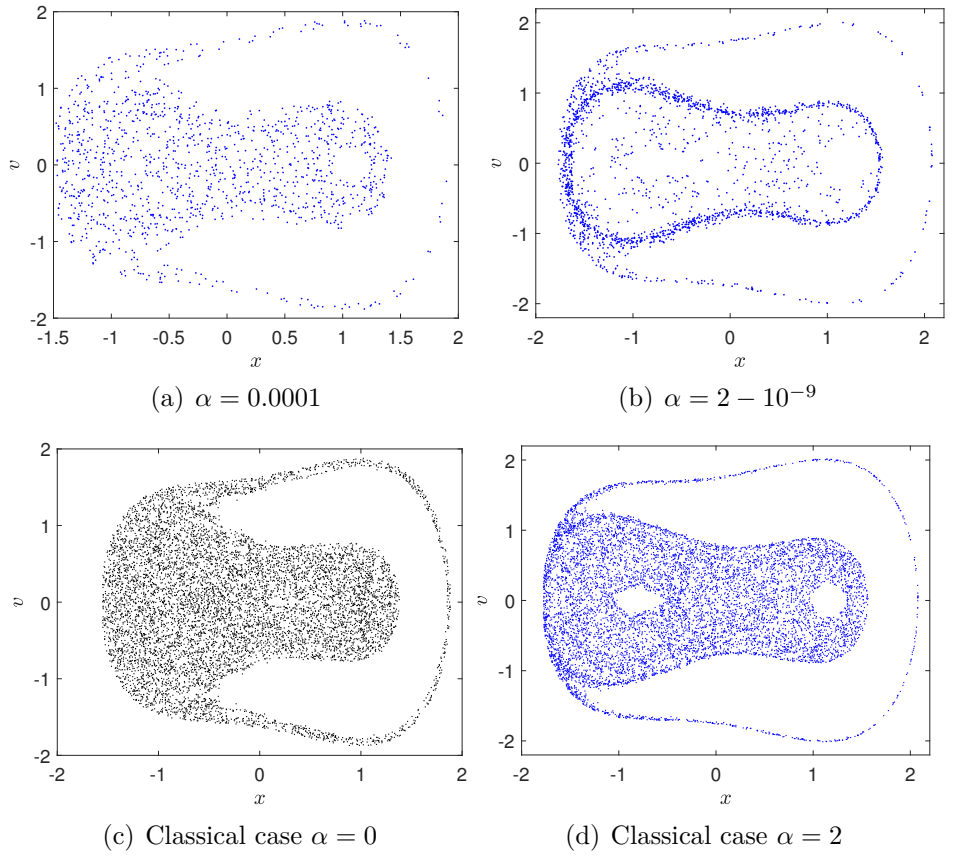


(a) $\alpha = 0.00001$ (b) $\alpha = 1.999999$

Figure 4.21: Stroboscopic maps for α near to 1 and 2 for $f_0 = 0.03$, $\gamma = 0.9$, $\omega = 1$.

The similarity is clear in comparison with the classical case Figure 4.17(a) and Figure 4.17(b).

- In Figure 4.22 for $f_0 = 0.1, \gamma = 0.25, x_0 = 0.25, v_0 = 0.2, \omega = 1$:



(a) $\alpha = 0.0001$ (b) $\alpha = 2 - 10^{-9}$

(c) Classical case $\alpha = 0$ (d) Classical case $\alpha = 2$

Figure 4.22: Stroboscopic maps showing the chaotic region of both limit cases: $f_0 = 0.1$.

We have computed the Lyapunov Dimension where we note that it is close to 2 in both limits as shown in Figure 4.9.

$\alpha \to 1$: The fractional derivative corresponds in this limit to the first order derivative [56]:

$$D_t^1 x(t) = \dot{x}(t), \tag{4.105}$$

and we obtain the classical Duffing equation (2.28). The strange attractor obtained as $\alpha \to 1$ with values above or below 1 tends to be the classical one (Section 2.3).

While the system lacks symmetry concerning α, this asymmetry does not impact the behaviour of the fractional system as it approaches any of the three classical limits. As α approaches 0 or 2, both limits manifest analogous behaviours, akin to a scenario suggestive of symmetry.

Chapter 5

Intermittency

Dynamical systems exhibit a range of behaviours, including periodic and chaotic patterns. Three main routes have been identified during the transition between these behaviours: period-doubling, quasiperiodicity, and intermittency [83, 90]. Intermittency, in particular, is frequently observed in various physical phenomena [126, 80]. In this chapter, we present our results concerning intermittency in the fractional equation. To analyse the behaviour in the fractional system, we start with the theory of intermittency, and especially, with results for the classical Duffing equation. We use this to validate the tools that we apply to analyse the fractional model.

5.1 Theory of the main types of chaotic intermittency

Intermittency denotes a phenomenon characterised by sporadic irregular behaviour. This behaviour is marked by chaotic bursts or abrupt transitions that occur intermittently, rather than continuously.

These bursts or transitions occur randomly over time, interspersed between regular periods. The duration of these stable periods, often referred to as laminar phases, varies in length.

However, as a control parameter is gradually increased, the system experiences a gradual reduction in the duration of these laminar phases until eventually transitioning into a state of chaos. The regular or laminar phases represent regions of pseudo-equilibrium, pseudo-periodic solutions, or quasi-invariant objects. In these phases, the system may persist for extended periods. Conversely, the burst phases are regions where the system's evolution becomes chaotic.

The intermittency phenomenon can be understood by considering a control parameter, represented by f. When f is below a critical value, the system's behaviour appears to be periodic, quasiperiodic, or in any case, regular. However, when the control parameter slightly exceeds this critical value (known as the intermittency threshold), the system enters an intermittent dynamic regime. Even though it is somewhat specific and special, the intermittent regime should still be regarded as a form of chaotic regime.

This intermittent regime becomes progressively more challenging until the system transitions into a state of full chaos.

Traditionally, intermittency has been categorized in three types I, II, and III based on the Floquet multipliers (see Appendix A) of the periodic solution in continuous systems, or the eigenvalues of the Jacobi matrix for fixed points in the local Poincaré map. In these classifications, when the control parameter f surpasses a critical threshold (let us denote it by f_c), a fixed point of the local Poincaré map (or a periodic solution of the system) becomes unstable or may disappear entirely.

Chaotic intermittency can be explored through Poincaré maps, with two primary characteristics defining it:

- Specific local map,
- Reinjection mechanism.

The local map dictates the type of intermittency, while the reinjection mechanism redirects the system from chaotic regions back to local regular or laminar zones.

This process is explained by the reinjection probability density (RPD) function, which is shaped by the system's chaotic dynamics. The RPD function quantifies the probability of trajectories being redirected into the laminar zone near the unstable fixed point. When combined with the local map, it facilitates the description of the intermittency process.

Apart from these two concepts, authors employ other statistical methodologies to illustrate chaotic intermittency [23], listed as the following:

- Estimating the probability density of the laminar length.
- Approximating the average length of laminar phases. It is necessary because these periods do not consistently exhibit the same number of iterations or length.
- Characteristic relation which establishes the correlation between the average length of laminar phases and the control parameter.

Typically, authors employ these concepts when they encounter a specific form of system map. To accurately characterise intermittent behaviour, they utilize the RPD function.

Intermittency has been commonly observed in many physical phenomena, such as forced nonlinear oscillators, turbulent flows, plasma physics, Rayleigh–Bénard convection, Lorenz system, electronic circuits, nonlinear Schrödinger equation [23].

We focus particularly on categorising this regime (intermittency), especially presenting the case of intermittencies occurring in various models of the Duffing equation. Later, we compare them with the fractional case to ascertain if similarities exist.

Manneville and Pomeau were the first who describe this behaviour when studying the Lorenz system [94, 78].

Using the Floquet analysis, the classification was based on the linear instability of the limit cycle, which explains the spontaneous amplification of fluctuations from a regime near the

periodic state.

Additionally, the discussion of the relaminarization process, in which intermittent bursts are interrupted and replaced by new regular oscillations, played a role in their classification. The initiation of these non-regular phases at the end of the periodic trajectory (laminar phase) is interpreted as an instability of the periodic motion.

The stability analysis of a limit cycle, employing Floquet theory, provides insights into three different types of instability that can arise (see Appendix A).

The classification of intermittency as type I, II, or III relies on the specific behaviour of the Floquet multiplier as it traverses the unit disk within the complex plane (see Figure A.1).

5.1.1 Type I intermittency

At the bifurcation point, a real Floquet multiplier crosses the unit circle at (+1) as shown in Figure 5.1.

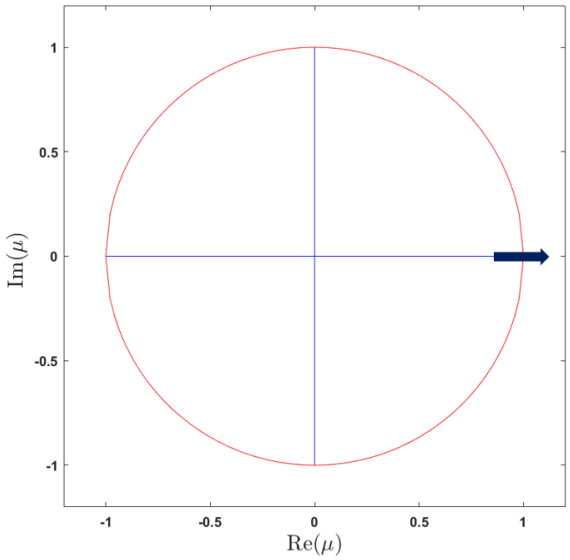


Figure 5.1: Floquet multipliers μ: type I.

This type has been described in the Lorenz model [94, 78].

In this case, one of the eigenvalues associated with the relevant fixed point on the Poincaré map departs from the unit circle in the direction of +1. The manifold linked to this eigenvalue holds crucial information about intermittency because dissipation occurs in all other directions [83]. This manifold guides the system's intermittent behaviour, as trajectories may stay close to the manifold for a while, showing regular behaviour, before suddenly deviating and leading to chaotic behaviour. To understand intermittency, we can study a one-dimensional map linked to this manifold:

$$x_{n+1} = P(x_n, \epsilon), \quad x_n, P \in \mathbb{R}, \tag{5.1}$$

where ϵ is the parameter of bifurcation:

$$\epsilon = \frac{f - f_c}{f_c}, \tag{5.2}$$

that passes through zero at the onset of intermittency f_c. This map can be approximated in the bifurcation region as:

$$x_{n+1} = x_n + ax_n^2 + \epsilon, \quad (a, \epsilon > 0) \tag{5.3}$$

- When $\epsilon < 0$ the return map intersects the identity map $x_{n+1} = x_n$ at two points: a stable fixed point x_s and an unstable fixed point x_u. These fixed points represent the presence of both stable and unstable limit cycles concurrently .
- At $\epsilon = 0$, the stable fixed point x_s and the unstable fixed point x_u converge and merge into a single fixed point x_*. This convergence point indicates a tangent bifurcation.
- When $\epsilon > 0$, the return map does not intersect the identity map. A narrow corridor or channel forms between the return map and the identity map for small positive values of ϵ. The trajectories that approach this channel move slowly through it, gathering successive iterates in its narrowest part.

  Outside the channel, the orbit undergoes irregular (chaotic) oscillations until it is reinjected into the channel when, by chance, the chaotic orbit comes close to the channel as shown in Figure 5.2.

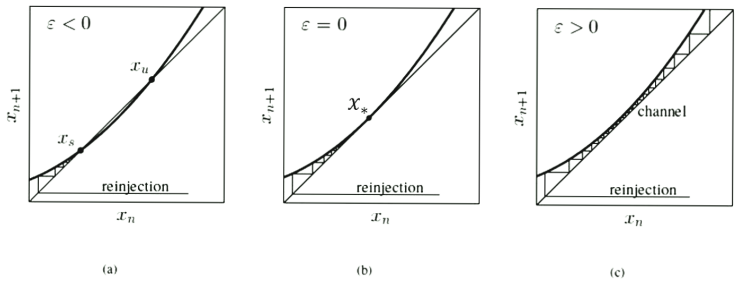


Figure 5.2: Type I intermittency, Tangent bifurcation. (a) Existence of two fixed points: one stable x_s and the other one unstable x_u. (b) Coalescence of both fixed points into a single fixed point. (c) Intermittency: occurrence of the channel [23].

The laminar length l can be interpreted as the integer value representing the number of iterations required or used to pass through the laminar interval. Alternatively, it can be understood as the time taken by each trajectory to cross the laminar zone $[x_{\min}, x_{\max}]$, where $x_{\min}$ and $x_{\max}$ denote the positions where the trajectory enters and exits the regular region with $x_{\max}$ being the upper limit of the laminar interval

To calculate this time (laminar length l), we presume ϵ to be a small positive value, resulting in very small steps in x with consecutive iterates within the channel, implying that $x_{n+1} - x_n$ is minimal.

This assumption permits us to approximate $x_{n+1} - x_n$ as dx/dl and subsequently substitute the discrete equation (5.3) with the differential equation:

$$\frac{dx}{dl} = \epsilon + ax^2. \tag{5.4}$$

By integrating (5.4), the time l needed for the orbit to pass through the interval $[x_{\min}, x_{\max}]$ is:

$$l = \frac{1}{\sqrt{a\epsilon}} \left[\arctan\left(\frac{x_{\max}}{\sqrt{\epsilon/a}}\right) - \arctan\left(\frac{x_{\min}}{\sqrt{\epsilon/a}}\right) \right]. \tag{5.5}$$

The number of iterations, and consequently the estimated time required to pass through the channel (average laminar length $< l >$ (mean time)), is

$$< l >= \frac{\pi}{\sqrt{\epsilon}} \approx \epsilon^{-1/2} = \left[\frac{f - f_c}{f_c}\right]^{-1/2}, \tag{5.6}$$

this means that the bursts of irregular oscillations will be separated by approximately periodic intervals of duration $\mathcal{O}(\epsilon^{-1/2})$.

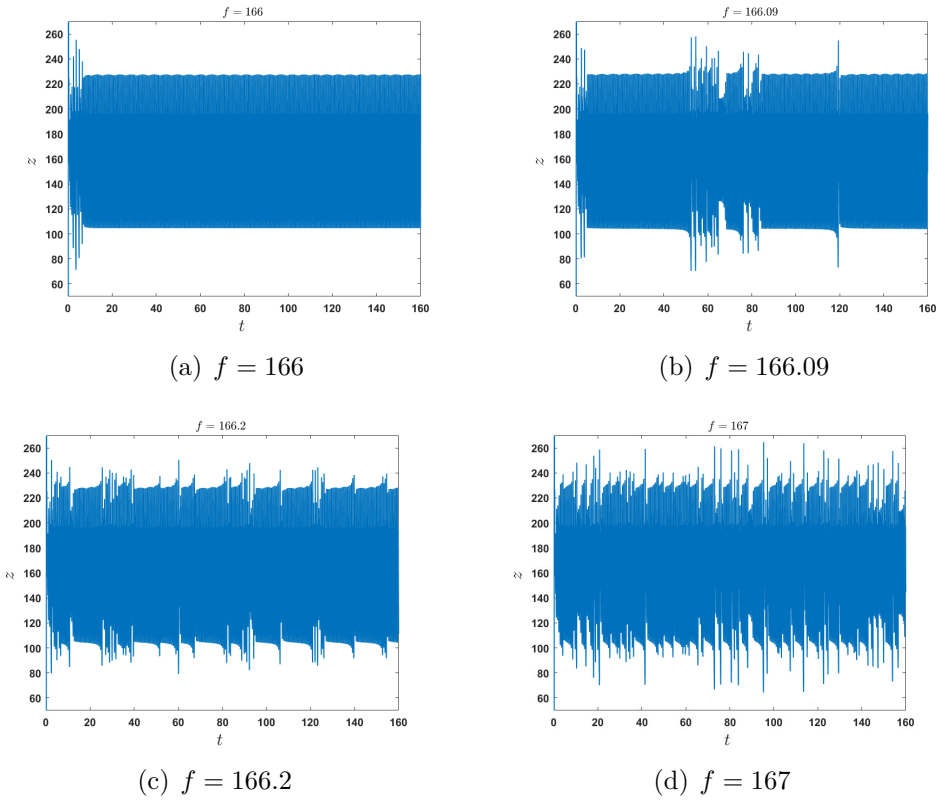
This relation (5.6) between the average laminar length $< l >$ and the ϵ is a characteristic relation. It can be generated in a general form as:

$$< l > \sim \epsilon^{-\beta} \tag{5.7}$$

The exponent β indicates the rate at which the average laminar length $< l >$ grows as the parameter ϵ decreases. For type I intermittency, $\beta = 1/2$ [96, 89, 83, 79].

As previously mentioned, Manneville and Pomeau were the first to describe this behaviour while studying the Lorenz system [78]. They illustrated the behaviour of type I intermittency by plotting the temporal evolution of the z-component for different f-values, as shown in Figure 5.3.

- For $f = 166$, Z exhibits strictly periodic variations (see Figure 5.3(a)).
- When f approaches $\{166.09, 166.2\}$ long laminar phases are abruptly disrupted by short chaotic intervals (see Figures: 5.3(b), 5.3(c)).
- As the control parameter is further increased ($f = 167$), the regular phases become progressively shorter until, eventually, irregular behaviour predominates (see Figure 5.3(c)).



(a) $f = 166$ (b) $f = 166.09$

(c) $f = 166.2$ (d) $f = 167$

Figure 5.3: Lorenz system: transitioning to chaos through type I intermittency.

Type I intermittencies typically exhibit a single reinjection channel, indicating the presence of only one type of observed laminar phase. However, in several systems, other studies have identified cases of type I intermittencies with two reinjection channels.

5.1.2 Type III intermittency

This type is associated with a subcritical period-doubling bifurcation scenario, where an unstable period-2 orbit interacts with and destabilizes a stable period-1 orbit.

It occurs when the Floquet multiplier is real and crosses the unit circle at (-1) as shown in Figure 5.4.

Because the absolute values of the Floquet multipliers are less than unity in other directions, the necessary information to represent intermittency is found in the manifold associated with the unstable Floquet multiplier. As such, this manifold $P(x_n, \epsilon)$ has a map associated with it. Hence, the map corresponding to this manifold takes the form of a one-dimensional map (5.1), which can be approximated near the intermittency threshold as follows [112, 83]:

$$x_{n+1} = P(x_n, \epsilon) = -(1+\epsilon)x_n + ax_n^2 + bx_n^3. \tag{5.8}$$

The constants a, b depend on the specific dynamical system being studied. In this context, $x = 0$ serves as a fixed point of this map for all ϵ and $a > 0$. When ϵ is small and positive,

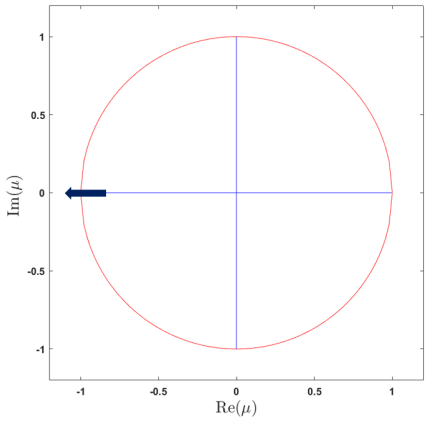


Figure 5.4: Floquet multipliers: type III.

the fixed point $x = 0$ becomes unstable, whereas, for negative values of ϵ, the fixed point $x = 0$ becomes stable. To analyse the map (5.8), the authors [83]: employ its second iterate x_{n+2} and simplify it to:

$$x_{n+2} = P^2(x_n, \epsilon) = (1 + 2\epsilon)x_n + a_1 x_n^3, \quad a_1 = -2(a^2 + b). \tag{5.9}$$

Intermittency is governed by the coefficient of the linear term $(1 + 2\epsilon)x_n$ in (5.9), which establishes the map's slope for $x_0 = 0$.

Type III intermittency occurs in connection with either a subcritical pitchfork bifurcation of $P^2(x_n, \epsilon)$ or a subcritical period-doubling bifurcation of $P(x_n, \epsilon)$.

This behaviour contrasts with that of type I intermittency, where a channel exists between the map and the bisector $x_{n+p} = x_n$ with $p = 1, 2, 3, \cdots$.

Approximating the difference $x_{n+2} - x_n$ by the derivative $\frac{dx}{dl}$ gives:

$$\frac{dx}{dl} = 2\epsilon x + a_1 x^3, \tag{5.10}$$

which is the normal form of a pitchfork bifurcation. By solving this equation, the average laminar length of type III intermittency is given by:

$$< l > \sim \frac{1}{\epsilon}. \tag{5.11}$$

Type III intermittency is linked to a subcritical period-doubling or flip bifurcation: an empirical demonstration of this phenomenon can be observed in Rayleigh-Bénard convection, as documented by Dubois in [20]. Dubois et al. experimentally plot its return map, highlighting that the observed behaviour may vary depending on the position of the measurement point relative to the convective structure.

5.1.3 Type II intermittency

It is associated with a pair of complex conjugate Floquet multipliers crossing the unit circle at $e^{\pm i\omega}$, as shown in Figure 5.5, and introducing an additional incommensurate frequency

with respect to the unstable periodic orbit at the onset of instability, therefore it can not occur in one-dimensional maps.

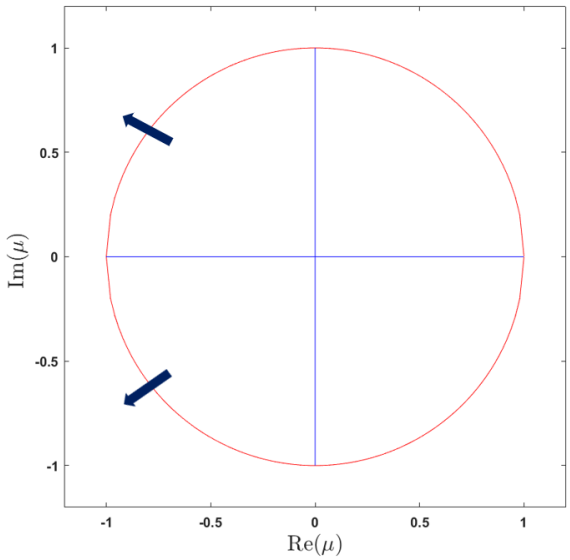


Figure 5.5: Floquet multipliers: type II.

This pair of complex-conjugate eigenvalues (Floquet multipliers) is linked to a two-dimensional manifold, where a Hopf bifurcation occurs for the fixed point of the map. The local Poincaré map of intermittency type II is, in the polar coordinates, of the form:

$$\begin{cases} r_{n+1} = (1+\epsilon)r_n + ar_n^3, \\ \theta_{n+1} = \theta_n + b + qr_n^2, \end{cases} \tag{5.12}$$

where a, b and q are constants, and ϵ is defined by (5.2). The intermittency can appear for $\epsilon > 0$.

The same statistical parameters used to describe types I and III intermittencies are also used to describe type II.

The laminar length l of this type is:

$$l = \frac{1}{2\epsilon} \ln \left(\frac{a + \epsilon/x_{\min}^2}{a + \epsilon/x_{\max}^2} \right). \tag{5.13}$$

Its average laminar length is given by:

$$< l >= \frac{1}{x_{\max}\sqrt{a\epsilon}} \arctan \left(x_{\max} \sqrt{\frac{a}{\epsilon}} \right) \tag{5.14}$$

The scaling law for type II intermittency is similar to that of type III intermittency (5.11), unlike type I intermittency (5.6) [23, 112, 83].

It has been observed for the periodic forced nonlinear oscillations [98]:

$$\dddot{x} + a\ddot{x} + b\dot{x} + cx + d_1x^2 + d_2\dot{x}^2 + d_3x\dot{x} + d_4x\ddot{x} + d_5x^2\ddot{x} = F\cos(\omega t). \tag{5.15}$$

Type II Pomeau-Manneville intermittency was also observed in an interconnected nonlinear oscillator circuit that incorporated a PN Junction diode along with linear oscillator components[42].

Sacher et al. successfully reported the first observation of type II intermittency in an optical system, specifically in the light intensity of a GaAs/GaAlAs semiconductor laser with external feedback during coherence collapse. A reconstructed Poincaré plot supports this explanation by confirming the spiralling tendency of type II intermittency [105]. The classical Duffing equation does not exhibit Type II intermittency.

5.1.4 Cases of intermittency in the classical Duffing equation

Cases of intermittency: type I

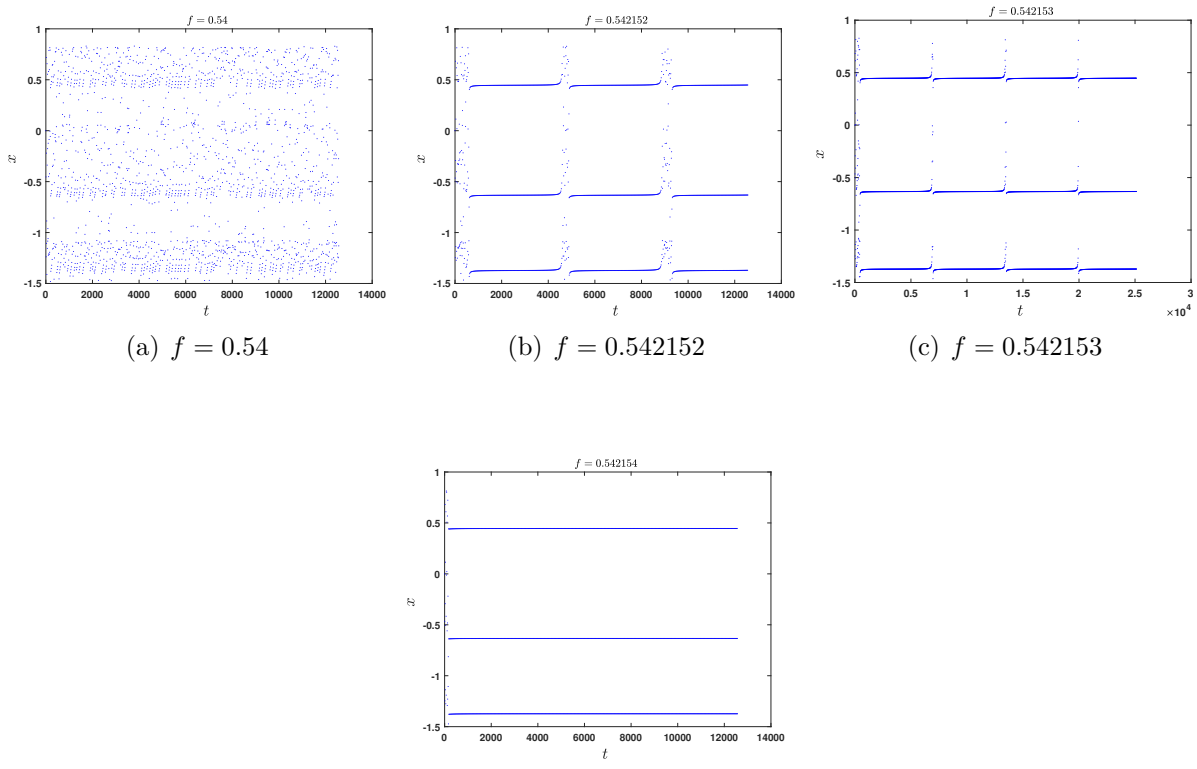
In [77], Malasoma et al. present the intermittency type I with two channels of reinjection in the Lorenz system and Rayleigh–Bénard convection. In [68], the authors investigated type I intermittencies with n channels of reinjection.

Intermittency of type I has been observed in various dynamical systems. However, our focus lies on instances where it manifests in different models of the Duffing equation. In [62], Lakshmanan et al. analysed the intermittency type I in this specific Duffing equation:

$$\ddot{x} + 0.5\dot{x} - x + x^3 = f\sin(\omega t), \tag{5.16}$$

The intermittency in this equation (5.16) is similar to the behaviour seen in the logistic map, which demonstrates type I intermittency.

The bifurcation phenomena of (5.16) have been studied in the range $f \in (0.538, 2.5445)$. Intermittency emerges at $f_c \approx 0.542152$. To observe this pattern, we explore various values of f close to f_c in Figure 5.6.



(a) $f = 0.54$ (b) $f = 0.542152$ (c) $f = 0.542153$

(d) $f = 0.54214$

Figure 5.6: Intermittent behaviour in (5.16).

Beyond $f = 0.542153$, a stable period-3T orbit is evident, illustrated in Figure 5.6(d) for $f = 0.5421$. Conversely, below $f = 0.542152$, chaos manifests, as shown in Figure 5.6(a) for $f = 0.54$. Intermittent dynamics are observed in Figure 5.6(b) and Figure 5.6(c).

For $f = 0.542152$, we have intermittency. In Figure (5.7), we represent the third return map x_n versus x_{n+3}. The straight line corresponds to the $x_{n+3} = x_n$ line, while the black dots denote a series of third iterates.

The values of x-component constituting the laminar phase are approximately $x \approx \{0.445, -0.633, -1.372\}$ (it means that there are three laminar zones close to $x \approx 0.445$, $x \approx -0.633$ and $x \approx -1.372$). These laminar zones are marked inside black squares in Figure 5.7.

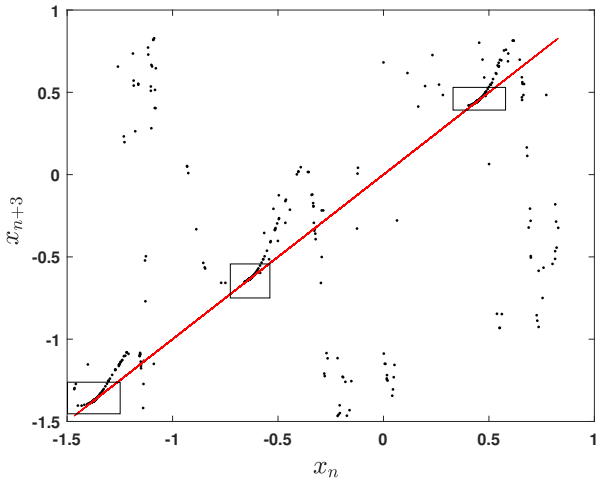


Figure 5.7: Third return maps constructed from experimental data of the Poincaré map for $f = 0.542152$, $x_0 = v_0 = 0$.

To see clearly how the iterates of x_n approach one of the values of $x \in \{0.445, -0.633, -1.372\}$, in Figure 5.8, we enlarged the view in the neighbourhood of the fixed point $x = -0.633$ to see the channel produced by the points of the return map versus the identity map points. The gradual advancement of the iterates, characterised by a staircase-like trajectory as x_n approaches $x = -0.633$, is observed.

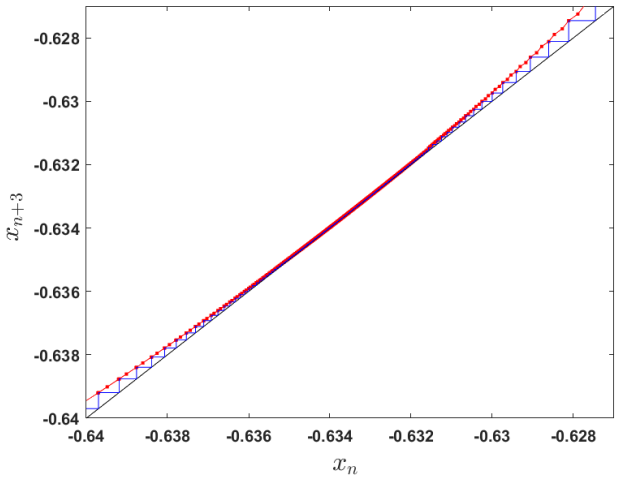


Figure 5.8: x_{n+3} versus x_n near $x = -0.633$ showing the slow passage of x thereby forming a laminar phase.

Following the passage through the narrowed channel presented in Figure 5.8, the iterates expand extensively and manifest chaotic behaviour until the orbit re-enters the constricted domain. Thus, with the decrease in the external force, a discernible transition from a period-

3T attractor to a fully developed chaotic attractor is evident (see Figure 5.6(a)), illustrating intermittent behaviour.

Similar intermittency patterns are observed in the context of the same equation (5.16), characterised by laminar phases exhibiting stable period-$6T$ orbits where 6 narrow channels are formed [97]. For $f_0 = 0.3603208$, we present that in Figure 5.9.

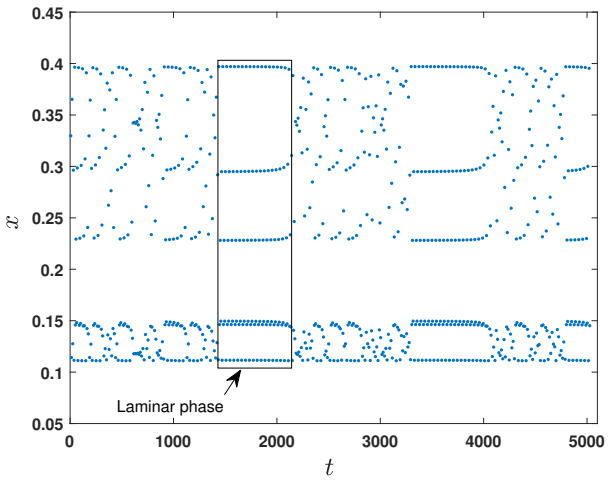


Figure 5.9: Intermittency patterns for $f_0 = 0.3603208$.

Most of the papers that studied the intermittency in the Duffing equation fixed the damping term at $\gamma = 0.5$.

In the following, we study it for $\gamma = 0.25$, as in our fractional case, with $F = f_0 \cos(\omega t)$ and fix $\omega = 1$. The theoretical threshold of chaos by Melnikov proves that the chaos in the classical Duffing equation may appear when the parameters satisfy (2.36).

Numerically, the value of the threshold appears to be at $f_0/\gamma = 1.06$. We utilise the bifurcation diagram to identify it.

To present this diagram, we keep $\gamma = 0.25$ and $w = 1$ constant, and we vary f_0, which serves as the control parameter for bifurcation. In the bifurcation diagram spanning $0.25 < f_0 < 0.42$, chaos initially emerges at $f_0 = 0.2649622$ as presented in Figure 5.10 with an intermittent pattern observed.

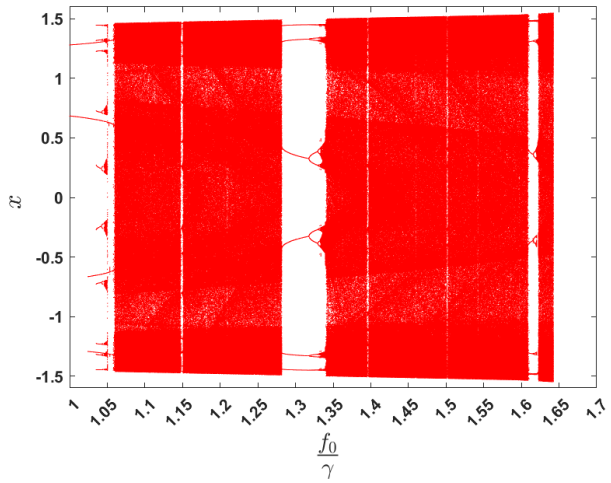


Figure 5.10: The bifurcation diagram for equation $\ddot{x} + 0.25\dot{x} - x + x^3 = f\cos(\omega t)$.

According to the definition of intermittency, the solution remains regular when the control parameter is below its chaos threshold. For $f = 0.26496 < 0.2649622$, the solution is regular as shown in Figure 5.11.

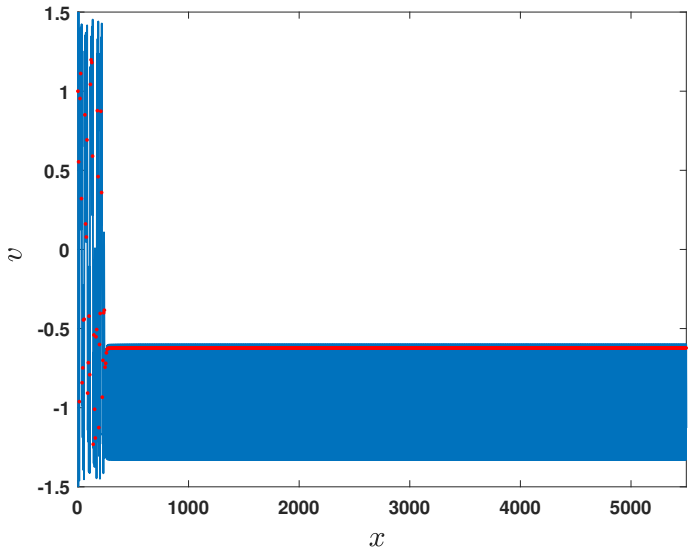


Figure 5.11: Regular solution for $f_0 = 0.26496$.

In Figure 5.12, at the intermittency threshold $f_0 = 0.2649622$, we observe chaotic bursts that disrupt the regular phases.

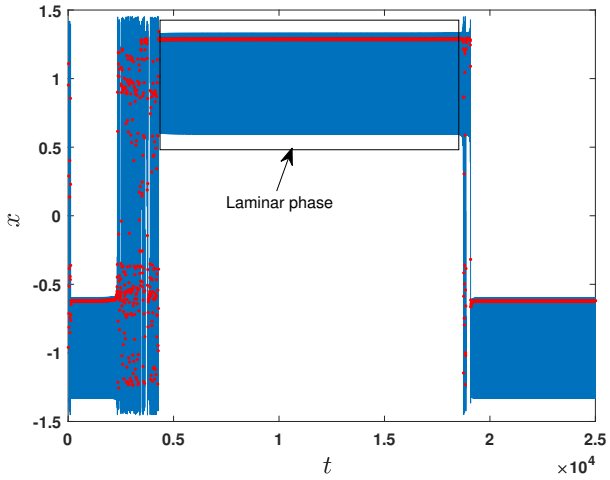


Figure 5.12: Intermittency for $f_0 = 0.2649622$.

Upon revisiting the bifurcation diagram in Figure 5.10, we notice multiple regions where the solution transitions between regular and chaotic regimes. In each region, intermittent behaviour is evident when the solution changes its behaviours from chaotic to regular or the opposite.

For $0.286 < f_0 < 0.288$, The system transitions into a regular zone around $f_0 = 0.2872$ and subsequently enters a new chaotic zone.

Following the regular regime experienced by the system, it is notable that the solution within that range does not start with chaotic behaviour but rather displays intermittent behaviour at $f_0 = 0.287644871$. In figure 5.13, we present a stroboscopic map that exhibits this behaviour.

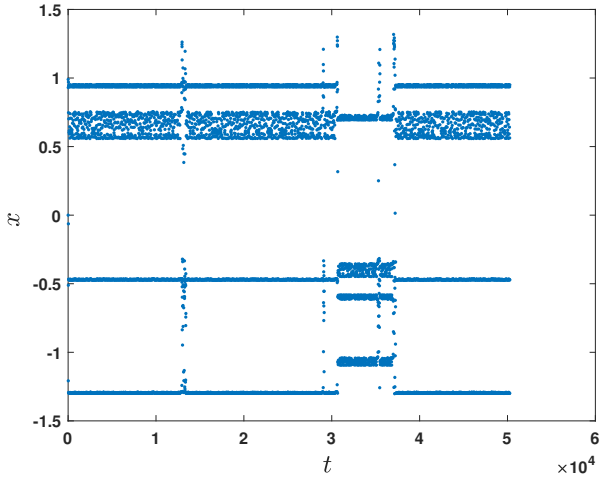


Figure 5.13: Intermittent behaviour for $f_0 = 0.287644871$.

In the range $0.32 < f_0 < 0.336$, the system exhibits full of chaos for $f_0 = 0.32$. However, before transitioning to complete regularity at $f_0 = 0.32459$, it passes through an intermittent

regime. This regime initiates with a very brief laminar phase at $f_0 = 0.3201$, which then gradually becomes more distinct and elongated, as shown in Figure 5.14 for $f_0 = 0.320452$.

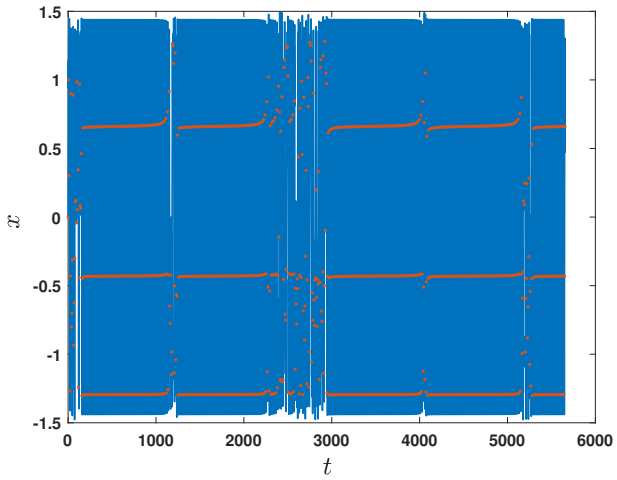


Figure 5.14: Intermittent behaviour for $f_0 = 0.320452$: the blue curve represents the solution $x(t)$ and the red dots are the stroboscopic map corresponding to this solution.

This intermittency is similar to the one found in [62], for $\gamma = 0.5$, $f_c = 0.542153$ with sinusoidal external force.

In the range $0.348 < f_0 < 0.35$, the intermittency is not clearly seen. Moreover, there exists a prolonged transient of chaos preceding the emergence of laminar phases which are very brief. In Figure 5.15, this phenomenon is illustrated for $f_0 = 0.34856$, where three channels can be observed.

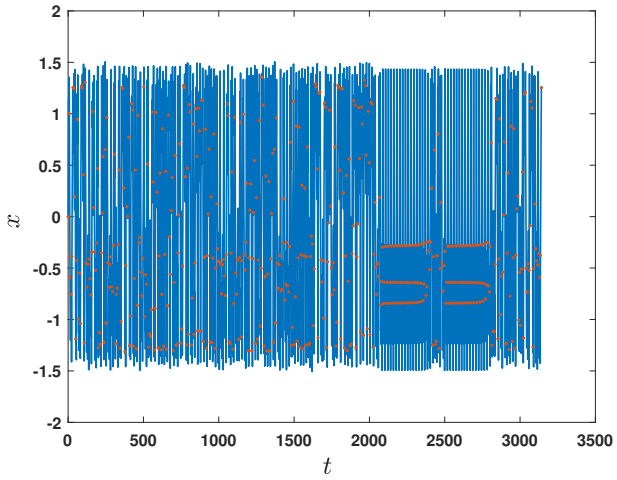


Figure 5.15: Intermittent behaviour for $f_0 = 0.34856$.

Similarly, in the range $0.4 < f_0 < 0.406$, we observe intermittency at $f_0 = 0.40214$ with two channels. Figure 5.16 represents this phenomenon.

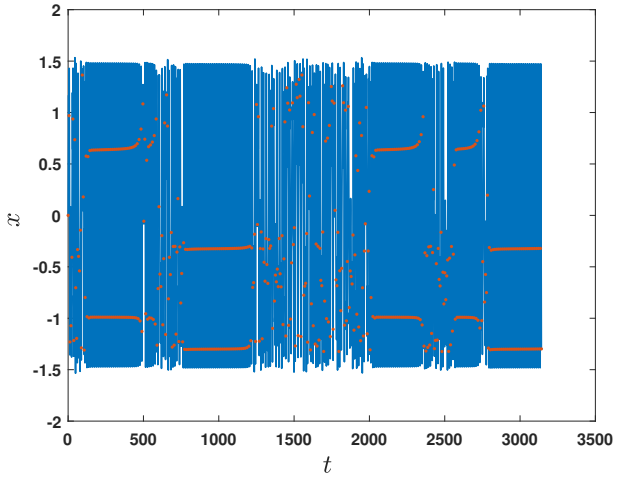


Figure 5.16: Intermittent behaviour for $f_0 = 0.40214$.

In the following analysis, our objective is to characterise the type of intermittency observed at $f_0 = 0.2649622$ using diverse numerical methods, including the return map, meantime approximation $< l >$, and Floquet multipliers estimation.

Classify the intermittency at $f_0 = 0.2649622$

To identify which type of intermittency it can be, we rely on several points.

1. **Using the return map**
   From the points of the Stroboscopic map presented in Figure 5.18, two channels appear.

   In Figure 5.12, we observe that the regular phases oscillate around any of the two fixed points $x \approx \{-0.6185, 1.28563\}$ which are the values of x constituting the laminar phase. In Figure 5.17, we present the return map that corresponds to Figure 5.12:

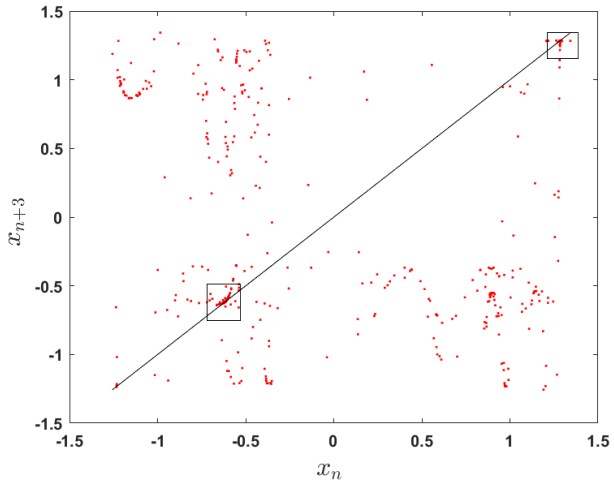


Figure 5.17: Third return map corresponds to $f_0 = 0.2649622$.

We enlarge the return map presented in Figure 5.17 in the neighbourhood of the fixed point $x \approx 1.28563$ to see the channel produced around it.

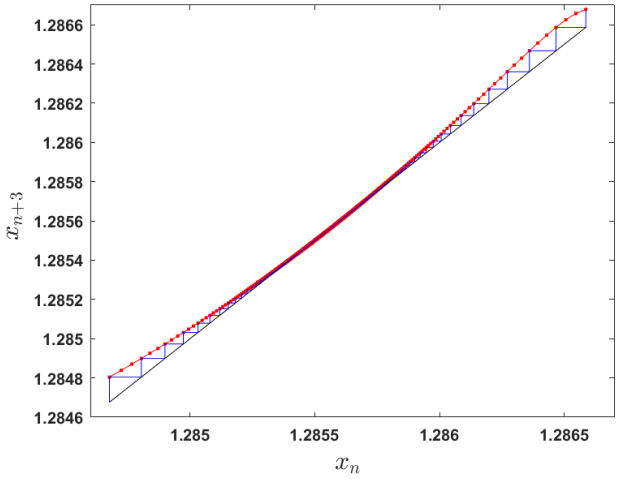


Figure 5.18: Third return map x_{n+3} versus x_n in the neighbourhood of the fixed point $x = 1.28563$.

The narrowed channel shown in Figure 5.18 emerges as a result of observing the gradual progression of the iterates, characterised by a staircase-like trajectory. This characterises type I intermittency.

2. **Approximate the meantime** $< l >$
   Also, we have determined by a computer analysis of our data, the meantime $< l >$ as a function of the injection current. We have taken the normalized injection current:

$$\epsilon = \frac{f - f_c}{f_c}. \tag{5.17}$$

Thus, we estimate the maximum lengths l of the laminar phases depending on the distance from the intermittency threshold f_c by extracting l from the phase space for several values of the control parameter.

Then, in Figure 5.19 we plot l versus ϵ on a double logarithmic scale. All the points lie almost on a straight line, and the slope obtained after using regression is $\beta = -0.5147$ which is close to the power-law (5.6), as predicted for type I intermittency.

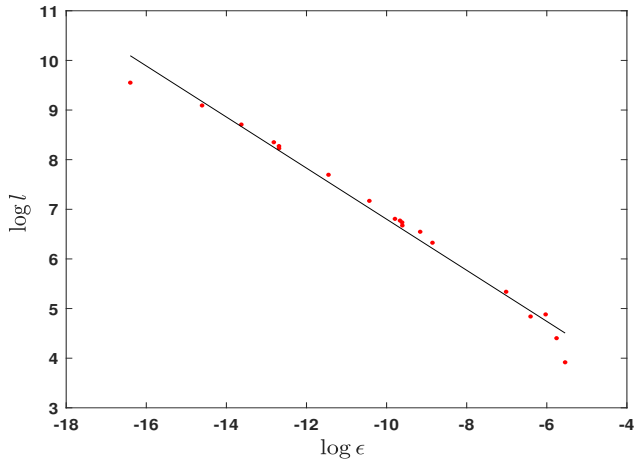


Figure 5.19: Double logarithmic scale of the maximum length l of the laminar sections in dependence of ϵ with slope equals to -0.5147.

3. **Approximate the Floquet multipliers**

We approximate the Floquet multipliers numerically using the Monodromy matrix as presented in Appendix A, relying on the Jacobi matrix of the classical Duffing equation (2.23).

Since intermittent behaviour begins at $f_0 = 0.2649622$, we need to use data related to this parameter to approximate the fundamental matrix solution. The eigenvalues of the monodromy matrix correspond to the eigenvalues of the fundamental matrix solution at each period $kT, k \in \mathbb{N}$, which are the Floquet multipliers μ_k.

From Figure 5.12, we have three laminar phases. The data presented are for the number of time steps $N = 3 \cdot 10^6$.

In Figure 5.20, we present the Floquet multipliers corresponding to this data: we see the Floquet multiplier μ_2 leaving the unit cycle through $+1$.

For further clarity, we specifically focus on the data surrounding the departure of μ_2 from the unit cycle. The initial leaving occurred via $+1$ with $\mu_2 = 1.0000001e + 00$ at $t = 1.1963185e + 04$ as highlighted in red in Table 5.1.

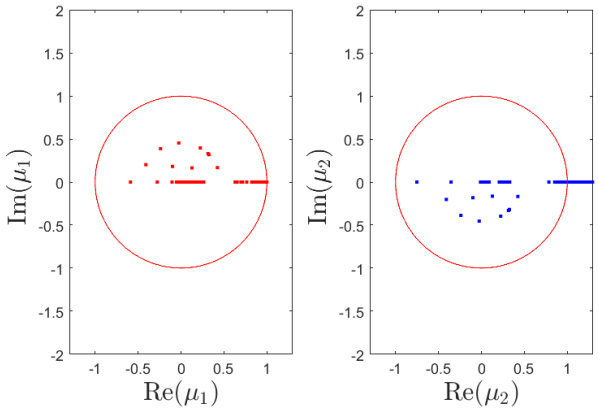


Figure 5.20: Floquet multipliers corresponding to Figure 5.12: The first crossing with the unit circle was throughout μ_2.

Floquet multipliers for $f_0 = 0.2649622$		
t	μ_1	μ_2
1.1919203e+04	2.0786555e-01	9.9997373e-01
1.1925486e+04	2.0786477e-01	9.9997748e-01
1.1931769e+04	2.0786399e-01	9.9998124e-01
1.1938052e+04	2.0786321e-01	9.9998502e-01
1.1944335e+04	2.0786242e-01	9.9998878e-01
1.1950618e+04	2.0786164e-01	9.9999254e-01
1.1956902e+04	2.0786086e-01	9.9999631e-01
1.1963185e+04	2.0786008e-01	1.0000001e+00

Table 5.1: Numerical data of the Floquet multipliers near the first crossing with the unit cycle.

Thus, we confirm that the classical Duffing equation exhibits a type I intermittency.

We know that one of the typical transitions to chaos is via intermittency through the process of injection is characterises type I intermittency. T. Karakisawa et al. [54] in their paper in 1998, prove that the absence of this process of injection does not mean there is no intermittency type I.

They studied the fifth-order system of magnetoconvection that displays a way to transition from a laminar phase to chaos without the reinjection process. They classified it using the characteristic relation that was found with a scaling power law equal to $-1/2$, which is consistent with the power law of type I intermittency.

Cases of intermittency: type III

Laugesen, Jakob, et al. [64] studied the statistical distribution of the laminar phase by using a one-dimensional map suggested by Pomeau to study this type of intermittency.

Ishii, Hiroaki et al. [44] studied the following equation of motion:

$$\ddot{x} + \gamma\dot{x} - 10x + 100x^3 = F\cos(3.5t) \tag{5.18}$$

Based on the results presented in the bifurcation diagram (Figure 5.10, they initially determined the critical value of chaos, with the amplitude F serving as the control parameter.

They obtained that if F takes the value zero, the solution tends to be one of the stable fixed points, as F increases they noted a periodic solution, before the transition to the chaotic motion.

They showed the intermittency characteristic when F approaches the critical value and they interpreted the migration between two wells as the bursts (chaotic parts) and the laminar phases (states) when the solution is located in one well.

Thus, if the solution is in a well it takes a long time to jump into the other one. They concluded that the similarity exponent introduced to analyse the intermittency characteristics satisfies a scaling law (5.7) with scaling power law equal to $0.7 - 0.8$ near the transition point.

In Figure 5.21, we represent the intermittency exhibit by (5.18) for $x_0 = 0.5, v_0 = 0.5, f = 0.8495$.

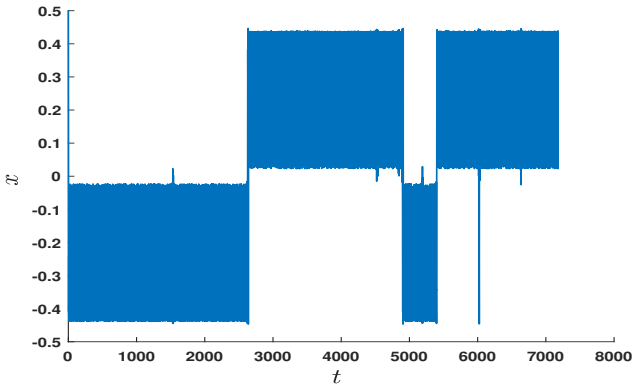


Figure 5.21: Intermittency type III in (5.19).

.

H. Bunz et al. also [8] checked the intermittency in the Duffing equation:

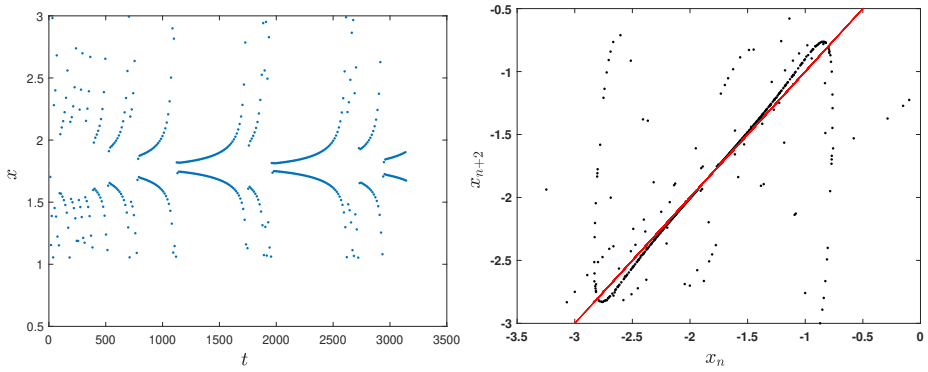
$$\ddot{x} + k\dot{x} + cx + x^3 = A\cos(t) \tag{5.19}$$

They examine the Floquet exponents using a period-doubling cascade, illustrating the presence of type III intermittency.

Additionally, they investigate the reinjection mechanisms and the duration of the laminar phases characteristic of this intermittent behaviour.

Their experimental analysis involves plotting the second iterate of the Poincaré section $x_{n+2} = x_n$ in proximity to the unstable period 1 solution. Notably, the map exhibits a structure consistent with type III intermittency.

For the same parameter of the paper $k = 0.2, c = -3.1, A = 4.6$, in Figure 5.22, we represent type III intermittency for $x_0 = 0.1, v_0 = 0.1$.



(a) local Poincaré map

(b) Second return of the Poincaré map x_{n+2} versus x_n

Figure 5.22: Type III intermittency $x_0 = v_0 = 0.1$.

5.2 Different cases of intermittency in the fractional Duffing equation

In this section, intermittency with one or several channels is analysed. Across the range, α, n-channels of reinjection emerge for various values of the fractional order α and f_0. These n-channels correspond to the n-stable periodic orbits, $n = \{1, 2\}$. We present them by cases, commencing with smaller values of α.

- In our study, we have discovered specific cases in which the regular-like phases of the solution that tend towards the T-periodic curve, exhibit oscillatory patterns around both centres of the underlying classical Hamiltonian system $(+1, 0)$ and $(-1, 0)$. Notably, this type of behaviour only manifests when the values of α are small and the amplitude is relatively large. These conditions play a crucial role in facilitating the observed oscillations around the system's centres. We present such a case in Figure 5.23.

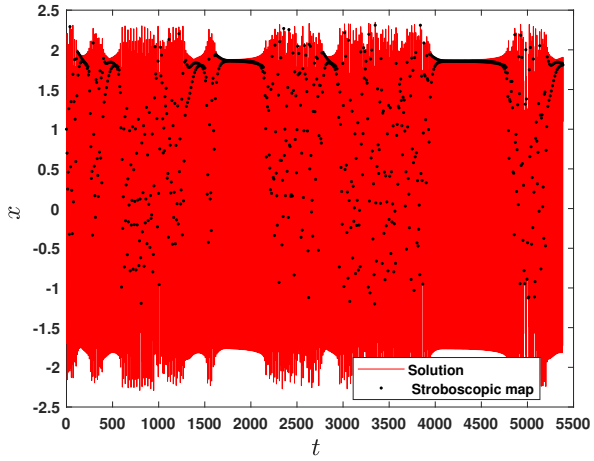


Figure 5.23: Intermittency with one channel of reinjection around both centres, $\alpha = 0.1, f_0 = 0.778, x_0 = 1, v_2 = 0$.

- Due to a continuity argument, the behaviour of the classical Duffing equation should smoothly transition as the parameter α approaches 1 either slightly less than 1 or slightly greater than 1. This agreement implies that the system's dynamics when α is very close to 1 should resemble the system's behaviour when α is exactly 1, displaying a continuous shift from fractional to classical dynamics. This consistency is important for validating the model and ensuring its behaviour aligns with expectations in the classical case.

  By observing this transition, we can confirm that the fractional model conforms to known classical dynamics as it shifts from fractional to classical behaviour. In our study, the intermittent behaviour appears for values of α near 1 with slightly smaller values. This behaviour closely resembles that seen in the classical case for the same range of f_0. An example is illustrated in Figure 5.24 for $\alpha = 0.99999$, demonstrating the similarity in behaviour.

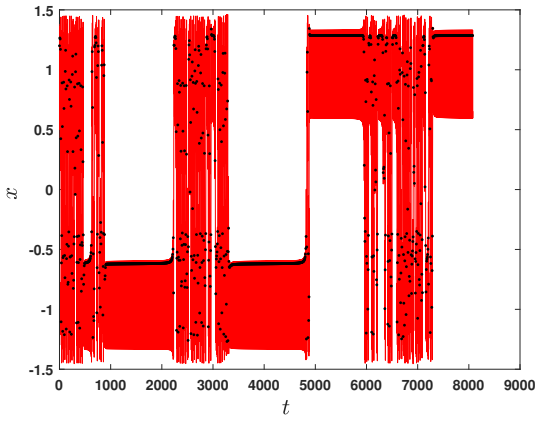


Figure 5.24: Intermittency for $\alpha = 0.99999, \quad f_0 = 0.26497, \quad x_0 = 1.2, v_0 = 0.3$.

- For values of α close to 1 and slightly higher, two-channel intermittency is detected. These 2-channels correspond to the 2-regular orbits that tend towards $2T$ periods. We present this case in Figure 5.25.

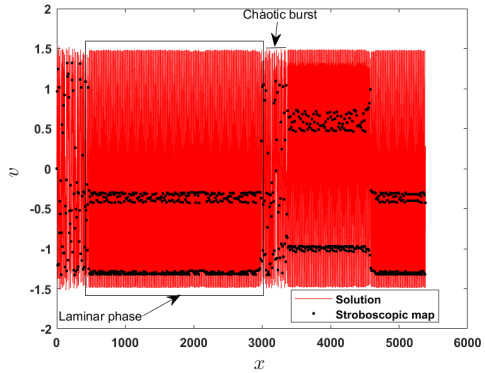


Figure 5.25: Intermittency for $\alpha = 1.000001, f_0 = 0.4057, x_0 = 0, v_0 = 0$.

In Figure 5.26, we see that one of the regular phases oscillates around both centres of the underlying classical Hamiltonian system and the second one oscillates around one of the two centres. we present that:

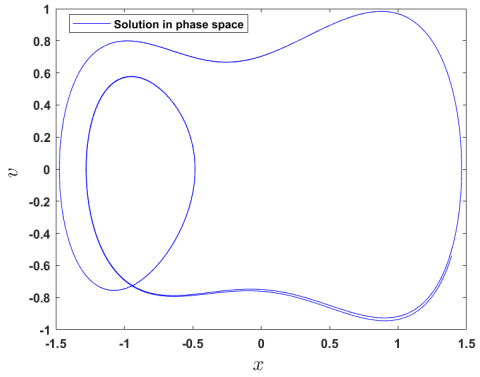


Figure 5.26: Intermittency for $\alpha = 1.000001, f_0 = 0.4057, x_0 = 0, v_0 = 0$.

- We have identified an intermittent behaviour with one channel, causing the regular-like phases of the solution to oscillate exclusively around one of the centres of the underlying classical Hamiltonian system $(+1, 0)$ or $(-1, 0)$.

  This phenomenon is visually represented in Figure 5.27 where the laminar phase tends towards a T-periodic curve.

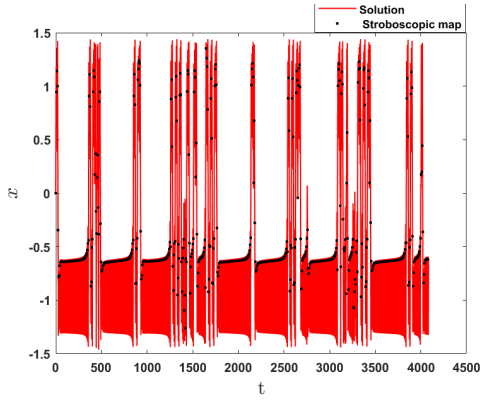


Figure 5.27: Intermittency with one channel, $\alpha = 1.25$, $f_0 = 0.2271$, $x_0 = 0.00101$, $v_0 = 0.002$.

- In other cases, we observe the presence of two channels of reinjection in the intermittent behaviour, where the regular-like phases of the solution can oscillate around either of the two centres. These phases transition intermittently from one centre to the other, periodically shifting their oscillations. This behaviour is shown in Figure 5.28.

5.2.1 Intermittency with two reinjection channels

Now, we study an intermittent behaviour with two reinjection channels for $\alpha = 1.1, x_0 = v_0 = 0$.

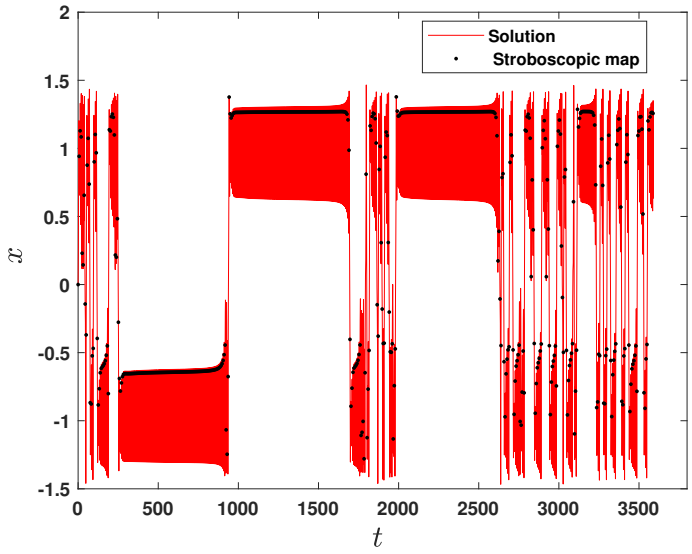
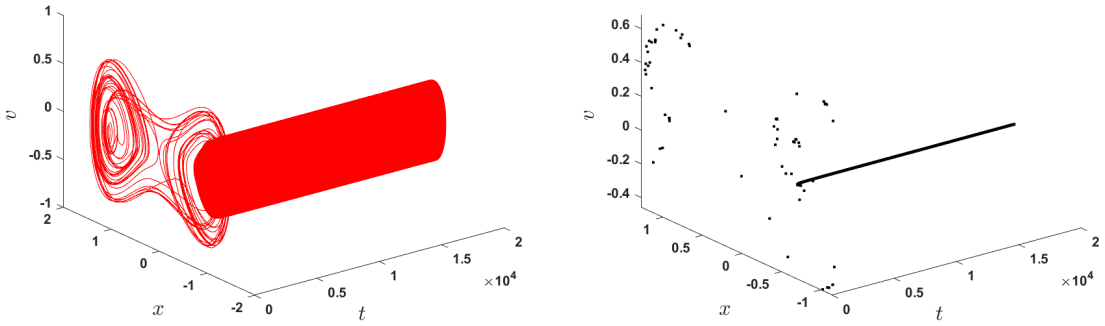


Figure 5.28: Intermittency with two channels, $\alpha = 1.35, f_0 = 0.2119, x_0 = v_0 = 0$.

- When the control parameter f_0 is below the critical value $f_{0c} = 0.250007$, the attractor takes the form of a regular curve with period T.

  For $f_0 = 0.25000699 < f_{0c}$, the system has a limit cycle. In Figure 5.29(a), we present in 3D false projection the phase space and the stroboscopic map that seems to tend to a fixed point as time increases in Figure 5.29(b).



(a) Phase space for $f_0 = 0.2500699$ (b) Stroboscopic map for $f_0 = 0.2500699$

Figure 5.29: Phase space and stroboscopic map for regular solution $f_0 = 0.25000699$.

- At the critical value $f_{0c} = 0.250007$, we observe a loss of stability in the solution. A chaotic burst interrupts the regular phase which oscillates between the two fixed points of the underlying Hamiltonian system, as shown in Figure 5.30

  The solution destabilizes after a long time t_c. It can be seen in Figure 5.31 where we present the stroboscopic map corresponding to the solution of Figure 5.30.

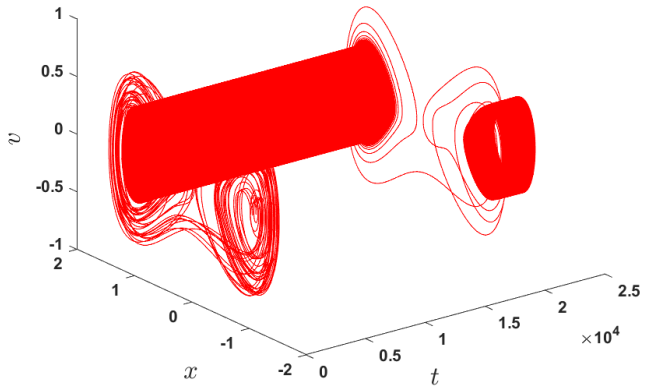


Figure 5.30: Chaotic intermittent behaviour with two re-injection channels $f_0 = 0.250007$.

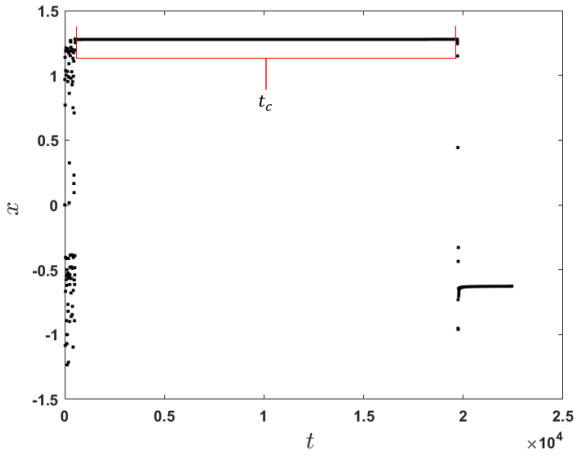
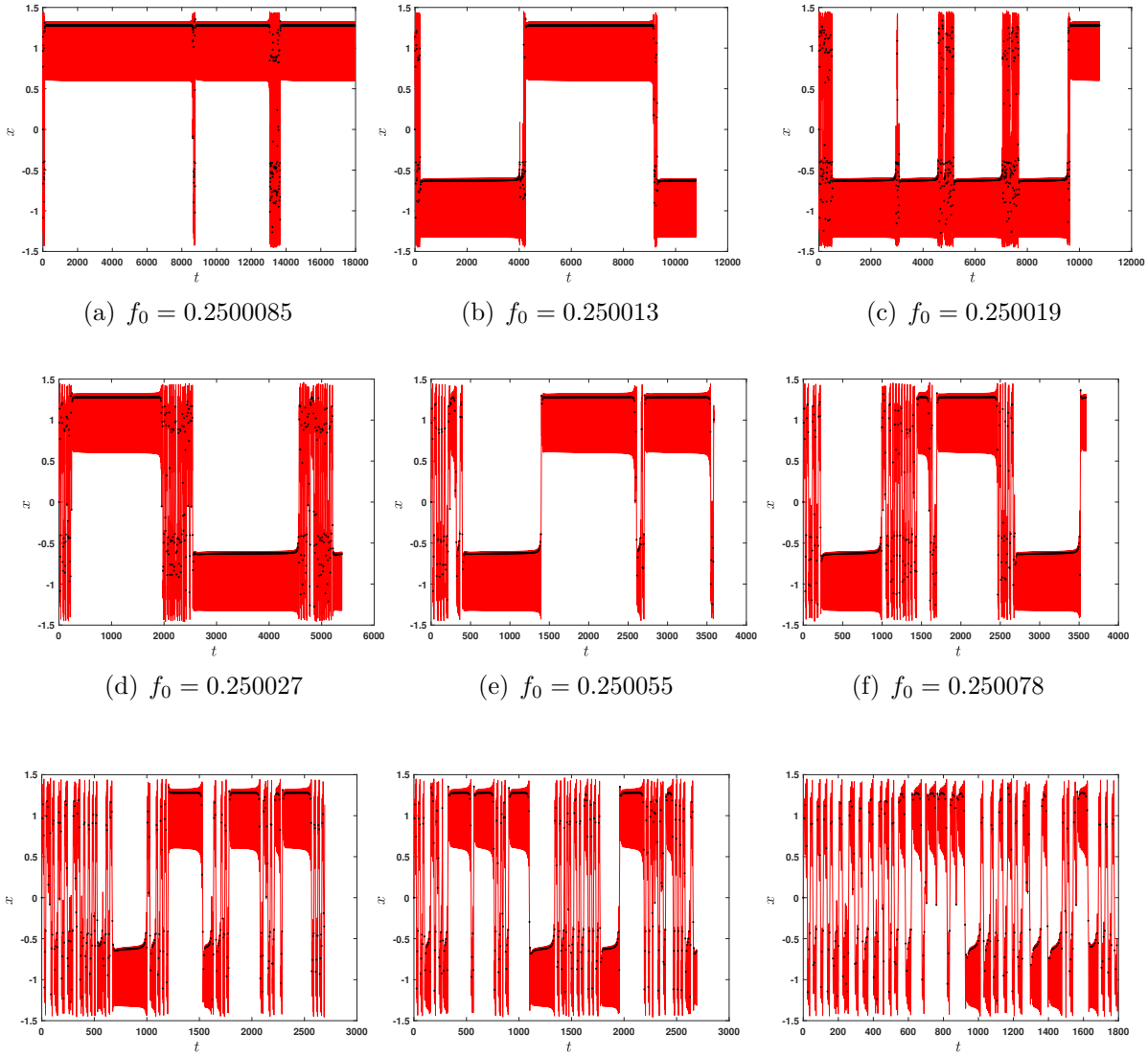


Figure 5.31: Stroboscopic map of two re-injection channels, $f_0 = 0.250007$.

- Upon increasing the control parameter f_0 above f_0c, the size of the laminar region diminishes, accompanied by a substantial increase in the frequency of chaotic bursts.

  As the parameter deviates significantly from the critical value associated with intermittency, the laminar phases disappear entirely, giving way to a state of complete chaos in the motion. Figure 5.32 illustrate that:

To explain the dynamical characteristics of this intermittency, we employ a return map constructed from numerical data. We present it in Figure 5.32(d). In Figure 5.33, we present the stroboscopic map for $f_0 = 0.250027$. The values of x constituting the laminar phase are approximately $x \approx \{1.278, -0.6276\}$.



(a) $f_0 = 0.2500085$ (b) $f_0 = 0.250013$ (c) $f_0 = 0.250019$

(d) $f_0 = 0.250027$ (e) $f_0 = 0.250055$ (f) $f_0 = 0.250078$

(g) $f_0 = 0.25028$ (h) $f_0 = 0.2506$ (i) $f_0 = 0.253$

Figure 5.32: Stroboscopic map and solution $x(t)$ showing the intermittent behaviour as f_0 increases with two re-injection channels.

Using the values x_n of the stroboscopic map, in Figure 5.34, we plot x_{n+1} versus x_n to see the two channels obtained near the points constituting the laminar phases.

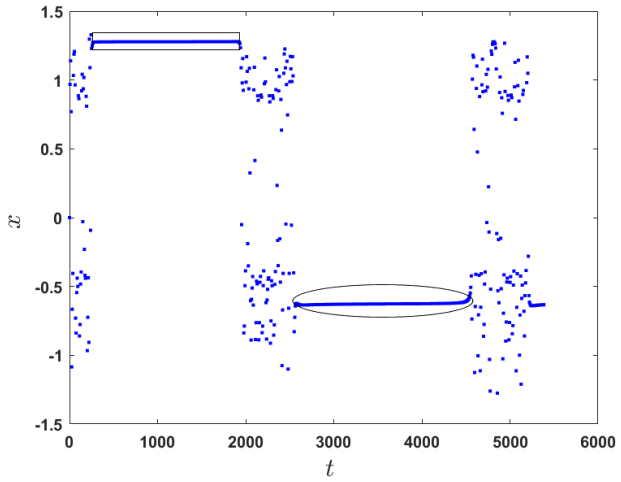


Figure 5.33: Stroboscopic map for $f = 0.250027$, where there exist two laminar phases.

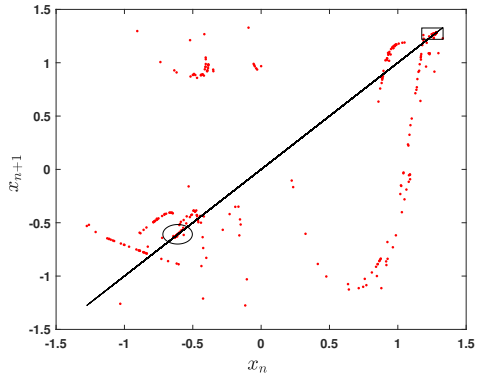


Figure 5.34: First return map for $f = 0.250027$, with two distinct re-injection channels.

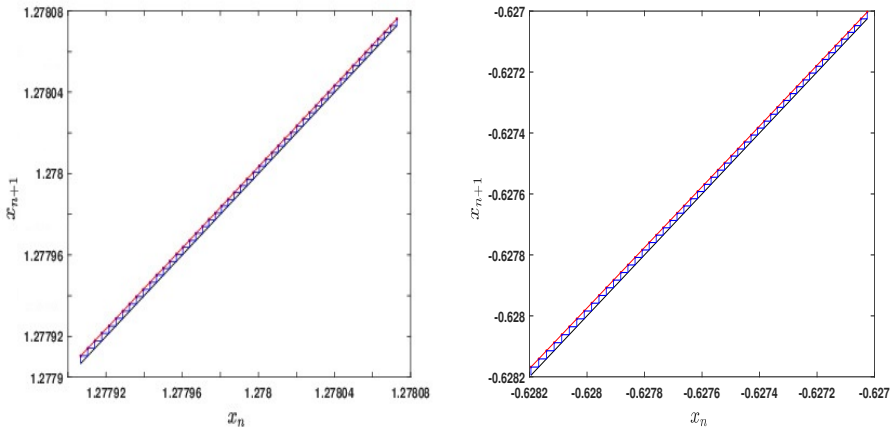
It is important to note that chaotic bursts are observed around two distinct re-injection channels. The points that form these two channels are indicated inside the square and the ellipse in Figures 5.33 and 5.34.

Presenting all the points of the Poincaré map in Figure 5.34 is not clear enough to see the two channels. To provide a clearer view of the channels formed around each fixed point, distinguishing the intermittent behaviour characteristic of type I intermittency, in Figure 5.35, we generate a return map focusing on the vicinity of the two stable fixed points $x \approx \{1.278, -0.6276\}$.

To validate the relation (5.6) proposed by Pomeau and Manneville, we calculate the average duration of the laminar phases $< l >$ for 85 different values of f_0 with $\epsilon = \frac{f_0 - f_{0c}}{f_{0c}}$.

For each value of f_0, we extract the maximum length of the laminar intervals l. From the numerical data, l represents the number of iterations required to traverse the channel.

These results are shown in Figure 5.36. The slope of the linear mean-square fit is $\beta = -0.59$,



(a) First return map in the neighbourhood of the fixed point $x = 1.278$

(b) First return map in the neighbourhood of the fixed point $x = -0.6276$

Figure 5.35: Two channels shown by the first return maps for $f = 0.250027$.

thus, near $-1/2$. We can conclude that this behaviour exhibits type I intermittency.

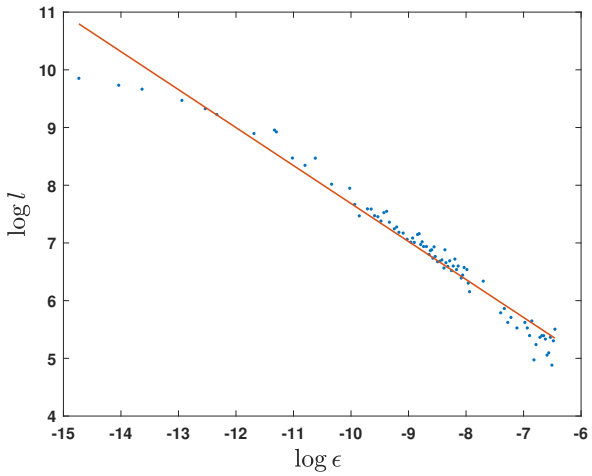


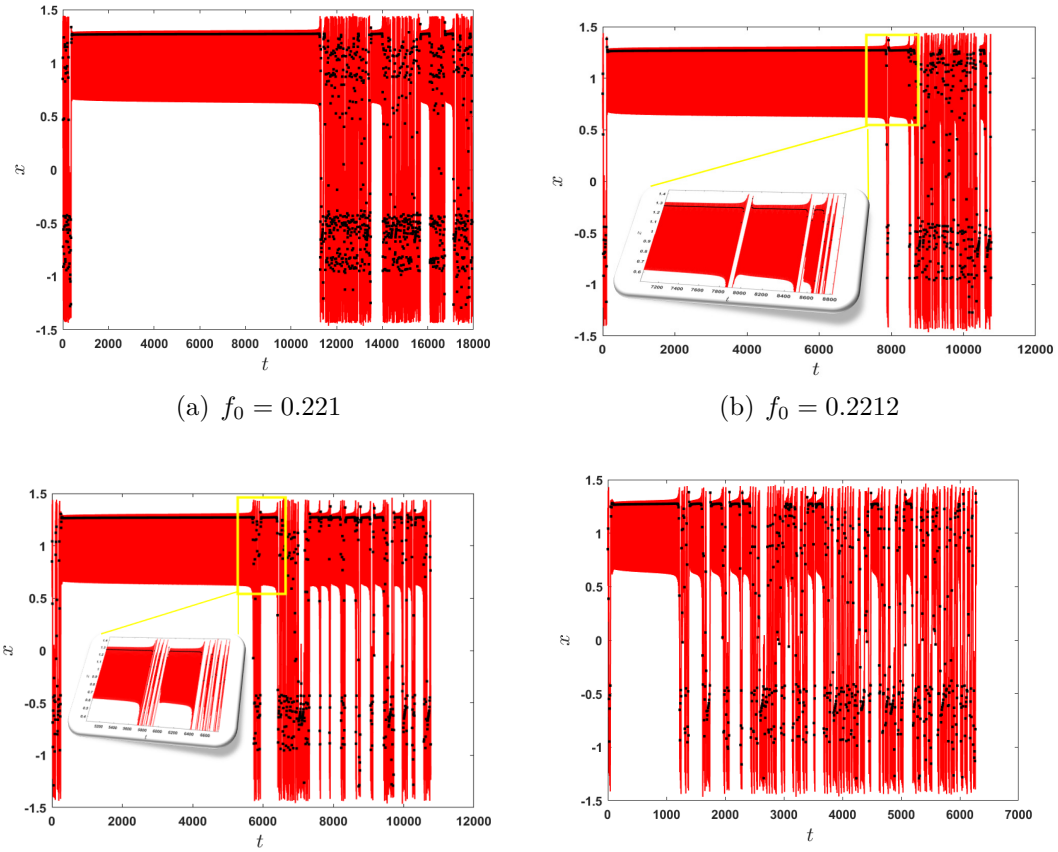
Figure 5.36: Power law for the mean value of the laminar phases with slope $\beta = -0.59$.

5.2.2 Intermittency with one reinjection channel

In the previous section, we illustrate a case of intermittency involving two reinjection channels. Now, for the parameter set $\alpha = 1.3, x_0 = 0.85, v_0 = 0.12$, we observe intermittency with only one channel. In Figure 5.37, we present the evolution of the solution and the stroboscopic map.

Following the onset of intermittent behaviour at $f_{0c} = 0.221$ (as shown in Figure 5.37(a)), we notice an extended period of laminar phase alongside shorter episodes, intermittently interrupted by chaotic bursts.

In Figures 5.37(b), 5.37(c), 5.37(d), we observe that as the control parameter f_0 moves further away from the intermittency threshold, the duration of the laminar phase decreases.



(a) $f_0 = 0.221$ (b) $f_0 = 0.2212$

(c) $f_0 = 0.2214$ (d) $f_0 = 0.2228$

Figure 5.37: Stroboscopic map and solution $x(t)$ showing the intermittent behaviour as f_0 increases with one re-injection channel.

- Approximating the LCEs for $f_{0c} = 0.221$

  At the intermittency threshold, the laminar phase is very long $l = 10850$, and the LCEs corresponding to this case are presented in Figure 5.38.

  In the rectangle illustrated in Figure 5.38, both LCEs initially show negative values,

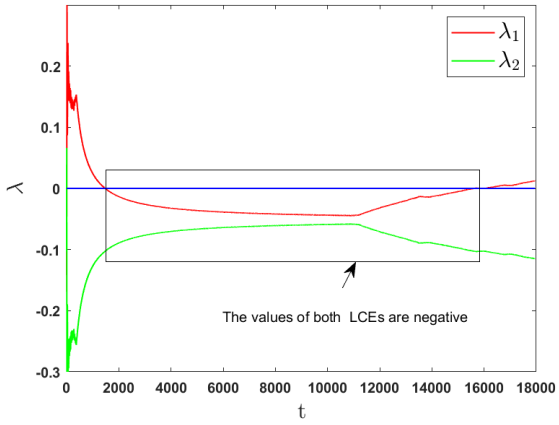


Figure 5.38: Estimation of the LCEs for an intermittent behaviour, $\alpha = 1.3$, $f_0 = 0.221$, $x_0 = 0.85$, $v_0 = 0.12$.

but, eventually, one of them, λ_1, transitions to a positive value.

- Approximate the Floquet multipliers

  In the previous approximation of the LCEs, we observe that they tend to be negative as the system enters the laminar phase. Subsequently, one of them becomes positive.

  A similar pattern is observed with the Floquet multipliers, which initially have small values with a modulus less than 1 ($|\mu_1|, |\mu_2| < 1$), indicating that both are inside the unit circle. Then, we notice that μ_1 exits the unit circle, reaching a value of +1.

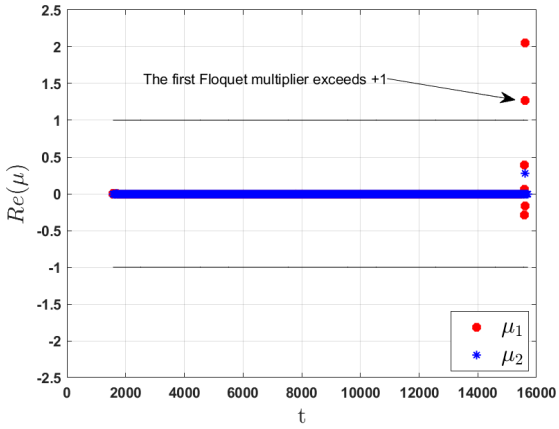


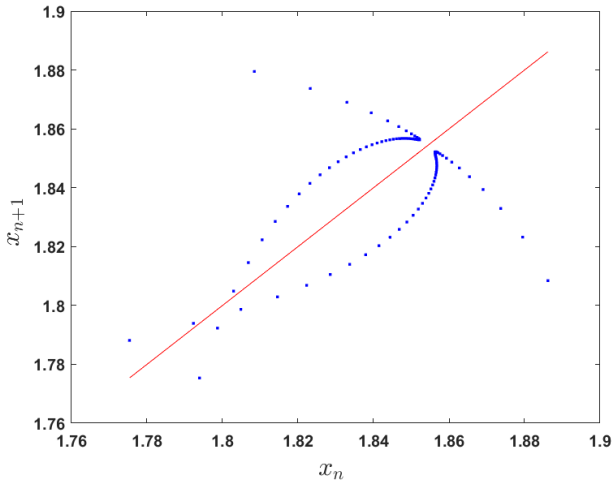
Figure 5.39: The Floquet multipliers associated with the data in Figure 5.37(a) intersect the +1 level line. The solid black lines represent the levels +1 and -1.

When the first Floquet multiplier crosses +1, this indicates a transition from stability to instability of the solution. As mentioned before, this transition is characteristic of type I intermittency.

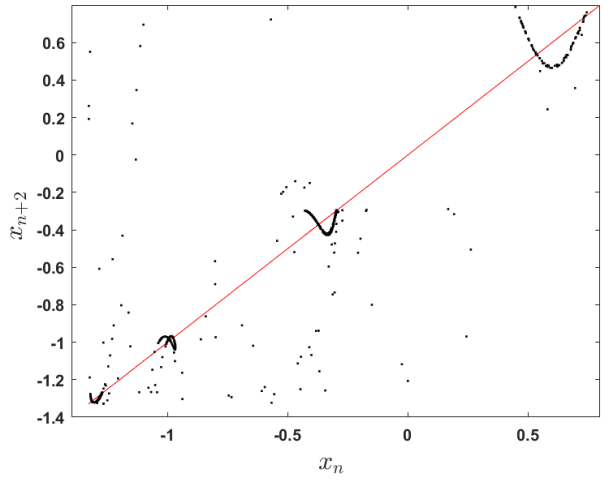
5.2.3 Future research

As we saw at the beginning of this chapter section 5.2, there is an intermittent behaviour where phase space surrounds both corners $(+1, 0)$ and $(-1, 0)$ as shown in Figure 5.23. Also, the intermittency detected for values of α close to 1 and slightly higher is presented in Figure 5.25.

These two cases have a return map different from the classical types we know. It could be an open work to discover their characteristics to classify them. In figure 5.40, we present the first return map corresponding to Figures 5.23 and 5.25 respectively.



(a) First return map for the intermittent behaviour with one channel of reinjection around both centres, $\alpha = 0.1, f_0 = 0.778, x_0 = 1, v_2 = 0$.



(b) Second return map for the intermittent behaviour for $\alpha = 1.000001, f_0 = 0.4057, x_0 = 0, v_0 = 0$.

Figure 5.40: Return map of intermittent behaviour.

Chapter 6

Conclusions

In this work, we study Duffing's equation with fractional damping term and linear stiffness using the Caputo fractional derivative. We have explored the equation in the range from $\alpha = 0$ to $\alpha = 2$. We have used two numerical methods, from two different approaches, that give consistent results.

We have numerically estimated the threshold in the parameters that separate regular and chaotic regimes. This classification is not simple. The system appears to be very sensitive to the values of the parameters and the initial conditions, especially in the region near the threshold. Small variations in any of the values can give rise to solutions with different behaviours, even in the case of regular solutions, where the attractor is not unique.

The presence of a fractional derivative taking the rôle of the first-order derivative introduces changes in the behaviour of the system. Some of the special features we have encountered are already present in the classical Duffing Equation but they are much enhanced in the fractional model.

For instance, we have the multiplicity of the regular attractors, given a fixed set of parameter values. The classical equation may present three attractors that correspond to periodic solutions around one of the two centres of the undisturbed Hamiltonian, or around both of them. In the fractional case we have found that the number of regular attractors that coexist is not limited to three and several different closed curves may be found. We understand that the relaxation of the dissipation and the long memory that the fractional derivative introduces allow more periodic attractors to be stable.

Certainly, in the classical Duffing equation, chaotic transients exist but their lengths are generally limited compared to their counterparts in the fractional model. Specifically, chaotic transients in the fractional model persist for a longer time, contrasting with the classical model where they are typically brief. Additionally, while both models may show a mix of regular and chaotic attractors, this mixture is more prevalent and pronounced in the fractional Duffing equation.

Moreover, in the fractional system, this feature presents high sensitivity to initial conditions, especially concerning the prolonged chaotic transient. Even slight deviations in the initial state

of the solution x_0 and velocity v_0 can yield substantial discrepancies, with minor deviations potentially leading to either brief or extended transients. This appears to be a significant feature of this system.

The regular attractors in the classical Duffing equation correspond to periodic curves in the phase plane that are symmetric under the change $x \to -x$, $v \to -v$. The same seems to occur in the fractional case. In both cases the transformation corresponds to an invariance in the equation but for a change of phase in the cosine term for half a period. This can give some insight into the long-time behaviour of the fractional system and the fact that, although there are no periodic solutions, the regular attractors correspond to periodic curves in the phase plane. The system can be considered to be embedded in a two-dimensional phase space. This provides a structured framework for analysis and prediction.

We have presented a way to effectively compute both Lyapunov Characteristic Exponents (LCEs) λ_1, λ_2 by approximating the Jacobi matrix of the linearized system. We gain useful insights into the fractional system's dynamic behaviour and stability. Our approximation enables us to understand the system's properties.

The agreement observed between the computed LCEs and the maximum LCE simulated using the fiduciary orbit technique underscores the accuracy of our approach. Our computational methodology captures the system's complex dynamics and evolution over time.

Additionally, we have compared the approximation of the LCEs λ_1, λ_2 obtained by the linearization method with $\lambda_{\max}$ obtained by the fiduciary orbit method.

The solution system was obtained through two numerical methods employed to approximate the solution of the fractional Duffing equation. The agreement between λ_1 and $\lambda_{\max}$ was good when using the SV + Odibat method while using the SV + Diethelm method showed a small gap between them. This agreement supports the accuracy of the new method.

As $\alpha \to 0^+$ or $\alpha \to 2^-$, the system becomes closer to the limit cases where chaos is present in the central region of the phase plane independently of the values of the parameters. The chaotic region becomes increasingly dense as we approach the limit, tending towards filling a two-dimensional area. This is in agreement with the shape of the chaotic attractor, the estimated values of D_L and the numerical estimation of the threshold of chaos.

In both limits, the system behaves similarly and tends to the classical case where no dissipation is present. In this sense, there is a closed transition that interpolates between these limits and the classical Duffing equation that corresponds to the intermediate limit $\alpha = 1$. Although the behaviour of the system is similar in both extreme limits, the intermediate behaviour is different on both sides of $\alpha = 1$.

In addition to the system's distinct behaviours, including regular, chaotic, long chaotic transient, long regular transient, and solutions transitioning from regular attractors, intermittent behaviour also occurs. However, this behaviour is not widely observed within the range of $0 < \alpha < 1$, except for specific values of α. The first occurrence is when α is very close to 0, with amplitudes ranging between $0.75 < f_0 < 0.8$. The second instance is when α approaches 1 with slightly values less than 1, where intermittency emerges at the same f_0 value as in the classical case.

Moving to the range of $1 < \alpha < 2$, intermittent behaviour becomes more prevalent, with variations depending on the number of reinjection channels. Some cases can be classified as intermittency type I through return map plots, which facilitate to note of the channels, along with approximations of the average laminar length corresponding to type I.

In other cases featuring very long laminar phases, where both Lyapunov Characteristic Exponents (LCEs) start negative but subsequently increase, leading to one becoming positive upon the emergence of chaos, the analysis follows the Floquet multipliers. Initially, these multipliers vary with time within the unit circle, until one crosses it through either $+1$ or -1.

Some cases remain unclassifiable due to their return maps deviating from known types. Addressing these cases will be considered for future research.

Further studies are ongoing, and initial findings reveal that the system exhibits a range of intermittency types, allowing us to classify certain cases. In the future, we will focus on a rigorous analysis of the unclassified cases, aiming to accurately identify and characterize them.

Appendix A

Stability of periodic solutions: Floquet theory

Let us consider a dynamical system given by a first-order differential equation of the form:

$$\dot{\vec{x}} = \vec{f}(t, \vec{x}), \quad \vec{x} \in \mathbb{R}^n \tag{A.1}$$

The system may depend, in general, on some control parameters, as in the (classical) Duffing equation. We suppose that the system has a special solution $\vec{u}(t)$ that is periodic with period T:

$$\forall t, \quad \vec{u}(t+T) = \vec{u}(t), \tag{A.2}$$

and we want to analyse the stability of this solution (A.2), specifically determining whether solutions that begin close in the vicinity of $\vec{u}(0)$ remain close or not to solution $\vec{u}$ as time evolves.

Let us consider a solution $\vec{x}(t)$ such that:

$$\vec{x}(t) = \vec{u}(t) + \vec{\delta}(t), \tag{A.3}$$

with $\delta_0 := \|\vec{\delta}(0)\|$ very small. From (A.1), and performing a Taylor expansion around $\vec{u}(t)$, we have:

$$\dot{\vec{\delta}}(t) = \vec{f}(t, \vec{x}) - \vec{f}(t, \vec{u}) = \vec{0} + Df(\vec{u}(t))\vec{\delta} + \mathcal{O}(\|\vec{\delta}(0)\|^2), \tag{A.4}$$

where Df is the Jacobi matrix of (A.1). To simplify the notation let us represent by J the Jacobi matrix of (A.1) computed on the periodic solution:

$$J(t) := Df(\vec{u}(t)). \tag{A.5}$$

If we consider the stroboscopic map with base period T, the first points for both solutions are $\vec{u}(0)$ and $\vec{x}(0)$. The next iteration of the stroboscopic map does not give a new point for the periodic solution, since $\vec{u}(T) = \vec{u}(t)$. The other solution gives a second point:

$$\vec{x}(T) = \vec{x}(0) + \vec{\delta}(T). \tag{A.6}$$

The difference $\vec{\delta}(T)$ can be approximated linearly as the solution at time T of the linear problem:

$$\begin{cases} \dot{\vec{\delta}}(t) = J(t)\vec{\delta}(t), \\ \vec{\delta}(0) = \vec{\delta}_0. \end{cases} \tag{A.7}$$

For instance, if J is a constant matrix (as in the examples below), the solution of (A.7) is given by:

$$\vec{\delta}(t) = e^{Jt}\vec{\delta}_0, \tag{A.8}$$

and thus (A.3) become:

$$\vec{x}(T) = \vec{u}(t) + e^{Jt}\vec{\delta}_0. \tag{A.9}$$

If J depends on time we can find a differential equation that it satisfies. Let us define a matrix $M(t)$ such that:

$$\vec{\delta}(t) = M(t)\vec{\delta}_0. \tag{A.10}$$

Differentiating (A.10), we obtain:

$$\dot{\vec{\delta}}(t) = \dot{M}(t)\vec{\delta}_0 \Leftrightarrow J(t)\vec{\delta}(t) = \dot{M}(t)\vec{\delta}_0 \Leftrightarrow J(t)M(t)\vec{\delta}_0 = \dot{M}(t)\vec{\delta}_0. \tag{A.11}$$

Requesting this to hold for any initial $\vec{\delta}_0$, we have, finally:

$$\begin{cases} \dot{M}(t) = J(t)M(t), \\ M(0) = I, \end{cases} \tag{A.12}$$

where the initial condition on M is to ensure that $\vec{\delta}(0) = \vec{\delta}_0$. The matrix M is the fundamental matrix solution.

Consequently, there exists a constant Matrix Φ, called the Monodromy matrix, such that:

$$M(t+T) = M(t)\Phi. \tag{A.13}$$

Since $M(0) = I$, we have $\Phi = M(T)$. In general, Φ cannot be defined analytically but must be obtained numerically.

To calculate the monodromy matrix, we integrate equation (A.12) for $0 < t < T$. As $J(t)M$ varies with $x(t)$, the Jacobi matrix should be provided at each t. So, we integrate simultaneously (A.1) with (A.12):

$$\begin{cases} \dot{\vec{x}}(t) = \vec{f}(t, \vec{x}), \quad x(0) = x_0, \\ \dot{M}(t) = J(t)M(t), \quad M(0) = I. \end{cases} \tag{A.14}$$

Finally, the Monodromy matrix is given by $\Phi = M(T)$, when we integrate (A.14) until $t = T$. The eigenvalues of Φ are the Floquet multipliers μ.

- If $|\mu| = 1$, there is a pseudo-periodic solution. If $\mu = \pm 1$, then the solution is asymptotically periodic with period T.

- If $|\mu| < 1$: all Floquet multipliers are within the unit circle centred at the origin of the complex plane, the stroboscopic map is contractive and the periodic solution is stable.
- Otherwise, If $|\mu| > 1$ the periodic solution is unstable [113].

The examination of the stability of the periodic orbit when one of the system's parameter changes can be achieved by analysing its bifurcations using the information derived from the Floquet multipliers. This stability relies on the specific behaviour of the Floquet multiplier as it traverses the unit disk within the complex plane.

Let us first define the bifurcation [36, 133, 100]. It is sudden qualitative changes in the behaviour of a dynamical system, that occur at critical control parameter value. It is divided into two principal classes:

Global bifurcation
Global bifurcations typically arise when extensive invariant sets within the system intersect, either among themselves or with the system's equilibria. Detecting them solely through stability analysis of equilibria (fixed points) is insufficient.

Local bifurcation:
Local bifurcations occur when small changes in system parameters lead to qualitative changes in the behaviour of the system near a particular equilibrium point, periodic orbit, or invariant set. They are typically analyzed by examining the linear stability properties of the system near the equilibrium points or periodic orbits.

According to whether an eigenvalue crosses the circle at $+1$ or -1 or whether a pair of conjugate complex eigenvalues crosses the unit circle, a different type of bifurcation takes place [27].

(i) A saddle-node bifurcation, a transcritical bifurcation or a pitchfork bifurcation can occur when a real Floquet multiplier μ_i moves out of the unit circle through $+1$ with the remaining Floquet multipliers staying inside.

(ii) A Neimark Sacker bifurcation can occur when a complex Floquet multiplier μ_i, and its complex conjugate, leave the unit circle together as a pair with the remaining Floquet multipliers staying inside.

(iii) A period-doubling bifurcation (flip) can occur when a real Floquet multiplier μ_i moves out of the unit circle through -1 with the remaining Floquet multipliers staying inside.

In Figure A.1, we explain how the Floquet multipliers leave the unit circle in these three different ways:

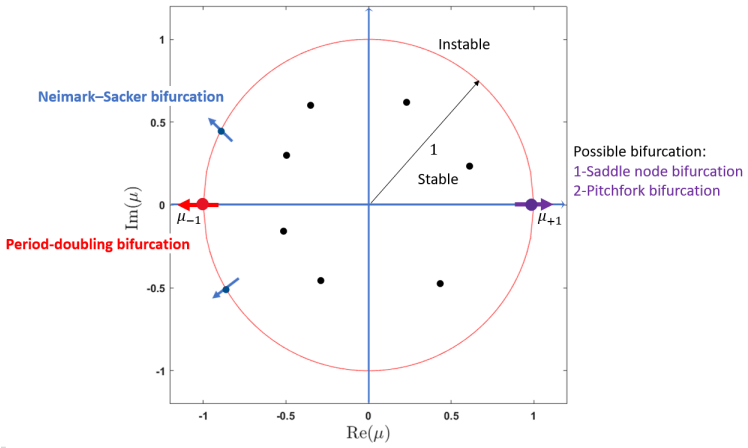


Figure A.1: A schematic illustrating the Floquet multipliers and the corresponding possible bifurcations.

Example 1 *we start with the following:*

A dissipative linear system with an external forcing

$$\ddot{x} = -x - \dot{x} + cos(t). \tag{A.15}$$

The general solution of (A.15) *is:*

$$x(t) = e^{-t/2}\left[c_1 \cos(\omega t) - c_2 \sin(\omega t)\right], \quad \omega = \frac{\sqrt{3}}{2}. \tag{A.16}$$

The fundamental matrix solution has the following components:

$$\begin{cases} a(t) = e^{-t/2}\left(\cos(\omega t) + \frac{1}{2\omega}\right), \\ b(t) = e^{-t/2}\frac{1}{\omega}\sin(\omega t), \\ c(t) = e^{-t/2}\frac{-1}{\omega}\sin(\omega t), \\ d(t) = e^{-t/2}\left(\cos(\omega t) - \frac{1}{2\omega}\sin(\omega t)\right). \end{cases} \tag{A.17}$$

Thus:

$$M(t) = \begin{bmatrix} a(t) & b(t) \\ c(t) & d(t) \end{bmatrix} = \begin{bmatrix} e^{-t/2}\left(\cos(\omega t) + \frac{2\sin(\omega t)}{\omega}\right) & e^{-t/2}\frac{\sin(\omega t)}{\omega} \\ -e^{-t/2}\frac{\sin(\omega t)}{\omega} & e^{-t/2}\left(\cos(\omega t) - \frac{2\sin(\omega t)}{\omega}\right) \end{bmatrix}. \tag{A.18}$$

At $T = 2\pi$, $\Phi(T) = M(T)$ *is the Monodromy matrix.*

$$\Phi_{Exact} = \begin{bmatrix} e^{-\pi}\left(\cos(\sqrt{3}\pi) + \frac{1}{\sqrt{3}}\sin(\sqrt{3}\pi)\right) & e^{-\pi}\frac{1}{\omega}\sin(\sqrt{3}\pi) \\ e^{-\pi}\frac{-1}{\omega}\sin(\sqrt{3}\pi) & e^{-\pi}\left(\cos(\sqrt{3}\pi) - \frac{1}{\sqrt{3}}\sin(\sqrt{3}\pi)\right) \end{bmatrix} \tag{A.19}$$

Thus:

$$\Phi_{Exact} \approx \begin{bmatrix} 0.01017787 & -0.03721651 \\ 0.03721651 & 0.04739438 \end{bmatrix}. \tag{A.20}$$

And numerically taking a very small step size at $T = 2\pi$, $\phi(T)$, is

$$\Phi_{num} \approx \begin{bmatrix} 0.01017786 & -0.03721648 \\ 0.03721648 & 0.04739435 \end{bmatrix}. \tag{A.21}$$

At $T = 4\pi$, the exact Monodromy matrix:

$$\Phi_{Exact} \approx \begin{bmatrix} e^{-2\pi}\left(\cos(2\sqrt{3}\pi) + \frac{1}{\sqrt{3}}\sin(2\sqrt{3}\pi)\right) & e^{-2\pi}\frac{1}{\omega}\sin(2\sqrt{3}\pi) \\ e^{-2\pi}\frac{-1}{\omega}\sin(2\sqrt{3}\pi) & e^{-2\pi}\left(\cos(2\sqrt{3}\pi) - \frac{1}{\sqrt{3}}\sin(2\sqrt{3}\pi)\right) \end{bmatrix}, \tag{A.22}$$

thus:

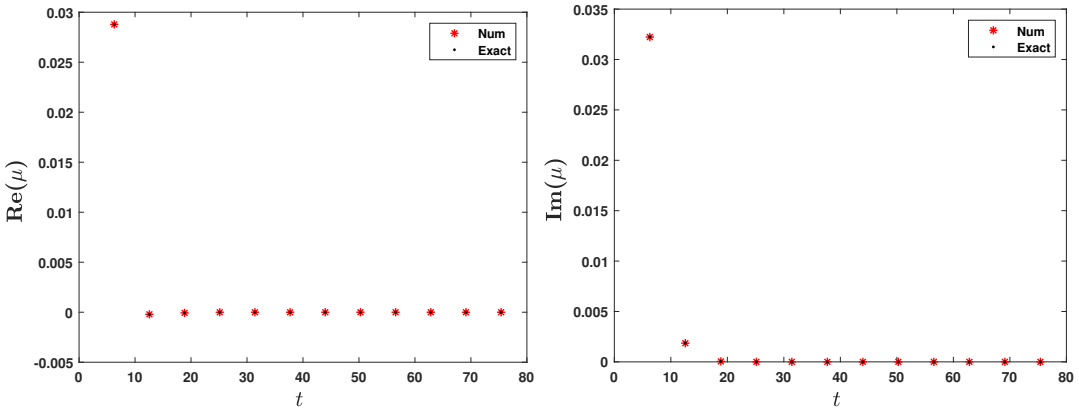
$$\Phi_{Exact} \approx \begin{bmatrix} -0.001281479 & -0.002142638 \\ 0.002142638 & 0.000861158 \end{bmatrix}, \tag{A.23}$$

and the numerical one approximated at $T = 4\pi$ is:

$$\Phi_{num} \approx \begin{bmatrix} -0.001281478 & -0.002142635 \\ 0.002142635 & 0.000861157 \end{bmatrix}. \tag{A.24}$$

We note that both results are close. This ensures that our program to approximate the Monodromy matrix is valid. In Figure A.2 We compare the Floquet multipliers of Φ_{Exact} and Φ_{num} which are the eigenvalues of these two matrices.

Both ways to calculate the Floquet multipliers, either numerically using the Jacobi matrix or using directly the exact formula of Monodromy matrices, give approximately the same results.



(a) (b)

Figure A.2: Comparison between exact and numerical Floquet multipliers (real and imaginary part).

***Remark**:*
As time increases the values of the Monodromy matrix tend to 0 (the same thing for the Floquet multipliers), thus the solution (A.16) *is stable.*

References

[1] Abel, N. H. "Solution de Quelques Problèmes à l'Aide d'Intégrales Définies, Werke 1". *Mag. Naturvidenkaberne* (1823), 10–12.

[2] Ahmad, W. M. and Sprott, J. C. "Chaos in fractional-order autonomous nonlinear systems". *Chaos, Solitons & Fractals* **16**.2 (2003), 339–351.

[3] Baleanu, D., Diethelm, K., Scalas, E., and Trujillo, J. J. *Fractional calculus: models and numerical methods*. **3**. World Scientific, 2012.

[4] Barba-Franco, J.J., Gallegos, A., Jaimes-Reátegui, R., and Pisarchik, A. N. "Dynamics of a ring of three fractional-order Duffing oscillators". *Chaos, Solitons & Fractals* **155** (2022), 111747.

[5] Birnir, B. "Dynamical systems theory". *Center for Complex and Nonlinear Dynamics and Department of Mathematics University of California* (2008).

[6] Brzezinski, D. W. "Computation of Gauss-Jacobi Quadrature Nodes and Weights with Arbitrary Precision". *2018 Federated Conference on Computer Science and Information Systems (FedCSIS)*. Vol. 15. IEEE. 2018, 297–306.

[7] Bülbül, B. and Sezer, M. "Numerical solution of Duffing equation by using an improved Taylor matrix method". *Journal of Applied Mathematics* **2013** (2013), 1–6.

[8] Bunz, H., Ohno, H., and Haken, H. "Subcritical period doubling in the Duffing equation-type 3 intermittency, attractor crisis". *Zeitschrift für Physik B Condensed Matter* **56** (1984), 345–354.

[9] Cao, J., Ma, C., Xie, H., and Jiang, Z. "Nonlinear dynamics of Duffing system with fractional order damping". *Journal of Computational and Nonlinear Dynamics* **5**.4 (2010), 1–6.

[10] Casartelli, M., Diana, E., Galgani, L., and Scotti, A. "Numerical computations on a stochastic parameter related to the Kolmogorov entropy". *Physical Review A* **13**.5 (1976), 1921.

[11] Chen, L., Wang, W., Li, Z., and Zhu, W. "Stationary response of Duffing oscillator with hardening stiffness and fractional derivative". *International Journal of Non-Linear Mechanics* **48** (2013), 44–50.

[12] Cicogna, G. and Papoff, F. "Asymmetric Duffing Equation and the Appearance of Chaos". *EPL (Europhysics Letters)* **3**.9 (1987), 963.

[13] Coccolo, M., Seoane, J. M., Lenci, S., and Sanjuán, M. A.F. "Fractional damping effects on the transient dynamics of the Duffing oscillator". *Communications in Nonlinear Science and Numerical Simulation* **117** (2023), 106959. ISSN: 1007-5704. DOI: https:

//doi.org/10.1016/j.cnsns.2022.106959. URL: https://www.sciencedirect.com/science/article/pii/S1007570422004464.

[14] Coccolo, M., Seoane, J. M., and Sanjuán, M. A.F. "Fractional damping induces resonant behavior in the Duffing oscillator". *Communications in Nonlinear Science and Numerical Simulation* **133** (2024), 107965.

[15] Diethelm, K. "Multi-term fractional differential equations, multi-order fractional differential systems and their numerical solution". *Journal européen des systèmes automatisés* **42**.6-8 (2008), 665–676.

[16] Diethelm, K. and Ford, N. J. "The analysis of fractional differential equations". *Lect. Notes Math* **2004** (2010), 3–12.

[17] Diethelm, K., Ford, N. J., Freed, A. D., and Luchko, Y. U. "Algorithms for the fractional calculus: a selection of numerical methods". *Computer methods in applied mechanics and engineering* **194**.6-8 (2005), 743–773.

[18] Diethelm, K., Ford, Neville J., and Freed, Alan D. "Detailed error analysis for a fractional Adams method". *Numerical algorithms* **36**.1 (2004), 31–52.

[19] Ding, T. "Boundedness of solutions of Duffing's equation". *Journal of differential equations* **61**.2 (1986), 178–207.

[20] Dubois, M., Rubio, M. A., and Berge, P. "Experimental evidence of intermittencies associated with a subharmonic bifurcation". *Physical review letters* **51**.16 (1983), 1446.

[21] Dugowson, S. "Les différentielles métaphysiques: histoire et philosophie de la généralisation de l'ordre de la dérivation". PhD thesis. Paris 13, 1994.

[22] Dutta, T. K. and Prajapati, P. K. "Some dynamical properties of the Duffing equation". *International Journal of Engineering Research & Technologies* **5**.12 (2016), 500–503.

[23] Elaskar, S. and Del Río, E. *New advances on chaotic intermittency and its applications*. Springer, 2017.

[24] Elías-Zúñiga, A. "A general solution of the Duffing equation". *Nonlinear Dynamics* **45** (2006), 227–235.

[25] Euler, L. "De progressionibus transcendentibus seu quarum termini generales algebraice dari nequeunt". *Commentarii academiae scientiarum Petropolitanae* (1738), 36–57.

[26] Euler, L. *The rational mechanics of flexible or elastic bodies 1638-1788: introduction to Vol. X and XI*. Springer Science & Business Media, 1980.

[27] Faust, G. and Haase, M. *An Exploration of Chaos: An Introduction for Natural Scientists and Engineers*. North-Holland, 1994.

[28] Fourier, B. J. *Theorie Analytique de la Chaleur*. **1**. Paris: Firmin Didot, 1822, 508.

[29] Frederickson, P., Kaplan, J. L., Yorke, E. D., and Yorke, J. A. "The Liapunov dimension of strange attractors". *Journal of differential equations* **49**.2 (1983), 185–207.

[30] Gao, X. and Yu, J. "Chaos in the fractional order periodically forced complex Duffing's oscillators". *Chaos, Solitons & Fractals* **24**.4 (2005), 1097–1104.

[31] Geist, K., Parlitz, U., and Lauterborn, W. "Comparison of different methods for computing Lyapunov exponents". *Progress of theoretical physics* **83**.5 (1990), 875–893.

[32] Georgiev, Z., Trushev, I., Todorov, T., and Uzunov, I. "Analytical solution of the Duffing equation". *COMPEL-The international journal for computation and mathematics in electrical and electronic engineering* **40**.2 (2021), 109–125.

[33] Gil, A., Segura, J., and Temme, N. M. "Asymptotic approximations to the nodes and weights of Gauss–Hermite and Gauss–Laguerre quadratures". *Studies in Applied Mathematics* **140**.3 (2018), 298–332.

[34] Grebogi, C., Ott, E., Pelikan, S., and Yorke, J. A. "Strange attractors that are not chaotic". *Physica D: Nonlinear Phenomena* **13**.1-2 (1984), 261–268.

[35] Greenspan, D. "Conservative numerical methods for x= f (x)". *Journal of Computational Physics* **56**.1 (1984), 28–41.

[36] Guckenheimer, J. and Holmes, P. *Nonlinear oscillations, dynamical systems, and bifurcations of vector fields*. **42**. Springer Science & Business Media, 2013.

[37] Gutermuth, D. "Picard's existence and uniqueness theorem". *Notes of Fundamental of Differential equations. https://embedded. eecs. berkeley. edu/eecsx44/lectures7Spring2013/Picard. pdf* (2013).

[38] Helmholtz, H. L. F. *On the Sensations of Tone as a Physiological Basis for the Theory of Music*. 2nd English. Dover Publications, 1954.

[39] Holmes, P. "A nonlinear oscillator with a strange attractor". *Philosophical Transactions of the Royal Society of London. Series A, Mathematical and Physical Sciences* **292**.1394 (1979), 419–448.

[40] Holmes, P. J. and Moon, F. C. "Strange Attractors and Chaos in Nonlinear Mechanics". *Journal of Applied Mechanics* **50**.4b (1983), 1021–1032.

[41] Hooke, R. "Lectures de potentia restitutiva of a spring explaining the power of spring bodies". *London, John Martin* **1678** (1960), 1638–1788.

[42] Huang, J. Y. and Kim, J. J. "Type-II intermittency in a coupled nonlinear oscillator: Experimental observation". *Physical Review A* **36**.3 (1987), 1495.

[43] Ilhan, E. "Interesting and complex behaviour of Duffing equations within the frame of Caputo fractional operator". *Physica Scripta* **97**.5 (2022), 054005.

[44] Ishii, H., Fujisaka, H., and Inoue, M. "Breakdown of chaos symmetry and intermittency in the double-well potential system". *Physics Letters A* **116**.6 (1986), 257–263.

[45] Jánosi, D. and Tél, T. "Chaos in Hamiltonian systems subjected to parameter drift". *Chaos: An Interdisciplinary Journal of Nonlinear Science* **29**.12 (2019), 121105.

[46] Al-Jawary, M. A. and Abd-Al-Razaq, S. G. "Analytic and numerical solution for Duffing equations". *International Journal of Basic and Applied Sciences* **5**.2 (2016), 115–119.

[47] Jeyakumari, S., Chinnathambi, V., Rajasekar, S., and Sanjuán, M. A. F. "Vibrational resonance in an asymmetric Duffing oscillator". *International Journal of Bifurcation and Chaos* **21**.01 (2011), 275–286.

[48] Jiménez, S. "Derivation of the discrete conservation laws for a family of finite difference schemes". *Applied Mathematics and Computation* **64**.1 (1994), 13–45.

[49] Jiménez, S., González, J., and Vázquez, L. "Fractional Duffing's equation and geometrical resonance". *International Journal of Bifurcation and Chaos* **23**.05 (2013), 1350089.

[50] Jiménez, S., Pascual, P., Aguirre, C., and Vázquez, L. "A panoramic view of some perturbed nonlinear wave equations". *International Journal of Bifurcation and Chaos* **14**.01 (2004), 1–40.

[51] Jiménez, S. and Zufiria, P. J. "Characterizing chaos in a type of fractional Duffing's equation". *Conference Publications*. Vol. 2015. special. American Institute of Mathematical Sciences. 2015, 660.

[52] Joo, J. M. "Chaos in the Damped and Forced Duffing Oscillator". *Chaos and Complexity Letters* **16**.1 (2022), 53–66.

[53] Kaplan, J. L. and Yorke, J. A. "Chaotic behavior of multidimensional difference equations". *Functional differential equations and approximation of fixed points*. Springer, 1979, 204–227.

[54] Karakisawa, T., Bekki, N., and Shimada, I. "Saddle-node bifurcation without a reinjection process in the temporal intermittency". *Physics Letters A* **247**.3 (1998), 235–240.

[55] Khan, M., Ali, S. H., and Qi, H. "On accelerated flows of a viscoelastic fluid with the fractional Burgers' model". *Nonlinear Analysis: Real World Applications* **10**.4 (2009), 2286–2296.

[56] Kilbas, A. A., Srivastava, H. M., and Trujillo, J. J. *Theory and applications of fractional differential equations*. **204**. elsevier, 2006.

[57] Klausmeier, C. A. "Floquet theory: a useful tool for understanding nonequilibrium dynamics". *Theoretical Ecology* **1** (2008), 153–161.

[58] Kovacic, I. and Brennan, M. J. *The Duffing equation: nonlinear oscillators and their behaviour*. John Wiley & Sons, 2011.

[59] Ku, Ja H. "JW Strutt, third Baron Rayleigh, The theory of sound, (1877–1878)". *Landmark Writings in Western Mathematics 1640-1940*. Elsevier, 2005, 588–599.

[60] Lacroix, S. F. *Trait.6 du Calcul Diffe'rentiel et du Calcul Int&gral*. 2nd ed. **3**. Paris: Courtier, 1819, 409–410.

[61] Lagrange, J.L. *Sur un nouvelle espèce de calcul relatif à la différentiation et à l'intégration des quantités variables*. **3**. Paris: Gauthier-Villars, 1849, 441–476.

[62] Lakshmanan, M. and Rajaseekar, S. *Nonlinear dynamics: integrability, chaos and patterns*. Springer Science & Business Media, 2012.

[63] Laskin, N. "Fractional schrödinger equation". *Physical Review E* **66**.5 (2002), 056108.

[64] Laugesen, J., Carlsson, N., Mosekilde, E., and Bountis, T. "Anomalous statistics for type-III intermittency". *Open Systems & Information Dynamics* **4**.4 (1997), 393–405.

[65] Lazarević, M. P., Rapaić, M. R., Šekara, T. B., Mladenov, V., and Mastorakis, N. "Introduction to fractional calculus with brief historical background". *Advanced topics on applications of fractional calculus on control problems, system stability and modeling* (2014), 3–16.

[66] Leibniz, GW. "1697. Letter from Hanover, Germany, to John Wallis, May 28, 1697". *Mathematische Schriften* (1962).

[67] Leibniz, GW. "Letter from hanover, germany, september 30, 1695 to ga L'hospital". *JLeibnizen Mathematische Schriften* **2**.301-302 (1849).

[68] Letellier, C., Werny, P., Malasoma, J. M., and Gilmore, R. "Multichannel intermittencies induced by symmetries". *Physical Review E* **66**.3 (2002), 036220.

[69] Lewandowski, R. and Baum, M. "Dynamic characteristics of multilayered beams with viscoelastic layers described by the fractional Zener model". *Archive of Applied Mechanics* **85** (2015), 1793–1814.

[70] Li, X., Wang, Y., and Shen, Y. "Cluster Oscillation of a Fractional-Order Duffing System with Slow Variable Parameter Excitation". *Fractal and Fractional* **6**.6 (2022), 295.

[71] Li, Z., Chen, D., Zhu, J.i, and Liu, Y. "Nonlinear dynamics of fractional order Duffing system". *Chaos, Solitons & Fractals* **81** (2015), 111–116.

[72] Liouville, J. "Mémoire sur l'intégration de l'équation $((mx^2 + nx + p)\frac{d^2y}{d^2x}y + (qx + r)\frac{dy}{dy} + sy = 0$ à l'aide des différentielles à indices quelconques". *Journal de l'École Polytechnique* **13**.cahier 21 (1832), 163–186.

[73] Liu, J., Dong, P., Xing, L., and Li, X. "Control of fractional order chaotic system via Hermit eigenvalue analysis". *2010 Chinese Control and Decision Conference*. IEEE. 2010, 2126–2131.

[74] LLC, MultiMedia. *MS Windows NT Kernel Description*. 2024. URL: https://en.wikipedia.org/wiki/Galileo_Galilei (visited on 04/19/2024).

[75] Lubich, C. "Runge-Kutta theory for Volterra and Abel integral equations of the second kind". *Mathematics of computation* **41**.163 (1983), 87–102.

[76] Mainardi, F. "Fractional relaxation-oscillation and fractional diffusion-wave phenomena". *Chaos, Solitons & Fractals* **7**.9 (1996), 1461–1477.

[77] Malasoma, J. M., Werny, P., and Boiron, M. A. "Multichannel type-I intermittency in two models of Rayleigh–Benard convection". *Chaos, Solitons & Fractals* **15**.3 (2003), 487–500.

[78] Manneville, P. and Pomeau, Y. "Intermittency and the Lorenz model". *Physics Letters A* **75**.1-2 (1979), 1–2.

[79] Marek, M. and Schreiber, I. *Chaotic behaviour of deterministic dissipative systems*. **1**. Cambridge University Press, 1995.

[80] Matthaeus, W., Wan, M., Servidio, S., et al. "Intermittency, nonlinear dynamics and dissipation in the solar wind and astrophysical plasmas". *Philosophical Transactions of the Royal Society A: Mathematical, Physical and Engineering Sciences* **373**.2041 (2015), 20140154.

[81] Moon, F.C. and Holmes, P. J. "A magnetoelastic strange attractor". *Journal of Sound and Vibration* **65**.2 (1979), 275–296.

[82] El-Nady, A. O. and Lashin, M. M. A. "Approximate solution of nonlinear Duffing oscillator using Taylor expansion". *Journal of Mechanical Engineering and Automation* **6**.5 (2016), 110–116.

[83] Nayfeh, A. H. and Balachandran, B. *Applied nonlinear dynamics: analytical, computational, and experimental methods*. John Wiley & Sons, 2008.

[84] Nayfeh, A. H. and Sánchez, N. E. "Bifurcations in a forced softening Duffing oscillator". *International Journal of Non-Linear Mechanics* **24**.6 (1989), 483–497.

[85] Niu, J., Liu, R., Shen, Y., and Yang, S. "Chaos detection of Duffing system with fractional-order derivative by Melnikov method". *Chaos: An Interdisciplinary Journal of Nonlinear Science* **29**.12 (2019), 123106.

[86] Nourazar, S. and Mirzabeigy, A. "Approximate solution for nonlinear Duffing oscillator with damping effect using the modified differential transform method". *Scientia Iranica* **20**.2 (2013), 364–368.

[87] Odibat, Z. "Approximations of fractional integrals and Caputo fractional derivatives". *Applied Mathematics and Computation* **178**.2 (2006), 527–533.

[88] Odibat, Z. "Computational algorithms for computing the fractional derivatives of functions". *Mathematics and Computers in Simulation* **79**.7 (2009), 2013–2020.

[89] Ott, E. *Chaos in dynamical systems*. Cambridge university press, 2002.

[90] Parker, T. S. and Chua, L. *Practical numerical algorithms for chaotic systems*. Springer Science & Business Media, 2012.

[91] Perko, L. *Differential equations and dynamical systems*. **7**. Springer Science & Business Media, 2013.

[92] Petráš, I. *Fractional-order nonlinear systems: modeling, analysis and simulation*. Springer Science & Business Media, 2011.

[93] Podlubny, I. *Fractional differential equations: an introduction to fractional derivatives, fractional differential equations, to methods of their solution and some of their applications*. Elsevier, 1998.

[94] Pomeau, Y. and Manneville, P. "Intermittent transition to turbulence in dissipative dynamical systems". *Communications in Mathematical Physics* **74** (1980), 189–197.

[95] Rahimi, M. A., Salarieh, H., and Alasty, A. "Stabilizing periodic orbits of fractional order chaotic systems via linear feedback theory". *Applied Mathematical Modelling* **36**.3 (2012), 863–877.

[96] Rasband, S. N. *Chaotic dynamics of nonlinear systems*. Courier Dover Publications, 2015.

[97] Ravichandran, V., Chinnathambi, V., and Rajasekar, S. "Effect of various periodic forces on Duffing oscillator". *Pramana* **67** (2006), 351–356.

[98] Richetti, P., Argoul, F., and Arneodo, A. "Type-II intermittency in a peroidically driven nonlinear oscillator". *Physical Review A* **34**.1 (1986), 726.

[99] Riemann, B. *Versuch einer allgemeinen Auffassung der Integration und Differentiation*. Reprint: Dover, New York, 1953. Leipzig: Teubner, 1876, 331–344.

[100] Robinson, C. *Dynamical systems: stability, symbolic dynamics, and chaos*. CRC press, 1998.

[101] Ross, B. *Fractional calculus and its applications: proceedings of the international conference held at the University of New Haven, June 1974*. **457**. Springer, 2006.

[102] Ross, B. "The development of fractional calculus 1695–1900". *Historia Mathematica* **4**.1 (1977), 75–89.

[103] Rossikhin, Y. A. and Shitikova, M. V. "New approach for the analysis of damped vibrations of fractional oscillators". *Shock and Vibration* **16**.4 (2009), 365–387.

[104] Rysak, A. and Sedlmayr, M. "Damping efficiency of the Duffing system with additional fractional terms". *Applied Mathematical Modelling* **111** (2022), 521–533.

[105] Sacher, J., Elsässer, W., and Göbel, E. O. "Intermittency in the coherence collapse of a semiconductor laser with external feedback". *Physical review letters* **63**.20 (1989), 2224.

[106] Salau, T., Olaiya, K. A., and Ajide, O. O. "Simulation of oscillators dynamics using selected versions of fourth order rungekutta scheme". *International Journal of Engineering and Technology* **4**.8 (2014), 444–450.

[107] Samko, S. G. "Fractional integrals and derivatives". *Theory and applications* (1993).

[108] Sánchez, N. E. and Nayfeh, A. H. "Prediction of bifurcations in a parametrically excited Duffing oscillator". *International Journal of Non-Linear Mechanics* **25**.2-3 (1990), 163–176.

[109] Sato, S., Sano, M., and Sawada, Y. "Practical methods of measuring the generalized dimension and the largest Lyapunov exponent in high dimensional chaotic systems". *Progress of theoretical physics* **77**.1 (1987), 1–5.

[110] Saxena, R. K., Mathai, A. M., and Haubold, H. J. "Fractional reaction-diffusion equations". *Astrophysics and space science* **305** (2006), 289–296.

[111] El-Sayed, A., El-Mesiry, A., and El-Saka, H. "Numerical solution for multi-term fractional (arbitrary) orders differential equations". *Computational & Applied Mathematics* **23**.1 (2004), 33–54.

[112] Schuster, H. G. and Just, W. *Deterministic chaos: an introduction*. John Wiley & Sons, 2006.

[113] Seydel, R. *Practical bifurcation and stability analysis*. **5**. Springer Science & Business Media, 2009.

[114] Shen, Y., Yang, S., Xing, H., and Gao, G. "Primary resonance of Duffing oscillator with fractional-order derivative". *Communications in Nonlinear Science and Numerical Simulation* **17**.7 (2012), 3092–3100.

[115] Sheu, L., Chen, H., Chen, J., and Tam, L. "Chaotic dynamics of the fractionally damped Duffing equation". *Chaos, Solitons & Fractals* **32**.4 (2007), 1459–1468.

[116] Singh, R., Rehman, A. U., Masud, M., et al. "Fractional order modeling and analysis of dynamics of stem cell differentiation in complex network". *AIMS Mathematics* **7**.4 (2022), 5175–5198.

[117] Sonin, N. Y. "On differentiation with arbitrary index". *Moscow Matem. Sbornik* **6**.1 (1869), 1–38.

[118] Sparrow, C. *The Lorenz equations: bifurcations, chaos, and strange attractors*. **41**. Springer Science & Business Media, 2012.

[119] Strauss, W. and Vázquez, L. "Numerical solution of a nonlinear Klein-Gordon equation". *Journal of Computational Physics* **28**.2 (1978), 271–278.

[120] Syta, A., Litak, G., Lenci, S., and Scheffler, M. "Chaotic vibrations of the Duffing system with fractional damping". *Chaos: An Interdisciplinary Journal of Nonlinear Science* **24**.1 (2014), 013107.

[121] Szempli, W. *Chaos Bifurcations and Fractals Around Us: A Brief Introduction*. **47**. World Scientific, 2003.

[122] Tabatabaei, K. and Gunerhan, E. "Numerical solution of Duffing equation by the differential transform method". *Appl. Math. Inf. Sci. Lett* **2**.1 (2014), 1–6.

[123] Torkzadeh, L. "Numerical behavior of nonlinear Duffing equations with fractional damping". *Rom. Rep. Phys* **73** (2021), 113.

[124] Truesdell, Clifford, Euler, Leonhard, et al. "The rational mechanics of flexible or elastic bodies, 1638-1788: introduction to Leonhardi Euleri Opera omnia, vol. X et XI seriei secundae". *(No Title)* (1960).

[125] Valli Priyatharsini, S., Meenakshi, S., Chinnathambi, V., and Rajasekar, S. "Horseshoe dynamics in Duffing oscillator with fractional damping and multi-frequency excitation". *Journal of Mathematical Modeling* **7**.3 (2019), 263–276.

[126] Vassilicos, J. C. *Intermittency in turbulent flows*. Cambridge University Press, 2001.

[127] Vázquez, L., Velasco, M. P., Usero, D., and Jiménez, S. "Fractional calculus as a modeling framework". *Monografias Matematicas Garcia de Galdean* **41** (2018), 187–197.

[128] Velasco, M. P., Usero, D., Jiménez, S., et al. "About some possible implementations of the fractional calculus". *Mathematics* **8**.6 (2020), 893.

[129] Wahi, P. and Chatterjee, A. "Averaging oscillations with small fractional damping and delayed terms". *Nonlinear dynamics* **38**.1 (2004), 3–22.

[130] Wang, J., Zhou, J., and Peng, B. "Weak signal detection method based on Duffing oscillator". *Kybernetes* **38**.10 (2009), 1662–1668.

[131] Wen, X. J., Wu, Z. M., and Lu, J.G. "Stability analysis of a class of nonlinear fractional-order systems". *IEEE Transactions on circuits and systems II: Express Briefs* **55**.11 (2008), 1178–1182.

[132] Wiggins, S. *Global bifurcations and chaos: analytical methods*. **73**. Springer Science & Business Media, 2013.

[133] Wiggins, S. *Introduction to Applied Nonlinear Dynamical Systems and Chaos*. Texts in Applied Mathematics. Springer New York, 2003. URL: https://books.google.es/books?id=RSI4RGdwnU4C.

[134] Wolf, A., Swift, J. B., Swinney, H. L., and Vastano, J. A. "Determining Lyapunov exponents from a time series". *Physica D: nonlinear phenomena* **16**.3 (1985), 285–317.

[135] Xing, W., Chen, E., Chang, Y., and Wang, M. "Threshold for chaos of a duffing oscillator with fractional-order derivative". *Shock and Vibration* **2019** (2019), 1230194.

[136] Xu, Y., Li, Y., Liu, D., Jia, W., and Huang, H. "Responses of Duffing oscillator with fractional damping and random phase". *Nonlinear Dynamics* **74**.3 (2013), 745–753.

[137] Yoder, J. G. "Christiaan Huygens, book on the pendulum clock (1673)". *Landmark Writings in Western Mathematics 1640-1940*. Elsevier, 2005, 33–45.

[138] Yuste, S. B. "Weighted average finite difference methods for fractional diffusion equations". *Journal of Computational Physics* **216**.1 (2006), 264–274.

[139] Yusufoğlu, Elçin. "Numerical solution of Duffing equation by the Laplace decomposition algorithm". *Applied Mathematics and Computation* **177**.2 (2006), 572–580.

[140] Zaslavsky, G. M., Stanislavsky, A. A., and Edelman, M. "Chaotic and pseudochaotic attractors of perturbed fractional oscillator". *Chaos: An Interdisciplinary Journal of Nonlinear Science* **16**.1 (2006), 013102.